

Snapshots of Radical Enzyme Catalysis: The Crystal Structures of Biotin Synthase and Lysine 5,6-Aminomutase.

By
Frederick Berkovitch

B.S. Biochemistry
Brandeis University, Waltham, MA

Submitted to the Department of Chemistry in
Partial Fulfillment of the Requirements for the Degree of

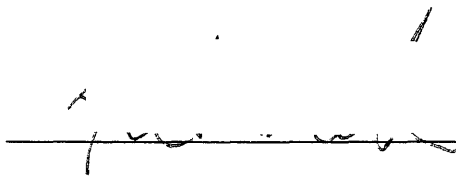
DOCTOR OF PHILOSOPHY
In Biological Chemistry

At the

Massachusetts Institute of Technology
September 2004

© 2004 Massachusetts Institute of Technology
All rights reserved

Signature of Author



Department of Chemistry
August 2004

Certified by

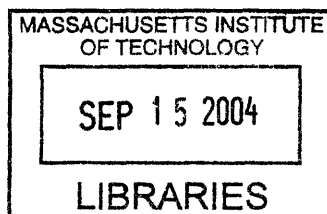
Catherine L. Drennan
Associate Professor
Thesis supervisor

Accepted by



Robert W. Field

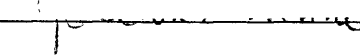
Chairman, Departmental Committee on Graduate Students



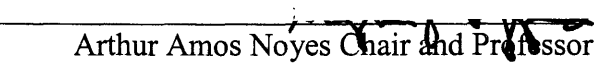
ARCHIVES

This doctoral thesis has been examined by a Committee of the Department of Chemistry as follows:


Professor JoAnne Stubbe


Committee Chairperson
Novartis Professor of Chemistry
Professor of Biology

Professor Stephen J. Lippard


Arthur Amos Noyes Chair and Professor of Chemistry

Professor Catherine L. Drennan


Thesis supervisor
Associate Professor of Chemistry

To my family and to Shaunna

Snapshots of Radical Enzyme Catalysis: The Crystal
Structures of Biotin Synthase and Lysine 5,6-aminomutase

by

Frederick Berkovitch

Submitted to the Department of Chemistry in September 2004 in Partial
Fulfillment of the Requirements for the Degree of Doctor of Philosophy

Abstract

“AdoMet radical” enzymes utilize a 4Fe-4S cluster and *S*-adenosylmethionine, in conjunction with a reducing system, to catalyze reactions that proceed through organic radical intermediates. Genomics studies suggest that at least 600 such enzymes exist across the archaea, bacteria, and eukaryotes, though few have been purified and characterized. AdoMet radical enzymes participate in several biomedically important processes, such as DNA biosynthesis and repair, cofactor biosynthesis, and bacterial pathogenesis. To gain insight into this enzyme family, the crystal structure of biotin synthase from *Escherichia coli*, in complex with its substrate dethiobiotin, was determined to 3.4 Å resolution. Biotin synthase catalyzes a remarkable reaction, the insertion of sulfur into dethiobiotin to form biotin (vitamin B₈). The structure of biotin synthase indicates that adenosylmethionine is coordinated to a unique Fe of the 4Fe-4S cluster, in agreement with spectroscopic investigations from other laboratories. Additionally, the structure reveals that the active site, located in the core of an (α/β)₈ barrel, contains a unique 2Fe-2S cluster, in addition to the 4Fe-4S cluster, adenosylmethionine, and dethiobiotin. Multiple lines of evidence suggest that in the AdoMet radical enzymes, adenosylmethionine is a source of 5'-deoxyadenosyl radical, an intermediate that is historically associated with the adenosylcobalamin-dependent radical enzymes. Interestingly, some of the adenosylcobalamin radical enzymes catalyze reactions that are very similar to those of AdoMet radical enzymes. One such example is adenosylcobalamin-dependent lysine 5,6-aminomutase, which is analogous to lysine 2,3-aminomutase, an AdoMet radical enzyme that is found in the same pathway. To further probe the relationship of the adenosylmethionine and adenosylcobalamin-dependent radical enzymes, the crystal structure of lysine 5,6-aminomutase was determined to 2.8 Å resolution. Like biotin synthase, the structure of lysine-5,6-aminomutase adheres to the general theme of barrels or barrel-like structures for enzymes that utilize 5'-deoxyadenosyl radicals in catalysis. Additionally, the structure of lysine-5,6-aminomutase implicates pyridoxal phosphate in a novel role, acting as a lock to prevent the formation of aberrant radicals in the absence of substrate.

Thesis supervisor: Catherine L. Drennan
Title: Associate professor

I thank Professors Drennan, Jarrett, Frey, Licht, Klibanov, Lippard and Stubbe, and their lab members, for enabling this work and for their counsel.

My brother Mike inspired me to go the distance, and continues to be a bottomless well of wisdom and experience. My mother and father have always reminded me of what my goal was, and had the utmost confidence in me. I always hoped that my success in graduate school would inspire my little cousins Joe, Brian, and Jenny to set and achieve their own goals. Their parents, my aunt and uncle, expected nothing less than success from me. My grandparents and great-grandparents lived a life of unimaginable hardship and sacrifice in order to give me, my brother, and my cousins the opportunity to live better lives. Through these last two years, I could always turn to Shaunna when things were difficult. She is the kindest, most beautiful person I have ever known. I don't know what I'd do without her. She took care of me during these last months - made me food, told me so when I needed to sleep... My experience at MIT was enriched by the company of the friends I've made. I thank them (you know who you are) for helping me, teaching me, and sharing their experiences with me. I guess the most poignant thing I learned in grad school is something that was so beautifully expressed by Edward Estlin Cummings:

O sweet spontaneous
earth how often have
the
doting

fingers of
prurient philosophers pinched
and
poked

thee
,has the naughty thumb
of science prodded
thy

beauty .how
often have religions taken
thee upon their scraggy knees
squeezing and

buffeting thee that thou mightest conceive
gods
(but
true

to the incomparable
couch of death thy
rhythmic
lover

thou answerest

them only with
spring)

Table of Contents

Abstract.....	4
Acknowledgements.....	5
Table of Contents.....	6
List of Tables.....	9
List of Figures.....	10

Chapter 1: Introduction to the structure of AdoMet and AdoCbl -dependent radical enzymes

Abbreviations.....	13
1.1 AdoCbl-dependent enzymes.....	14
1.2 AdoMet radical enzymes.....	16
1.3 Why two radical cofactors?	17
1.4 The diversity of 5'-deoxyadenosyl radical enzymes.....	20
1.5 AdoCbl and AdoMet -dependent radical enzymes: structural information.....	21
1.5.1 Methionine synthase, the canonical base-off Cbl binding protein	
1.5.2 Methylmalonyl-CoA mutase: a large-scale conformational change upon substrate binding	
1.5.3 Diol and glycerol dehydratases: Base-on enzymes with a catalytic K ⁺ ion in their active sites	
1.5.4 Glutamate mutase: a theory of radical propagation	
1.5.5 Class II ribonucleotide reductase: a ten-stranded $\alpha\beta$ barrel	
1.5.6 Lysine 5,6-aminomutase	
1.6 AdoMet radical enzymes.....	32
1.6.1 Lysine 2,3-aminomutase: reversible cleavage of AdoMet	
1.6.2 Pyruvate formate lyase activase: a model for AdoMet binding	
1.6.3 Class III ribonucleotide reductase activase: reductive cleavage of AdoMet	
1.6.4 Biotin and lipoyl synthases: sulfur insertion enzymes	
1.6.5 Coproporphyrinogen III oxidase: a new fold for an Ado• enzyme	
1.7 Summary.....	38
1.8 Figures.....	39
1.9 References.....	54

Chapter 2: Preliminary crystallographic characterization of biotin synthase

Abbreviations.....	66
2.1 Protein purification, Fe-S cluster reconstitution, and addition of substrates.....	67
2.2 Crystallization and preliminary analysis.....	67
2.3 Tables.....	76
2.4 Figures.....	81
2.5 References.....	87

Chapter 3: Crystal structure of biotin synthase	
Abbreviations.....	89
3.1 Introduction.....	90
3.2 Materials and methods.....	93
3.3 Results.....	95
3.3.1 Overall structure and the location of Fe-S clusters	
3.3.2 A PLP binding site is not observed in the structure	
3.3.3 The novel 2Fe-2S cluster of BioB	
3.3.4 The 4Fe-4S cluster and AdoMet	
3.3.5 The methionyl moiety	
3.3.6 The dethiobiotin binding site	
3.4 Discussion.....	101
3.4.1 Arginine as an Fe ligand	
3.4.2 Structural insight into the reaction catalyzed by BioB	
3.4.3 Questions arising from the structure of BioB	
3.5 Tables.....	105
3.6 Figures.....	109
3.7 References.....	122
Chapter 4: Crystal structure of lysine 5,6-aminomutase	
Abbreviations.....	127
4.1 Introduction.....	128
4.2 Materials and methods.....	131
4.2.1 Protein preparation	
4.2.2 Storage, handling, and crystallization of protein samples, and crystal cryoprotection	
4.2.3 Crystal properties, phasing, model building, and refinement	
4.3 Results.....	134
4.3.1 Overall structure	
4.3.2 PLP-protein interactions	
4.3.3 Cobalamin-protein interactions	
4.3.4 The CxxCxxxC motif of lysine 5,6 aminomutase	
4.4 Discussion.....	140
4.4.1 A hypothetical conformational change to bring AdoCbl into the active site	
4.4.2 Questions arising from the structure of 5,6-LAM	
4.5 Tables.....	144
4.6 Figures.....	147
4.7 References.....	164

Chapter 5: Conclusions

Abbreviations.....	166
5.1 Structural comparison of BioB and coproporphyrinogen III oxidase.....	167
5.2 Structural comparison of BioB with diol dehydratase.....	168
5.3 A novel role for PLP in a 5'-deoxyadenosyl radical enzyme.....	169
5.4 5'-deoxyadenosyl radical enzymes: barrel structures with reaction-specific accommodations.....	169
5.5 Figures.....	171
5.6 References.....	173

Appendices

1 Summary of 5,6-LAM crystallization experiments.....	174
2 Curriculum Vitae.....	175

List of Tables

Table 2.1. Timeline of BioB crystallization.....	76
Table 2.2. Hampton Research screens used to find BioB crystallization conditions....	77
Table 2.3. Additives used to optimize BioB crystallization conditions.....	78
Table 2.4. Data collected from a single crystal grown in condition BioB3.....	79
Table 2.5. Data collected from crystals grown in condition BioB5 and used to solve the structure of BioB.....	80
Table 3.1. Maximal BioB activity.....	105
Table 3.2. Data collection and refinement statistics.....	106
Table 3.3. Metal-nitrogen (guanidine) distances from crystallographic structures of metal-guanidine complexes.....	107
Table 3.4. Fe-S cluster-ligand distances.....	107
Table 3.5. Electrostatic interactions and potential hydrogen bonds between BioB and AdoMet.....	108
Table 3.6. Potential hydrogen bonds between BioB and DTB.....	108
Table 4.1. 5,6-LAM data collection and refinements statistics.....	144
Table 4.2. Potential PLP-5,6-LAM hydrogen bonding and electrostatic interactions..	145
Table 4.3. Potential AdoCbl-5,6-LAM hydrogen bonding interactions.....	146

List of Figures

Figure 1.1. Molecular structures of AdoCbl, Ado•, and AdoMet.....	39
Figure 1.2. Simplified catalytic cycle of AdoCbl-dependent mutases.....	39
Figure 1.3. Selected AdoMet-dependent enzymatic reactions.	40
Figure 1.4. The biotin biosynthetic pathway.....	41
Figure 1.5. The AdoCbl-dependent enzymatic reactions.....	42
Figure 1.6. Several moderately or well -characterized AdoMet radical enzyme reactions.....	43
Figure 1.7. The AdoMet cycle.....	44
Figure 1.8. Crystal structure of the MeCbl-binding domain of methionine synthase...	45
Figure 1.9. Crystal structure of methylmalonyl-CoA mutase.....	46
Figure 1.10. Crystal structure of diol dehydratase.....	47
Figure 1.11. Crystal structure of glutamate mutase.....	48
Figure 1.12. Crystal structure of class II ribonucleotide reductase.....	48
Figure 1.13. Crystal structure of the substrate-free AdoCbl-PLP-5,6-LAM complex..	49
Figure 1.14. Radical generation by the 4Fe-4S cluster and AdoMet in the AdoMet radical enzymes.....	50
Figure 1.15. Mechanism proposed by Frey and coworkers for the 2,3-LAM reaction.....	51
Figure 1.16. Crystal structure of BioB.....	52
Figure 1.17. Crystal structure of HemN.....	53
Figure 2.1. SDS-PAGE analysis of BioB crystals grown in condition BioB2.....	81
Figure 2.2. Lattice contacts in the final structure of BioB.....	82
Figure 2.3. BioB crystals.....	83
Figure 2.4. First diffraction from a BioB crystal.....	84
Figure 2.5. 5.5 Å data from crystals grown in condition BioB3.....	85
Figure 2.6. Location of putative Fe sites in BioB.....	86
Figure 3.1. Overall reaction of BioB.....	109
Figure 3.2. Mechanisms proposed for the BioB reaction.....	110
Figure 3.3. Stereo figure showing the electron density of the Fe-S clusters of BioB...	111
Figure 3.4. Solvent flattened, two-fold NCS-averaged 3.7 Å resolution experimental electron density map of BioB.....	111
Figure 3.5. Ramachandran plot of the BioB monomer.....	112
Figure 3.6. Overall structure of BioB.....	113
Figure 3.7. The BioB monomer.....	115
Figure 3.8. Space-filling model of BioB.....	116
Figure 3.9. Lattice packing in BioB crystals.....	117
Figure 3.10. Stereo alpha carbon trace of a single BioB subunit, showing the locations of all Lys residues in the structure.....	117
Figure 3.11. The BioB active site.....	118
Figure 3.12. 2Fe-2S and 4Fe-4S clusters with incomplete cysteinyl ligation.....	119
Figure 3.14. Conservation of residues across the AdoMet radical enzymes.....	120

Figure 3.15. The carboxylate tail of DTB interacting with residues T292 and T293...	121
Figure 4.1. Aminomutases in the bacterial lysine fermentation pathway.....	147
Figure 4.2. Proposed mechanism of 5,6-LAM.....	148
Figure 4.3. 1,2-imino shift under radical-generating conditions and rearrangement of the aziridylcarbinyl radical.....	149
Figure 4.4. Various crystal forms of 5,6-LAM.....	150
Figure 4.5. Solvent-flattened 3.0 Å resolution experimental electron density of 5,6- LAM.....	152
Figure 4.6. Ramachandran plot of 5,6-LAM.....	153
Figure 4.7. Overall structure of 5,6-LAM and location of cofactors.....	154
Figure 4.8. Topology diagram of the 5,6-LAM $\alpha\beta$ heterodimer.....	155
Figure 4.9. Lattice packing interactions for 5,6-LAM	156
Figure 4.10. The five established PLP-binding enzyme families, plus 5,6-LAM.....	157
Figure 4.11. Superposition of the TIM barrels of alanine racemase and 5,6-LAM.....	159
Figure 4.12. PLP in the putative active site of 5,6-LAM.....	160
Figure 4.13. The AdoCbl binding site of 5,6-LAM	161
Figure 4.14. A stereo view of the local structure of the CxxCxxxC sequence.....	161
Figure 4.15. Hypothetical conformational change of 5,6-LAM and observed conformational change of MCM.....	162
Figure 4.16. A cleft leading to the putative active site of 5,6-LAM.....	163
Figure 5.1. Superposition of BioB and coproporphyrinogen III oxidase.....	171
Figure 5.2. Superposition of BioB and diol dehydratase.....	172

Chapter 1

Introduction to AdoCbl and AdoMet -dependent radical enzyme structures

Abbreviations:

2,3-LAM	Lysine 2,3-aminomutase
5,6-LAM	Lysine 5,6-aminomutase
Ado	5'-deoxyadenosyl group
Ado•	5'-deoxyadenosyl radical
AdoCbl	Adenosylcobalamin, Coenzyme B ₁₂
AdoH	5'-deoxyadenosine
AdoMet	<i>S</i> -adenosylmethionine
APCbl	Adeninylpentylcobalamin
BioB	Biotin synthase
Cbl	Cobalamin
CNCbl	Cyanocobalamin, Vitamin B ₁₂
CoA	Coenzyme A
Cob(II)	Cob(II)alamin
DDH	Diol dehydratase
DTB	Dethiobiotin
EAL	Ethanolamine ammonia lyase
ENDOR	Electron nuclear double resonance
EPR	Electron paramagnetic resonance
ESEEM	Electron spin-echo envelope modulation
EXAFS	Extended X-ray absorption fine structure
GDH	Glycerol dehydratase
GM	Glutamate mutase
HemN	Coproporphyrinogen III oxidase
ICM	Isobutyryl-coenzyme A mutase
LipA	Lipoyl synthase
MCM	Methylmalonyl-coenzyme A mutase
MGM	Methyleneglutarate mutase
MS	Methionine synthase
OAM	Ornithine aminomutase
PFL	Pyruvate formate lyase
RNR	Ribonucleotide reductase
SAH	<i>S</i> -adenosylhomocysteine
SAM	<i>S</i> -adenosylmethionine

Certain enzymatic reactions require the activation of saturated carbons in order to effect difficult reactions. One general mode of accomplishing this daunting task is to recruit metallocofactors, which supply reactivity beyond that of the set of naturally occurring amino acids and organic cofactors. Carbon-based radical intermediates are sometimes involved in such metal-based activation processes. Two particular cofactors are frequently recruited to abstract a hydrogen atom from an organic substrate, generating free radical intermediates. The first of these, adenosylcobalamin (AdoCbl, or coenzyme B₁₂, Fig. 1.1a), is the coenzyme form of the cobalt-containing vitamin B₁₂, one of the oldest known organometallic compounds. A second common radical-generating cofactor is *S*-adenosylmethionine (AdoMet or SAM, Fig. 1.1c) in complex with a 4Fe-4S cluster. The immediately obvious feature that is common to both cofactors is the adenosyl group.

1.1 AdoCbl-dependent enzymes

The clinical importance of vitamin B₁₂ is rooted in the history of pernicious anemia, an autoimmune disease of the gastrointestinal system that results in poor nutrient absorption. If left untreated, the condition invariably results in death. The first reports of the disease date back to the 18th and 19th centuries¹. In 1926, Minot & Murphy demonstrated that pernicious anemia could be cured by feeding patients large amounts of liver², a discovery that would later win them the Nobel Prize in Medicine and Physiology. The groups of Folkers³ and Lester-Smith⁴ eventually isolated cyanocobalamin (CNCbl or vitamin B₁₂), a derivative of the “anti pernicious anemia factor” present in liver. Other serious human diseases arising from vitamin B₁₂ deficiency were later discovered, including methylmalonic aciduria and homocysteinuria. Both of these are genetic disease caused

by mutation in either the *MutAB* genes⁵, which encode AdoCbl-dependent methylmalonyl-CoA mutase (MCM), or in one of the *MmmA-H* genes, which encode proteins associated with Cbl uptake and metabolism⁶.

In 1958, Barker and coworkers showed that crude cell extracts of *Clostridium tetanomorphum* required a coenzyme form of vitamin B₁₂ to convert glutamate to 3-methylaspartate. This work led to the discovery and purification of AdoCbl⁷. AdoCbl dependence in a purified enzyme system (MCM) was first reported by Stadtman and coworkers^{8,9} two years after Barker's discovery of the coenzyme. Eggerer *et al* proposed that AdoCbl-dependent MCM catalyzes the formation of paramagnetic species on the reaction pathway⁹. Their hypothetical mechanism fell short of recognizing C-Co bond cleavage, (Fig. 1.2) but made an intellectual leap forward in asserting that the rearrangement of methylmalonyl-CoA to succinyl-CoA involved radical intermediates.

Thirty years after Minot and Murphy's successful treatment of pernicious anemia, Hodgkin and coworkers solved the X-ray crystal structure of CNCbl¹⁰, for which she was awarded the 1964 Nobel Prize in Chemistry. The structure revealed a single octahedral Co(III) center, coordinated equatorially by the four pyrrole nitrogens of a corrin macrocycle. The lower axial ligand is a nitrogen atom of the cofactor's dimethylbenzimidazole moiety, and the upper axial ligand is cyanide, an artifact of purification. In 1961, Hodgkin solved the structure of the coenzyme form of B₁₂¹¹, illuminating the structural basis for the reactivity of AdoCbl. At the heart of AdoCbl's reactivity is its alkyl cobalt bond: the 5'-deoxyadenosyl group (Ado) is covalently bound

to Co(III) in the upper axial position. AdoCbl is one of the largest known biological cofactors; it has the chemical formula $C_{72}H_{100}N_{18}O_{17}PCo$, and contains 18 chiral centers.

In 1966, R.H. Abeles and P.A. Frey first showed that diol dehydratase (DDH) catalyzes the transfer of tritium atoms between $[1-^3H]$ propanediol and the 5' carbon of AdoCbl¹². Furthermore, the resultant $[5'-^3H]$ AdoCbl was able to transfer its tritium into propionaldehyde, the product of the diol dehydratase reaction. In the early 1970's, other key investigators of AdoCbl enzymes, including Blakley and Babior, observed the kinetically competent formation of a paramagnetic species in the reactions of class II RNR¹³ and EAL^{14,15}. These and other pioneering experiments, over years of investigation, have led to the hypothesis that the C-Co bond of AdoCbl is homolytically cleaved, resulting in the transient intermediates Cob(II)alamin [Cob(II)] and 5'-deoxyadenosyl radical (Ado•, Fig. 1.1b and Fig. 1.2), which is thought to be responsible for the H atom abstractions that initiate AdoCbl-dependent reactions. Several excellent reviews covering the reactivity of AdoCbl enzymes are available¹⁶⁻²³.

1.2. AdoMet radical enzymes

Twenty three years after demonstrating the 3H atom transfers in DDH, Frey published analogous experiments on AdoMet-dependent lysine 2,3-aminomutase²⁴ (2,3-LAM), supporting the hypothesis that Ado• is the agent that is responsible for H atom abstraction in the enzymatic reaction. Significantly, Barker's work on 2,3-LAM first demonstrated that the enzyme is pyridoxal 5'-phosphate-(PLP) and Fe -dependent²⁵.

Compared to AdoCbl, AdoMet is a relatively simple molecule (Fig. 1.1). The C-Co bond of AdoCbl (~30 kcal/mol) is replaced by a much stronger (~60 kcal/mol) bond between the 5' carbon of Ado and the sulfur atom of the methionyl group. AdoMet is involved in a number of unusual reactions (Fig. 1.3). Two such reactions appear in the biotin (vitamin B₈) biosynthetic pathway (Fig. 1.4). In the first of these reactions, AdoMet acts as an amino group donor in the PLP-dependent transformation of 7-keto-8-aminoperlarginic acid to 7,8-diaminoperlarginic acid²⁶. The second unusual reaction is that of biotin synthase (BioB). BioB is an iron-dependent protein that requires AdoMet to form biotin from dethiobiotin²⁷⁻²⁹ (DTB). Marquet and coworkers have shown that BioB transfers deuterium from deuterated DTB into 5'-deoxyadenosine (AdoH)³⁰. These deuterium transfer experiments support the hypothesis that AdoMet abstracts substrate hydrogen atoms in BioB, as it does in 2,3-LAM.

1.3. Why two radical cofactors?

Since the early work on AdoCbl enzymes, a total of 10 AdoCbl- and 6 AdoMet-dependent radical enzymes have been purified and reasonably well characterized (Figs. 1.5 and 1.6). Recently, Sofia and coworkers proposed that over 600 unique sequences of AdoMet radical enzymes exist³¹. Several fascinating questions arise from this work: Why has nature evolved two analogous cofactors to abstract H atoms from metabolic intermediates? What is the evolutionary relationship between the two cofactors and the enzymes that require them? What are the evolutionary determinants of cofactor preference for a given enzyme? It is tempting, upon initial inspection, to speculate that

the AdoMet radical enzymes are the molecular ancestors of the AdoCbl radical enzymes.

Proponents of this theory may point to a few salient facts:

1. All of the known AdoMet radical enzymes require a 4Fe-4S cluster and, with one known exception, anoxic conditions for activity. Fe-S clusters are widely regarded as ancient and ubiquitous cofactors, capable of carrying out catalysis in the ancient, anoxic atmosphere³²⁻³⁴.
2. AdoMet biosynthesis (Fig. 1.7) requires far fewer enzymes than does AdoCbl biosynthesis (this argument does not take into account the enzymes required for Fe-S cluster biosynthesis or cluster reduction).
3. Several equivalents of AdoMet are required as methylating agents in the biosynthesis of AdoCbl³⁵.
4. Sequence analysis on probable AdoMet radical enzymes by Sofia *et al* reveals that some of these enzymes contain part of the "base-off" AdoCbl-binding sequence motif (DxHxxG...Sxl...GG) that is found in all of the AdoMet-dependent mutases.
5. Several AdoMet radical enzymes catalyze steps in central pathways of metabolism, including DNA biosynthesis and repair, acetyl-CoA biosynthesis, and coenzyme biosynthesis.

These and other reasons have led some to classify AdoMet radical enzymes as the "molecular fossils" of AdoCbl radical enzymes. In particular, this speculation has been applied with respect to the ribonucleotide reductases^{36,37}. Others believe that AdoCbl

may be the ancestral radical cofactor, and that the various arguments of the AdoMet ancestor proponents are weak. This opinion is bolstered by several lines of reasoning:

1. Corrinoid-like molecules are thought to date back to the primordial soup³⁸.
2. Many (but not all) organisms require methylcobalamin to synthesize AdoMet via the cobalamin-dependent methionine biosynthetic pathway³⁹.
3. The presence of the “base-off” AdoCbl binding motif in AdoMet radical enzyme sequences implies no directionality in evolution.
4. Several AdoCbl-dependent enzymes catalyze steps in central pathways of metabolism, including DNA biosynthesis, such as the class II ribonucleotide reductase (RNR).
5. In comparison to the AdoMet radical enzyme activases, where an entire protein, AdoMet, and a 4Fe-4S cluster are required to generate a catalytic radical on a separate enzyme, one can argue that AdoCbl is the simpler radical-generating machinery.

Some AdoCbl-dependent enzymes, such as the class II RNR, lysine 5,6-aminomutase (5,6-LAM), and diol dehydratase (DDH) have AdoMet-dependent counterparts that catalyze similar reactions. Perhaps these enzymes provide the best opportunity for understanding how the two enzyme superfamilies may be related.

1.4. The diversity of 5'-deoxyadenosyl radical enzymes

Many AdoCbl radical enzymes share a set of common steps in their reaction mechanisms, shown in general terms in Fig. 1.2. Briefly, Ado• abstracts a non-activated hydrogen atom from the substrate. The substrate then rearranges via a vicinal group migration to the original radical center, and then re-abstracts a hydrogen atom from AdoH, resulting in the reformation of AdoCbl. The exception to this general mechanistic scheme is the class II RNR reaction, in which the radical is propagated to a Cys residue, generating a catalytic thiyl radical^{13,40,41}. A key question in the field is how the AdoCbl enzymes, in the presence of either substrate or effectors, accelerate C-Co bond homolysis by a factor of $\sim 10^{12}$ over the non-enzymatic cleavage^{17,42-46}.

In contrast, AdoMet radical enzymes catalyze more diverse reactions (Fig. 1.6), and have substrates that vary in size from small molecules to proteins to DNA. The reaction mechanisms of AdoMet-dependent radical enzymes cannot be generalized beyond the abstraction of an H atom by Ado•. While some AdoMet radical enzymes go through a reaction sequence similar to those of AdoCbl enzymes, others utilize AdoMet as a substrate rather than a cofactor, resulting in the production of one or more equivalents of methionine and AdoH per substrate consumed.

Why are AdoMet radical enzymes so much more versatile than AdoCbl radical enzymes? What are the implications of this diversity on the theory that AdoMet is the ancestral radical cofactor? Given the current state of the field, the answers to these and other

questions about the relationship between AdoCbl and AdoMet radical enzymes remain unknown. Some of the answers may lie in the structural details of the two superfamilies.

1.5. AdoCbl and AdoMet -dependent radical enzymes: structural information

This section briefly reviews some of the more well-characterized AdoCbl and AdoMet-radical enzymes, with emphasis on structural information. The study of several of these enzymes has benefited from the availability of X-ray or NMR structures. A unifying theme in the structures of these enzymes is the dominance of α/β barrel folds⁴⁷, in which a central β -sheet is surrounded by α helices, and the prevalence of the TIM barrel fold in particular.

The TIM barrel is an ancient, ubiquitous, and adaptable protein fold^{48,49}. TIM barrel proteins carry out an astonishing number of diverse metabolic functions. Twenty-six protein superfamilies use the TIM barrel architecture to bind their substrates and to place their catalytic elements in their active sites⁴⁷. There is no apparent theme to the enzymatic reactions carried out by TIM barrels, and at least one TIM barrel has no associated enzymatic activity⁵⁰. With the exception of class II RNR, all AdoCbl-dependent radical enzymes of known structure have the same protein motifs, consisting of a TIM barrel substrate-binding domain and an AdoCbl binding domain that docks on top of the TIM barrel. The work described in this thesis reveals that BioB, an AdoMet dependent radical enzyme, is a TIM barrel. Furthermore, the structure of 5,6-LAM, an enzyme which bridges the AdoCbl and AdoMet radical superfamilies, adheres to the general scaffold of AdoCbl-dependent radical enzymes.

One interesting conclusion that is illuminated by structural and biophysical studies of cobalamin- (Cbl) binding proteins is that they can be grouped based on their mode of binding to the protein. The group I (“base-off”) proteins use a histidine residue to displace the intrinsic DMB moiety of the cofactor as the lower axial ligand to cobalt. This group includes methylcobalamin-dependent methionine synthase (MS)⁵¹, MCM⁵², GM⁵³, 5,6-LAM⁵⁴ (this work), and, presumably, isobutyryl-CoA mutase (ICM)⁵⁵, methyleneglutarate mutase (MGM)⁵⁶, and ornithine aminomutase (OAM)⁵⁷. For the group I enzymes that utilize AdoCbl, catalysis is initiated by abstraction of a H atom from a non-activated substrate carbon having only hydrocarbon substituents. The group II (“base-on”) proteins, which include DDH⁵⁸, EAL⁵⁹, class II RNR⁶⁰, the periplasmic CNCbl-binding protein BtuF⁶¹, and the ATP:corrinoid adenosyltransferase⁶², bind the with the DMB moiety in place as the lower axial ligand. The AdoCbl-dependent group II enzymes initiate catalysis by abstracting H from a heteroatom (class II RNR) or from a carbon with heteroatom substituents (EAL, DDH, GDH).

1.5.1. Methionine synthase, the canonical base-off Cbl binding protein

In 1994, Drennan *et al* solved the crystal structure of the Cbl-binding domain of MS⁵¹ (PDB code 1BMT), providing the first structure of protein-bound Cbl and the canonical model of a base-off Cbl-binding enzyme (Fig. 1.8a). The structure of the Cbl-binding subunit is a Rossmann-like fold, which is the norm for base-off Cbl binding. One of the most important results of this study was the establishment of the structural role of the base-off Cbl binding sequence DxHxxG...Sxl...GG (Fig. 1.8b). This sequence is found in all base-off Cbl-binding enzymes. The DxH portion is involved in Co ligation, where

the Asp sidechain hydrogen bonds to the imidazole ring of the His ligand. The downstream Gly residue leaves a cavity in which the phosphate of the Cbl nucleotide can bind. The Ser residue of the Sxl portion hydrogen bonds to imidazole ring of DMB, and the two Gly residues at the end of the sequence pack against the DMB moiety.

1.5.2. Methylmalonyl-CoA mutase: a large-scale conformational change upon substrate binding

MCM catalyzes the interconversion of methylmalonyl-CoA and succinyl-CoA (Fig. 1.5a). From a structural perspective, MCM is one of the most thoroughly characterized AdoCbl enzymes. Two years after the publication of the structure of the Cbl-binding portion of MS, Mancina *et al* published the structure of MCM in complex with a substrate fragment and with AdoCbl⁵² (PDB code 1REQ; Fig. 1.9a). The Ado moiety was not modeled in this structure due to its poor electron density. As in MS, a His residue coordinates the Co of Cbl. Remarkably, homolysis of the C-Co bond of the enzyme-bound cofactor is accelerated by approximately a trillion-fold^{42,45}. Unlike MS, the His N-Co distance in MCM is somewhat long (2.5 Å) compared with the DMB N-Co distance in the crystal structure of free cofactor⁶³ (2.237 Å), which lead the authors to conclude that *trans* effects^{64,65} in the protein-bound cofactor were responsible for promoting C-Co bond homolysis when substrate is bound. Structural comparison reveals that the lower axial His ligand of MCM and the Asp sidechain that hydrogen bonds to it superimpose with the His/Asp couple in MS, and that relative to MS, the cofactor has elevated *B* factors and is slightly farther away from the Rossmann domain. Thus, it is not protein differences that give rise to variations in N-Co bond length, but rather cofactor disorder

that appears to be responsible. One source of cofactor disorder may be X-ray irradiation, which is also responsible for the loss of the Ado ligand⁶⁶ in this crystal structure. Regardless of the source of cofactor disorder, the long N-Co bond length reported for MCM is not likely to be catalytically relevant, since extended X-ray absorption fine structure (EXAFS) analysis⁶⁷ does not support the *trans* effects hypothesis in MCM.

The ~23 Å-long substrate fragment desulfo-CoA (coenzyme A without the terminal thiol group) is bound along the entire length of the TIM barrel axis, with the end that would contain the thiol located ~11 Å from the cobalt of the cofactor, near the C-terminal end of the barrel. This suggested that the true substrate binds with its methylmalonyl group positioned near the Ado moiety of AdoCbl. Indeed, when a combination of true substrate/product was observed in the structure of the AdoCbl-MCM complex⁶⁸ (PDB code 4REQ), proximity of the substrate/product to AdoH was confirmed, as well as the identification of several key residues that bind the true substrate. H244 interacts with the carbonyl of the thioester, consistent with the thought that partial protonation of the carbonyl oxygen of the migrating group may facilitate the reaction⁶⁹⁻⁷¹ (see Fig. 1.5a). Mutation of this residue results in a ~10³-fold reduction in k_{cat} .

The crystal structure of the substrate-free MCM-AdoCbl complex⁶⁸ (PDB code 3REQ; Fig. 1.9b) revealed a drastically different conformation of the enzyme. Remarkably, the TIM barrel is distended to the point of rupture. The carbonyl-amide backbone hydrogen bonds of the internal beta sheet cylinder are interrupted by a gap in the side of the barrel, leaving enough room for substrate to enter the TIM barrel. The overall *B* factor of 80 Å²

suggests that this structure is conformationally dynamic. Unlike crystals of the desulfo-CoA MCM complex, the spectrum of substrate-free crystals was consistent with the presence of Co(III), which is expected of an intact, six-coordinate AdoCbl species. Features of electron density consistent with an Ado group still bonded to Co allowed Mancina and Evans to model the intact cofactor in this structure. Contrary to the previous hypothesis concerning *trans* effects in the presence of substrate, there was no evidence for a shorter Co-N bond length in the substrate-free structure. As in the desulfo-CoA MCM complex, the *B* factors of the cofactor are high. Finally, Mancina and Evans published structures of two inhibitor-MCM complexes (PDB codes 6REQ, 7REQ)⁷². In the CoA MCM complex, the CoA is disordered and the enzyme adopts a conformation like that of the open-barrel, substrate-free MCM-AdoCbl structure.

One of the most interesting results of the structural work on MCM is the observation of a conformational change of Y89, a conserved residue of the Cbl-binding site. In the substrate-free structure, Y89 is located above the intact cofactor, with its aromatic ring roughly parallel to the adenine of Ado. In the substrate-bound structure⁶⁸ (PDB code 4REQ), the sidechain of Y89 occupies the former Ado site and hydrogen bonds to the substrate. This destroys the Ado binding site, and is thought to be a major factor contributing to the rate acceleration of C-Co bond homolysis in MCM. The significance of the hydrogen bond between the phenolic oxygen of Y89 and the substrate is reflected in kinetic studies of the Y89F mutant, which shows a 1000-fold reduction in k_{cat} ⁷³. Moreover, formation of Cob(II) in either the pre-steady state or in the steady state is not observed in the Y89F mutant⁷³, as it is with the wild-type protein.

The structural work on MCM, combined with biochemical studies, gives us a more complete picture of how an AdoCbl enzyme accelerates C-Co bond homolysis in the presence of substrate. The substrate free structure adopts a conformation which allows the substrate to enter the active site, causing closure of the TIM barrel. A change in the conformation of Y89, caused by substrate binding, destroys the Ado binding site and seems to play a key role in C-Co homolysis.

1.5.3. Diol and glycerol dehydratases: Base-on enzymes with a catalytic K⁺ ion in their active sites

Diol dehydratase (DDH) was first purified and characterized by Lee and Abeles, who found a monovalent cation requirement for activity⁷⁴. DDH and glycerol dehydratase (GDH) are similar but distinct enzymes that catalyze a 1,2 hydroxyl group shift followed by the elimination of water to give an aldehyde product⁷⁵ (Fig. 1.5e, f). The structure of DDH in complex with CNCbl and (*S*)-1,2-propanediol⁷⁶ (PDB code 1DIO), published in 1999 by Yasuoka and coworkers, highlighted several fascinating aspects of this enzyme. Most strikingly, Cbl is bound in the base-on conformation (Fig. 1.10a). The protein is a dimer of heterotrimers, ($\alpha\beta\gamma$)₂, which binds two equivalents of AdoCbl. Cbl is bound by the β subunit, with the upper face of the corrin ring projected into the substrate-binding TIM barrel (α subunit). The γ subunit is proposed to stabilize the heterotrimer. Like MCM, a long N-Co bond (2.5 Å) was observed for the structure of the DDH-CNCbl complex. The upper axial CN ligand was not modeled due to poor electron density, presumably caused by radiolytic damage.

The base-on configuration of DDH-bound Cbl requires a Cbl binding subunit that is different from the Rossmann-like domain that invariably binds Cbl in MS and the mutases (Fig. 1.10b). The β subunit of DDH consists of a central β -sheet with peripheral α -helices. The cofactor binds on the face of the β -sheet, flanked by two helices. The orientation of the cofactor with respect to the β -sheet does not resemble the arrangement of AdoCbl in the Rossmann domains of base-off enzymes.

The crystallographic data indicate the presence of a K^+ ion in the active site, located deep in the core of the TIM barrel (Fig. 1.10b). The K^+ ion is coordinated by the hydroxyl groups of the substrate, implying that it participates directly in catalysis⁷⁶, perhaps by lowering the energy barrier to a hypothetical oxycation radical transition state (Fig. 1.10c). The observation of a K^+ ion in the active site is consistent with Abeles' initial finding of a monovalent cation requirement for DDH⁷⁴. Interestingly, in the substrate-free DDH-CNCbl complex, two water molecules coordinate the K^+ ion, rather than the hydroxyl groups of 1,2-propanediol. A similar observation was made by Liao *et al* in their structural studies of substrate-bound vs. substrate-free GDH⁷⁷.

Structural comparison of the DDH-adeninylpentylcobalamin (APCbl; an AdoCbl analog) substrate complex⁵⁸ (PDB code 1EEX) with the substrate-free DDH-CNCbl complex⁷⁸ (PDB code 1IWB) reveals that the β subunit and the corrin macrocycle move away from the α subunit when substrate binds. Assuming that the Ado moiety is held in the same position as in the substrate-free structure, movement of the corrin macrocycle would lengthen the C-Co bond and cause its cleavage. This idea has been referred to as an

adenine-attracting effect; the affinity for the adenine moiety is so strong that when the Cbl-binding domain moves away as substrates bind, the Ado group is held in place and the C-Co bond cleaves.

For both MCM and DDH, conformational changes upon substrate binding suggest mechanisms by which the proteins can enhance the rate of C-Co bond homolysis. For MCM, substrate binding causes the dramatic closure of the $(\alpha/\beta)_8$ barrel and the movement of Tyr 89 into the Ado-binding site, displacing Ado from the upper axial position. In DDH, the enzyme binds both ends of the AdoCbl cofactor, and substrate binding causes the Ado moiety and the Cbl portion to pull away from each other. Interestingly, prior to crystallographic analyses of Cbl-dependent enzymes, mechanisms to explain the increased rates of C-Co bond homolysis of the enzyme-bound cofactor focused on fine-tuning of the nucleophilicity of the lower axial ligand to Co. Structural data has shifted the focus to “brute-force” mechanisms for C-Co bond homolysis rate enhancement.

1.5.4. Glutamate mutase: a theory of radical propagation

Glutamate mutase (GM) catalyzes the interconversion of (*S*)-glutamate and (2*S*,3*S*)-3-methylaspartate, facilitating the fermentation of glutamate to acetate, CO₂, and NH₃⁷⁹ (Fig. 1.5c). The enzyme is a heterotetramer, $\epsilon_2\sigma_2$, where ϵ is a large subunit and σ is a small subunit. Kratky and coworkers have determined structures of GM in complex with AdoCbl and substrate⁸⁰ (PDB code 1I9C; Fig. 1.11), CNCbl and a substrate mimic (PDB code 1CCW)⁵³, and MeCbl and a substrate mimic⁵³ (PDB code 1CB7). GM binds two

AdoCbl molecules, one in each Rossmann-like domain (σ subunit). Like all of the AdoCbl-dependent mutases, GM binds AdoCbl in the base-off conformation. EXAFS studies of GM do not indicate an unusually long N-Co bond⁶⁶, which is confirmed by the crystallographic bond length of 2.2 Å. The top face of the corrin macrocycle is presented at the C-terminal end of the substrate-binding TIM barrel (ϵ subunit). Arguably, the most important result from the crystallographic analysis of GM is the observation of two conformations of the Ado moiety of AdoCbl. The 1.9 Å resolution structure suggests a mixed conformation for Ado, with one population in the C2'-endo conformation, and the other in the C3'-endo conformation. The interconversion of these two conformations, termed “ribose pseudorotation,” is proposed to be the basis of radical propagation from Ado• to the substrate. In the C2'-endo conformation, C5' is positioned ~3.1 Å directly above the Co atom, whereas in the C3'-endo state, C5' is ~4.5 Å removed from the Co and positioned such that it can abstract an H atom from C4 of the substrate, as expected from mechanistic studies⁸¹.

In addition to the crystallographic structures, solution structures of the σ subunit are available⁸²⁻⁸⁵. The solution structures are generally similar to the X-ray structures, but indicate that the loop containing the coordinating His residue, as well as the helix that precedes this loop, are in a dynamic equilibrium between relatively structured and unstructured states when AdoCbl is not bound. These studies suggest that the protein locks onto AdoCbl and adopts a more rigid structure when the cofactor is bound.

1.5.5. Class II ribonucleotide reductase: a ten-stranded $\alpha\beta$ barrel

Class II RNR carries out a unique AdoCbl-dependent reduction of nucleoside triphosphates or diphosphates (Fig. 1.5h). The class II RNR from *L. Leichmannii*, for which a structure has been determined⁶⁰, acts on nucleoside triphosphates. A system capable of multiple turnovers requires dithiols or the physiological thioredoxin/thioredoxin reductase system^{13,86,87}. In addition to nucleoside triphosphate reduction, *L. leichmannii* class II RNR catalyzes the exchange of 5' hydrogens of AdoCbl with solvent, in the presence of effector but not substrate^{88,89}. A protein based, cysteine derived thiyl radical has been shown to be generated in a kinetically competent fashion^{40,41,86}, and several other cysteine residues were shown to play a role in delivering reducing equivalents to the active site⁸⁶. Formation of the thiyl radical is AdoCbl dependent. Whether or not formation of the thiyl radical is concerted with C-Co bond homolysis has been the subject of several investigations^{23,90}.

Electron paramagnetic resonance (EPR) studies demonstrated that class II RNR from *L. leichmannii* binds AdoCbl in the base-on configuration⁹¹. This was confirmed by the crystal structure of the class II RNR in complex with APCbl (PDB code 1LIL; Fig. 1.12)⁶⁰. The structure of the class II RNR is largely dissimilar to the known structures of other AdoCbl binding enzymes, including the base-on enzyme DDH. Based on the location of Cys 408, which gives rise to the catalytic thiyl radical, the active site is located in the middle of a 10-stranded $\alpha\beta$ barrel. Cbl is bound to an "AdoCbl binding region" above the barrel. A structure of the apoenzyme is also available⁶⁰, and comparison with the APCbl-bound structure reveals a clamping-down of the AdoCbl

binding region over the barrel when Cbl is bound. The solvent accessibility of the active site Cys residue in the APCbl-bound structure suggests that the AdoCbl binding region is not fully closed over the barrel, resulting in a ~ 10 Å separation between the active site Cys in the barrel and the Co atom of Cbl. EPR spectroscopy was used to show that the Co-Cys distance is 5.5-7.5 Å in the catalytically active enzyme-coenzyme complex⁴¹. The openness of the APCbl-RNR structure was attributed to lack of bound effector. Effector binding promotes C-Co bond homolysis^{92,93}, perhaps by causing a more complete movement of the AdoCbl binding region, which would also bring the cofactor and active site Cys residue into proximity. Since the adeninylpentyl moiety of APCbl was not interpretable, the details of how clamping-down of the AdoCbl binding region would effect C-Co bond homolysis are unknown at this time.

A striking feature of the class II RNR structure is that the global fold of the enzyme is an $(\alpha\beta)_{10}$ barrel, unlike any other AdoCbl enzyme of known structure. This structure is similar to those of the class I⁹⁴ and III⁹⁵ RNRs and suggests that, as a class of enzymes, the RNRs are more closely related to one another than the class II enzyme is to other AdoCbl enzymes.

1.5.6. Lysine 5,6-aminomutase

5,6-LAM is an AdoCbl⁹⁶⁻⁹⁹ and PLP dependent^{100,101} enzyme in the bacterial lysine fermentation pathway¹⁰². This enzyme catalyzes the interconversion of DL-lysine or of β -L-lysine to 2,5-diaminohexanoate or to 3,5-diaminohexanoate, respectively (Fig. 1.5i). 5,6-LAM is similar to 2,3-LAM in terms of its substrates and reaction, but 2,3-LAM is an

AdoMet radical enzyme. Frey and coworkers have overexpressed, purified and characterized recombinant 5,6-LAM from *C. sticklandii*^{54,103}. Interestingly, computational analyses suggest a role for PLP in stabilizing radical intermediates on the reaction pathway¹⁰³, though Danen and West demonstrated that the 1,2 amino shift occurs in the absence of any aromatic substituent in the simplest model, the aziridylcarbinyl radical¹⁰⁴. The crystal structure of 5,6-LAM (Fig. 1.13), a major contribution to this thesis, was determined in collaboration with the Frey laboratory and suggests a novel role for PLP. The structure will be discussed in further detail in chapter 4.

1.6. AdoMet radical enzymes

In this section, the well or moderately-well -characterized AdoMet radical enzymes are introduced. Only two X-ray structures for AdoMet radical enzymes are published, though spectroscopic studies have provided structural insight into the coordination environment of the 4Fe-4S clusters in these enzymes.

1.6.1. Lysine 2,3-aminomutase: reversible cleavage of AdoMet

2,3-LAM, another enzyme of the bacterial lysine fermentation pathway¹⁰², was purified by Barker and coworkers from *Clostridium subterminale* SB4²⁵. The enzyme catalyzes the interconversion of L-lysine and L- β -lysine (Fig. 1.6c). 2,3-LAM is a homohexamer, with each monomer containing 1 molecule of PLP¹⁰⁵, 1 molecule of AdoMet^{24,106-109}, and an oxygen labile 4Fe-4S cluster^{110,111}. Like all known AdoMet radical enzymes, 2,3-LAM has a conserved CxxxCxxC motif. Frey and coworkers have made major contributions to our understanding of 2,3-LAM, which is one of the best- characterized

AdoMet radical enzyme. As mentioned earlier in this chapter, ^3H transfer from substrate to AdoMet was demonstrated by Moss and Frey in 1987²⁴. Unlike many other AdoMet radical enzymes, AdoMet cleavage is reversible in the 2,3-LAM reaction¹⁰⁹, i.e. 2,3-LAM utilizes AdoMet as a true cofactor rather than as a substrate. Cleavage of AdoMet to Ado• and Met requires the 4Fe-4S cluster to be reduced to the +1 state, which itself requires the presence of AdoMet¹¹¹. AdoMet cleavage also requires the presence of substrate¹⁰⁸. Spectroscopic investigations have led to a hypothetical mechanism for reductive cleavage of AdoMet by the catalytic $[4\text{Fe-4S}]^{1+}$ cluster (Fig. 1.14), in which the AdoMet amino and carboxyl groups chelate a unique Fe of the cluster, and the AdoMet sulfur is a ligand to the unique Fe after cleavage^{106,109}.

Spectacular model chemistry¹¹² and spectroscopic¹¹³⁻¹¹⁶ investigations with substrate and with substrate analogs have allowed Frey and coworkers to propose a mechanism for 2,3-LAM, in which PLP forms a benzylic radical at the imine carbon, facilitating a 1,2 imine shift via an aziridylcarbinyl radical (Fig. 1.15). In the spectroscopic studies, EPR, electron spin-echo envelope modulation (ESEEM) spectroscopy, and rapid freeze quench techniques were used to identify a kinetically competent radical intermediate in the reaction of 2,3-LAM with substrate. The studies of 2,3-LAM have provided the basis for many of the mechanistic proposals for 5,6-LAM, which will be discussed further in chapter 4.

1.6.2. Pyruvate formate lyase activase: a model for AdoMet binding

PFL catalyzes the reversible conversion of pyruvate and CoA to acetyl CoA and formate, an essential step in anaerobic glucose fermentation. PFL requires an activating enzyme, first described by Knappe and coworkers¹¹⁷⁻¹¹⁹. PFL activase contains a protein-bound 4Fe-4S cluster^{120,121}, which is ligated by the CxxxCxxC motif, and is active in the 1+ oxidation state¹²². Cluster reduction is dependent on the flavodoxin/flavodoxin reductase/NADPH system¹²³. PFL activase abstracts an H atom from the α carbon of PFL at Gly 734 (Fig. 1.6d), which is incorporated into AdoH, a product of the reaction¹²⁴.

PFL activase has been a model system for studying AdoMet-Fe-S cluster interactions in AdoMet radical enzymes. Mössbauer studies by Huynh and Broderick revealed the presence of a unique Fe in the 4Fe-4S cluster¹²⁵, and electron nuclear double resonance (ENDOR) studies by Broderick and Hoffman demonstrated chelation of AdoMet to the unique Fe of the cluster via the amino acid moiety¹²⁶. In these ENDOR studies, the AdoMet was labeled at the carboxyl group with ¹⁷O and ¹³C, and at the amino group with ¹⁵N. The model derived from these studies is shown in Fig. 1.14b. Although details of the sulfonium interaction with the cluster remain to be established, this model appears to represent the general mode of AdoMet binding in this superfamily, and has withstood the test of additional spectroscopic studies on other AdoMet radical enzymes, and two crystal structure determinations.

1.6.3. Class III ribonucleotide reductase activase: reductive cleavage of AdoMet

Class III RNR from *E. coli* is responsible for deoxyribonucleotide biosynthesis under anaerobic conditions. It was first described by Fontecave *et al*¹²⁷, and like PFL, it is a glyceryl radical enzyme. The reductase is activated by H atom abstraction (Fig. 1.6d) under anaerobic conditions by an activase, generally called β , which is dependent on one equivalent of AdoMet¹²⁸⁻¹³⁰ and contains a 4Fe-4S cluster ligated by a CxxxCxxC motif^{131,132}. EPR investigations on dithionite-reduced activase by Fontecave and coworkers showed that the [4Fe-4S]¹⁺ cluster reduces AdoMet to produce AdoH and Met^{129,130}. Flavodoxin/flavodoxin reductase/NADPH is thought to be the physiological reducing system for the 4Fe-4S cluster and is competent for glyceryl radical formation *in vitro*¹³³. These experiments on the class III RNR were crucial in establishing the role of the essential 4Fe-4S cluster in the AdoMet radical enzymes. Interestingly, Fontecave and coworkers propose that reduction of the cluster by flavodoxin is thermodynamically coupled to formation of AdoH and the glyceryl radical on the target protein¹³³. A crystal structure of the activase alone, and in complex with flavodoxin and the reductase, would be invaluable for learning more about the mechanism by which this thermodynamic coupling is achieved.

1.6.4. Biotin and lipoyl synthases: sulfur insertion enzymes

BioB catalyzes the final step in the biotin (vitamin B₈) biosynthetic pathway (Fig. 1.4), the conversion of dethiobiotin to biotin^{134,135} (Fig. 1.6a). BioB contains one 4Fe-4S cluster and one 2Fe-2S cluster¹³⁶. The 4Fe-4S cluster, which is responsible for radical

generation, is ligated by AdoMet and by the three cysteines of the CxxxCxxC motif, which is common to all AdoMet radical enzymes¹³⁷⁻¹³⁹. The 2Fe-2S cluster is ligated by three Cys residues and one Arg residue¹³⁷, and has been proposed to be the S donor in the reaction^{137,140-143}, but this is a subject of dispute^{144,145}. BioB is not known for its catalytic prowess: the *E. coli* enzyme catalyzes only one turnover at a rate of minutes to hours. The only report of multiple turnovers is for BioB from *Arabidopsis*, which catalyzes >2 turnovers per hour¹⁴⁶. The crystal structure of BioB¹³⁷ (PDB code 1R30, Fig. 1.16) is a major contribution to this thesis. The structure of BioB and the remarkable reaction this enzyme performs will be discussed in further detail in chapter 3.

The lipoyl group is an essential cofactor in several important enzymes¹⁴⁷, including the pyruvate dehydrogenase complex. Lipoyl synthase (LipA) catalyzes the conversion of octanoylated proteins to lipoylated proteins¹⁴⁸⁻¹⁵⁰ (Fig. 1.6b). In many respects, LipA is similar to BioB. Like BioB, LipA catalyzes the formation of C-S bonds at nonactivated carbon positions and contains two Fe-S clusters per polypeptide (one of which is a 4Fe-4S cluster that is, presumably, ligated by the protein's CxxxCxxC motif and by AdoMet). Also like BioB (according to Marquet's report¹⁴²), LipA consumes two equivalents of AdoMet per product. Despite the similarities of their reactions, some important differences between LipA and BioB do exist. Whereas BioB produces one equivalent of product per monomer, two equivalents of LipA are required to produce one lipoyl product, and the sulfur insertion reaction proceeds with inversion of configuration^{149,151}, in contrast to the retention of configuration in BioB¹⁵². As the biochemical and biophysical characterization of BioB and LipA continue, it will be fascinating to compare

and contrast how these two enzymes use different types of Fe-S clusters to catalyze similar reactions.

1.6.5. Coproporphyrinogen III oxidase: a new fold for an Ado• enzyme

Coproporphyrinogen III oxidase (HemN) oxidatively decarboxylates propionate side chains of coproporphyrinogen III to vinyl groups¹⁵³⁻¹⁵⁶, an essential step in heme and chlorophyll biosynthesis under certain growth conditions (Fig. 1.6f). The enzyme was overexpressed and purified from *E. coli*¹⁵⁶ and is known to contain a 4Fe-4S cluster, ligated by the three Cys residues of the CxxxCxxC motif, and by AdoMet at a unique Fe of the cluster^{156,157}. Surprisingly, the crystal structure of HemN¹⁵⁷ revealed not one, but two AdoMet molecules bound to the enzyme (PDB code 1OLT; Fig. 1.17). Both of these AdoMet sites were interpreted as physiologically relevant, but structural comparison with BioB suggests that the second AdoMet molecule may be occupying the substrate-binding site (discussed in chapter 5). Interestingly, the fold of HemN is not the same as that of BioB, but the interactions of the 4Fe-4S cluster with AdoMet are almost identical between the two enzymes (discussed in chapter 5).

1.7. Summary

AdoCbl- and AdoMet- dependent radical enzymes catalyze difficult reactions via radical-based mechanisms. Both families of enzymes must prevent aberrant free-radical reactions while still maintaining proper reactivity for catalysis. Ado● is implicated in the reactions of both enzyme families. The AdoMet radical enzymes require a catalytic [4Fe-4S]¹⁺ cluster in order to produce Ado●, and reduction of the cluster to the 1+ oxidation state requires a physiological reducing system, whereas AdoCbl-dependent enzymes require homolytic cleave of the C-Co bond to produce Ado●. Several AdoCbl radical enzymes have AdoMet radical enzyme analogs, such as the class II and class III RNRs and 5,6-LAM/2,3-LAM.

This thesis addresses key questions in the field of Ado● enzymes, such as: What is the structural basis for AdoMet binding by the AdoMet radical enzymes? What, if any, structural relationship exists between the AdoMet radical enzymes and the AdoCbl radical enzymes? How do Ado● enzymes prevent radical propagation in the absence of substrate or effector? Chapters 2 and 3 describe the crystallization, structure determination, and structure analysis of the AdoMet radical enzyme BioB. Chapter 4 describes the crystallization, structure determination, and structure analysis of the AdoCbl radical enzyme 5,6-LAM. Chapter 5 provides a few final thoughts on the relationship between these two superamilies of Ado● radical-producing enzymes.

1.8. Figures

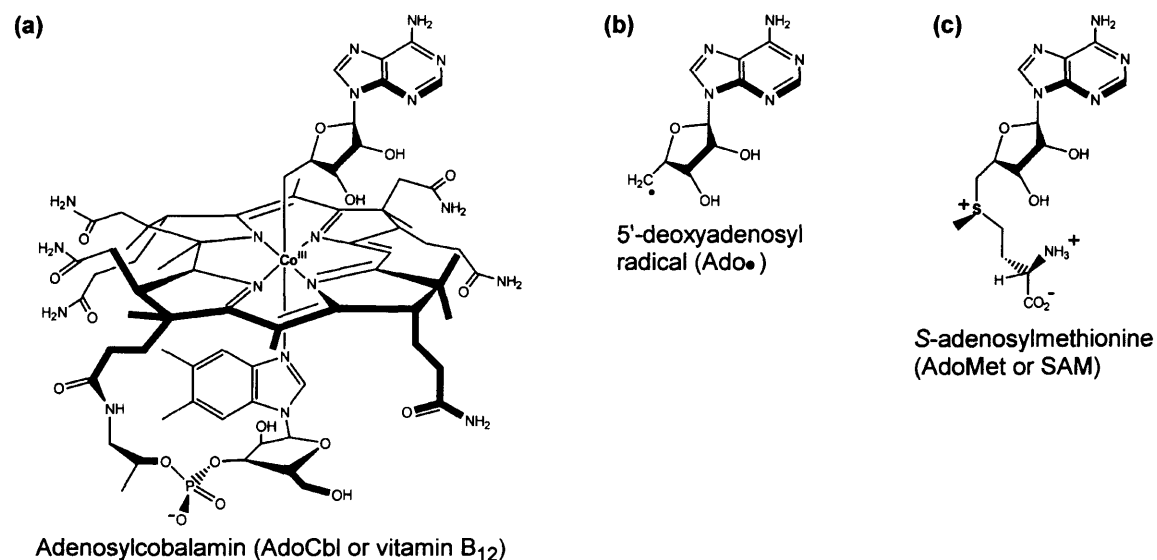


Figure 1.1. Molecular structures of (a) AdoCbl, (b) Ado•, and (c) AdoMet.

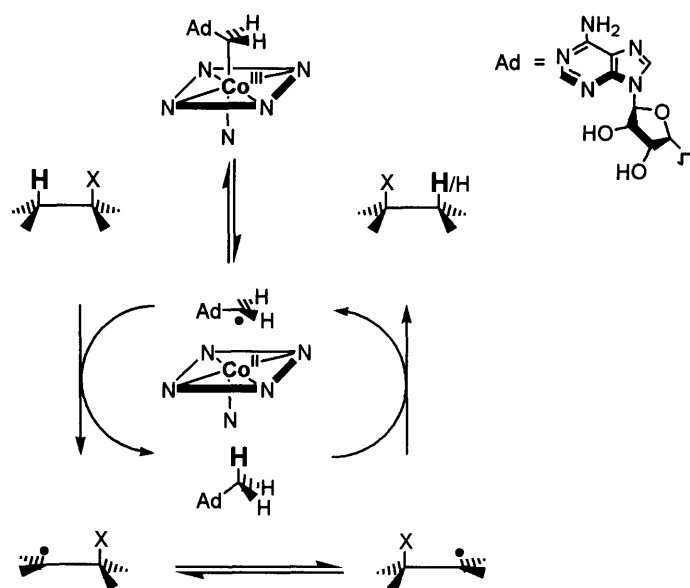


Figure 1.2. Simplified catalytic cycle of AdoCbl-dependent mutases. Carbon-cobalt bond homolysis leads to the formation of Ado• and Cob(II). Ado• abstracts a hydrogen atom from the substrate, initiating the 1,2 shift, which is simplified in this scheme. The product-derived radical abstracts an H atom from AdoH, reforming the Ado•/Cob(II) couple, which recombine to regenerate the intact cofactor. The stereochemical course of the reaction differs from enzyme to enzyme. Adapted from reference¹⁵⁸.

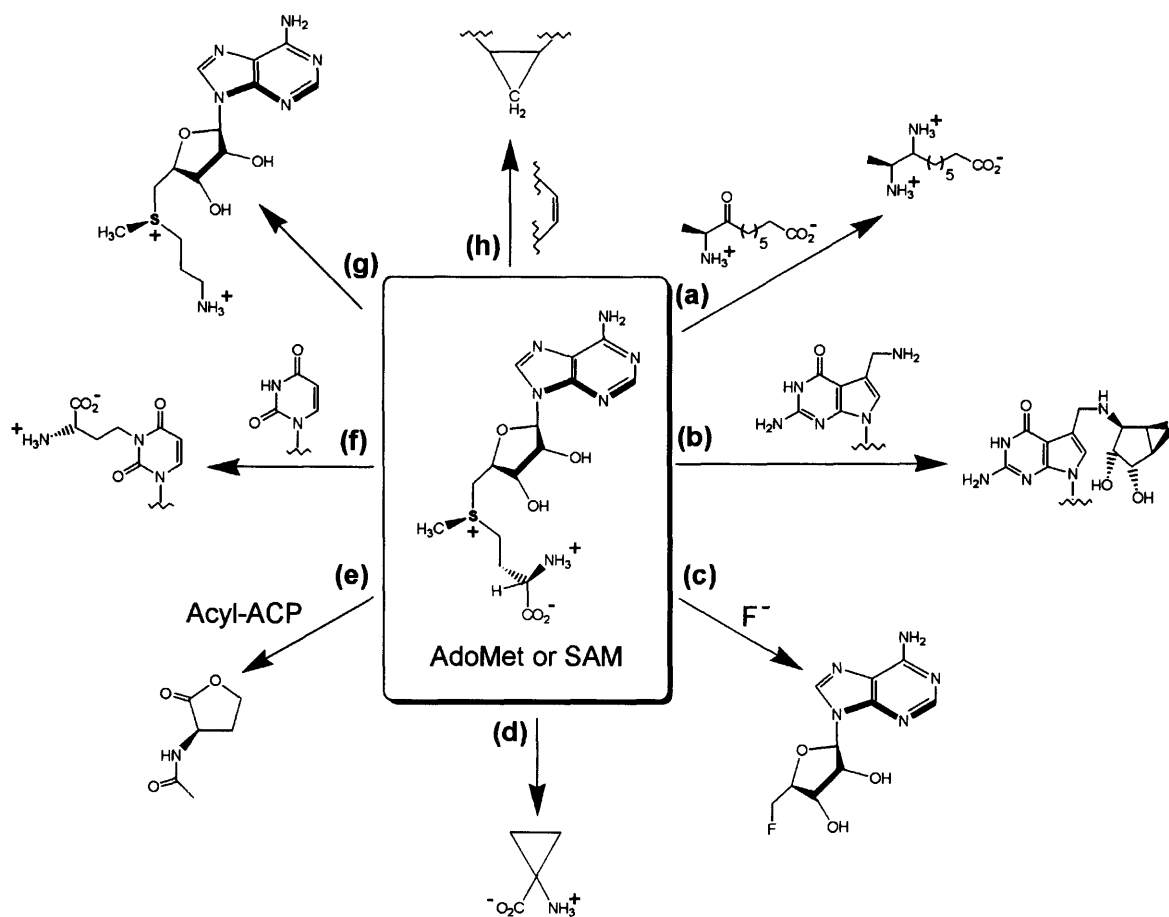


Figure 1.3. Selected AdoMet-dependent enzymatic reactions. The enzymes that carry out these reactions are: **(a)** DAPA synthase²⁶ (see also Fig. 1.4); **(b)** SAM-tRNA ribosyltransferase-isomerase¹⁵⁹; **(c)** 5'-deoxyfluoroadenosine synthase¹⁶⁰; **(d)** 1-aminocyclopropane-1-carboxylate synthase¹⁶¹; **(e)** acylhomoserine lactone synthase¹⁶² (ACP = acyl carrier protein); **(f)** 3-(3-amino-3-carboxypropyl) uridine synthase¹⁶³; **(g)** SAM decarboxylase¹⁶⁴; **(h)** Cyclopropane fatty acid synthase¹⁶⁵. Adapted from reference¹⁶⁶.

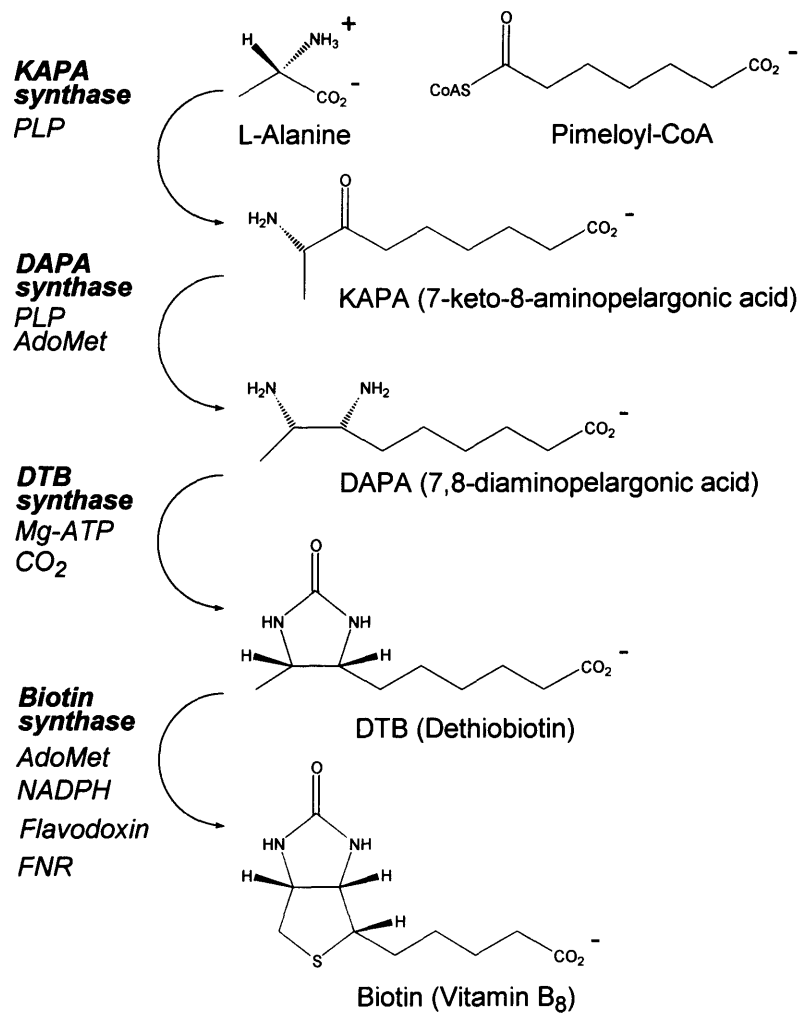
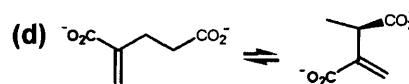
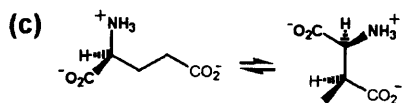
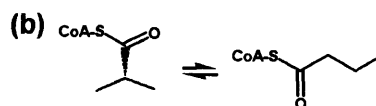
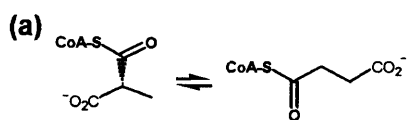
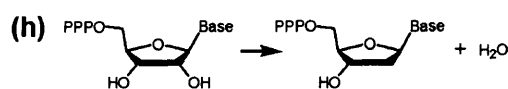
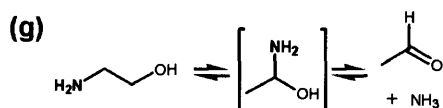
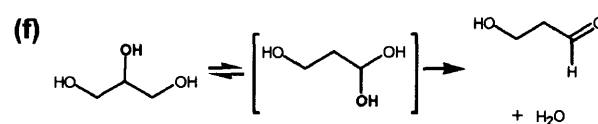
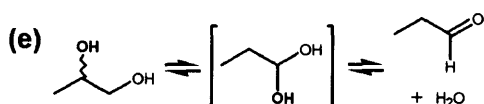


Figure 1.4. The biotin biosynthetic pathway. Enzymes in the pathway are in bold typeface. Cofactors, co-substrates, and other enzymes involved in pathway reactions (flavodoxin, flavodoxin-NADPH oxidoreductase [FNR]) are listed in italics.

Class I: Carbon skeleton mutases



Class II: Eliminases



Class III: Aminomutases

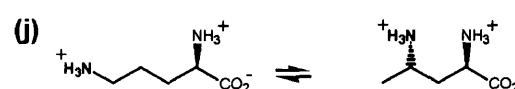
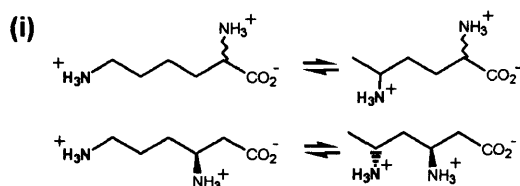
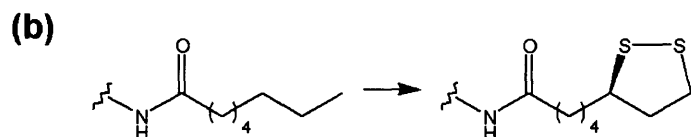
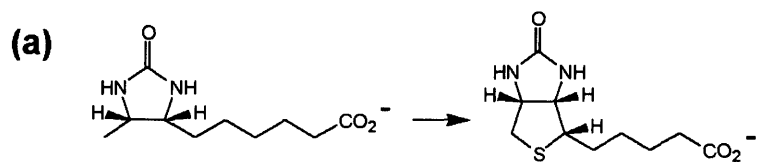
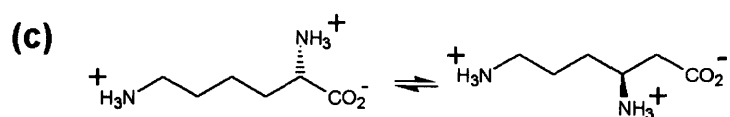


Figure 1.5. The AdoCbl-dependent enzymatic reactions. Reactions are sorted into general classes according to Buckel and Golding²². The reactions are catalyzed by: (a) MCM; (b) ICM; (c) GM; (d) MGM; (e) DDH; (f) GDH; (g) EAL; (h) class II RNR; (i) 5,6-LAM; (j) OAM. See text for references.

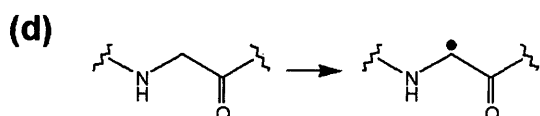
Sulfur insertase



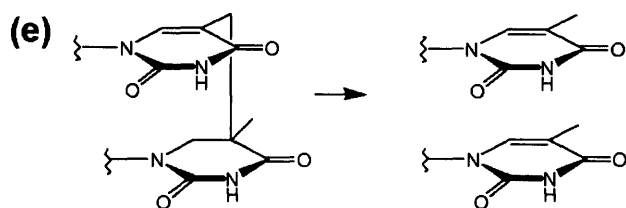
Mutase



Activase



Lyase



Oxidoreductase

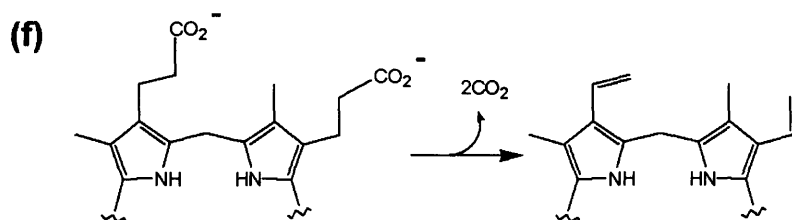


Figure 1.6. Several moderately or well-characterized AdoMet radical enzyme reactions, sorted into categories. The reactions are those of (a) BioB; (b) LipA; (c) 2,3-LAM; (d) the activases of class III RNR and PFL; (e) SPL; (f) HemN. See text for references.

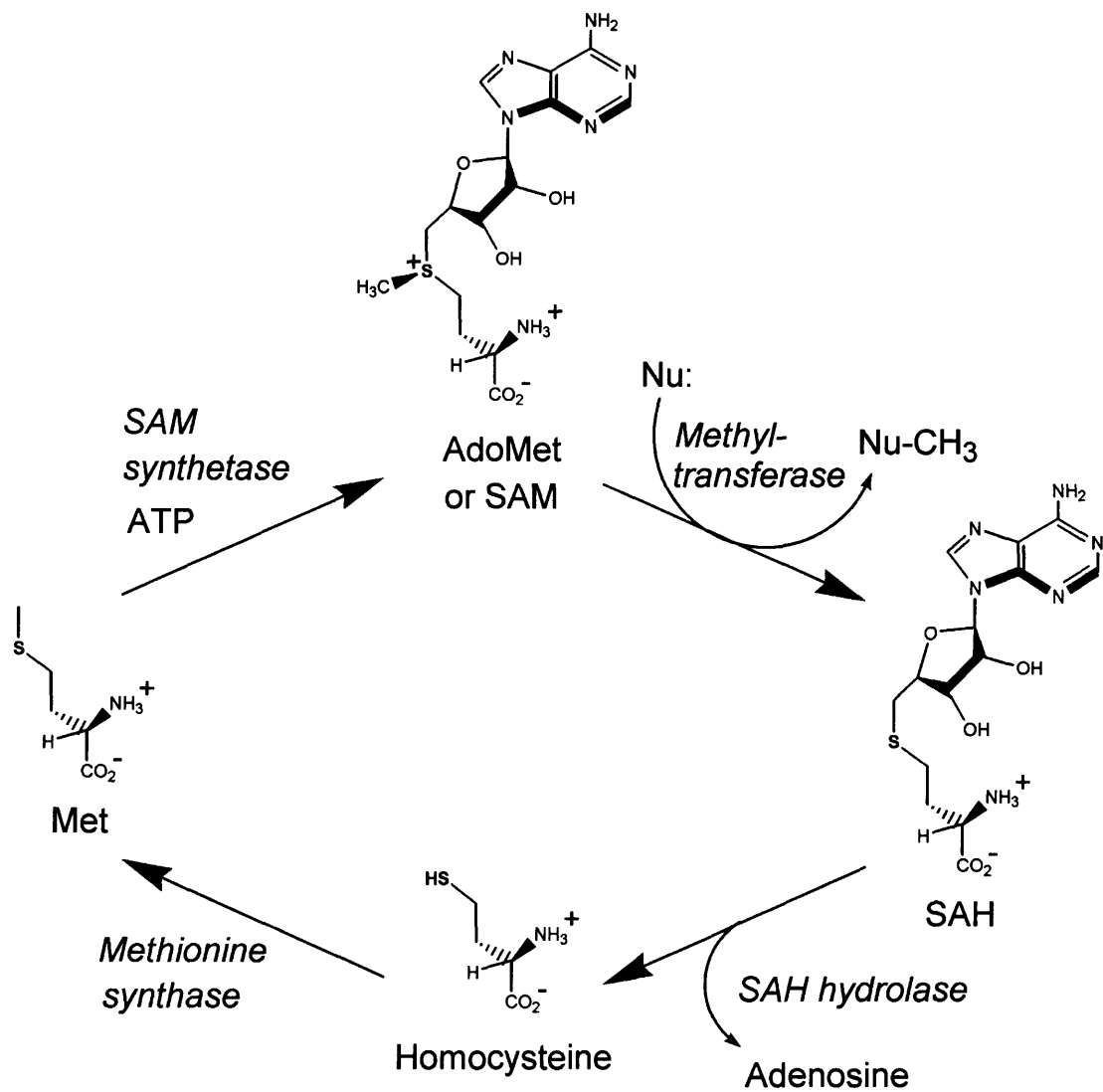


Figure 1.7. The AdoMet cycle. Enzymes involved in recycling AdoMet are shown in italics. The reaction most often associated with AdoMet, methylation of a nucleophile with production of *S*-adenosylhomocysteine (SAH), is shown as part of the cycle. Adapted from reference¹⁶⁶.

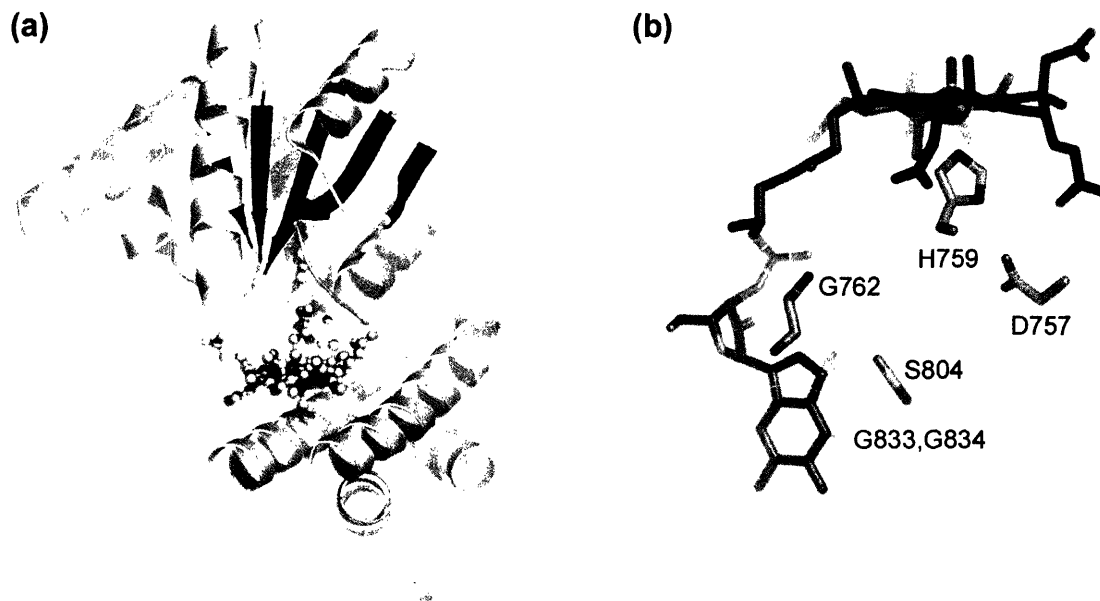


Figure 1.8. Crystal structure of the MeCbl-binding domain of MS⁵¹. **(a)** Ribbon representation of the MeCbl-binding Rossmann domain. β -strands are colored dark blue and MeCbl is shown in a ball-and-sphere representation in pink. This coloring scheme is used in all ribbon diagrams in this chapter. **(b)** Details of the base-off binding of MeCbl to MS, showing the conserved residues of the DxHxxG...SxI...GG sequence characteristic of all base-off binding enzymes (see text). The coloring scheme for this and all other Figures is: C, gray; O, red; N, blue; P, green. The carbon atoms of MeCbl are shown in black. All structural Figures were made with PyMol¹⁶⁷.

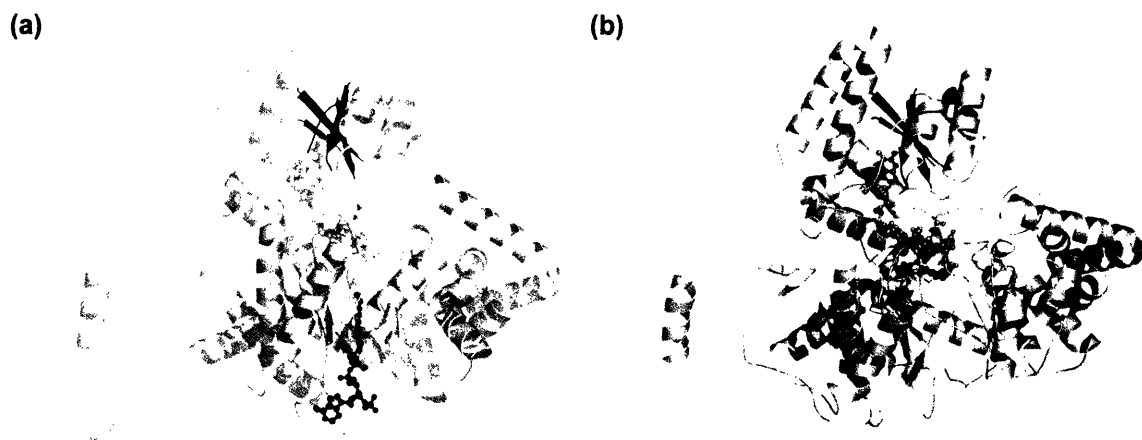


Figure 1.9. Crystal structure of MCM. **(a)** The MCM-Cbl-desulfo-CoA complex⁵². Desulfo-CoA is shown in a ball-and-stick representation in black. The substrate-binding TIM barrel is shown in green. **(b)** The substrate-free MCM-AdoCbl complex⁶⁸. The adenosyl group is colored in red. In this structure, the TIM barrel is spliced open relative to the MCM-Cbl-desulfo-CoA complex.

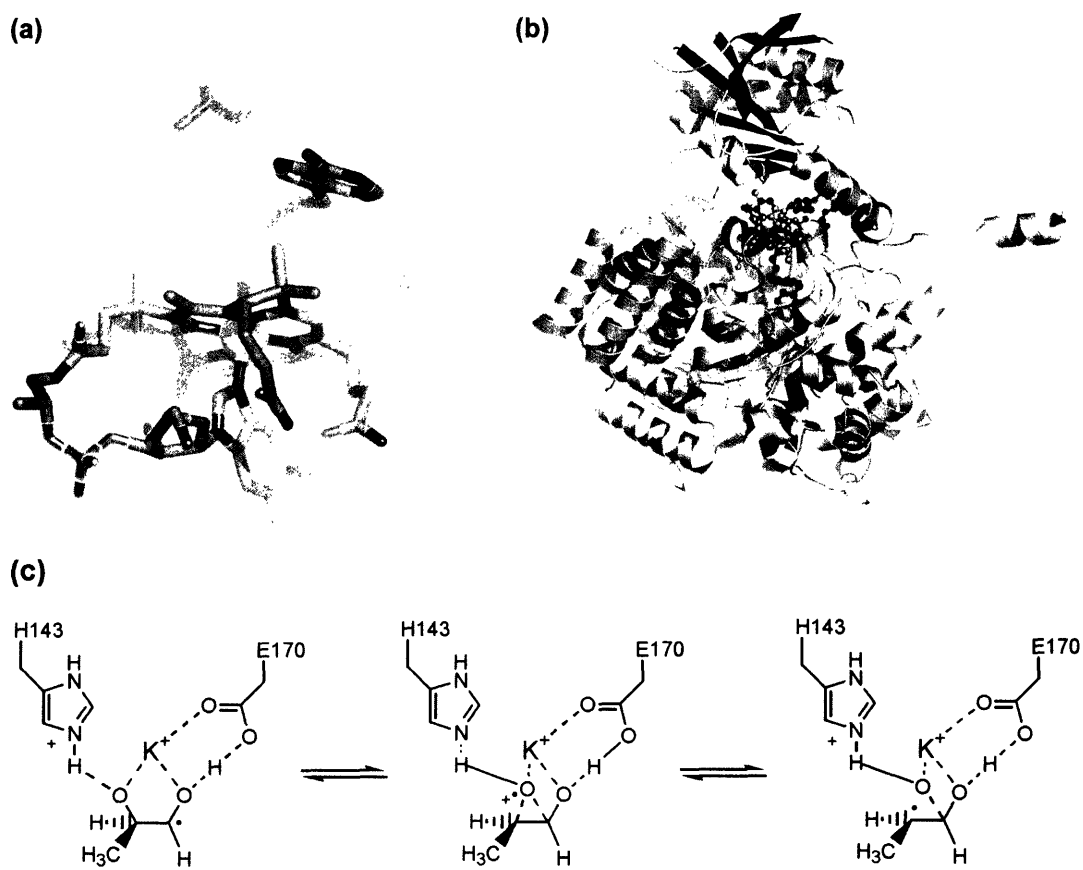


Figure 1.10. Crystal structure of DDH⁷⁶. **(a)** Close-up view of APCbl, the substrate (1,2 propanediol), and a potassium ion (orange sphere) in the active site. **(b)** Ribbon diagram of DDH showing the substrate-binding TIM barrel in green and the AdoCbl-binding subunit in light blue, with the central β -sheet in dark blue. The adeninylpentyl moiety of APCbl is shown in red, Cbl in pink, the substrate in dark grey, and the potassium ion is shown as an orange sphere. **(c)** A hypothetical mechanism for the 1,2 shift in DDH, wherein the K^+ ion is directly involved in catalysis (adapted from reference¹⁵⁸).



Figure 1.11. Crystal structure of GM in complex with substrate and AdoCbl⁸⁰. Only the C2'-endo conformation of Ado (red) is shown. Gruber *et al* modeled a mixture of substrate (L-glutamate, shown here in black) and product ([2*S*,3*S*]-3-methylaspartate, not shown) into the active site. The TIM barrel is shown in green.



Figure 1.12. Crystal structure of class II RNR⁶⁰. The AdoCbl-binding region is shown in blue, with the central β -hairpin highlighted in dark blue. APCbl is bound in the base-on configuration and shown in pink. The adeninylpentyl moiety is disordered and is not shown in this Figure.



Figure 1.13. Crystal structure of the substrate-free AdoCbl-PLP-5,6-LAM complex, a major contribution to this thesis (discussed in chapter 4). The protein is an $\alpha_2\beta_2$ tetramer; only the $\alpha\beta$ unit is shown. The AdoCbl binding Rossmann domain is colored in blue, with the central β -sheet highlighted in dark blue, and the remainder of the protein is colored green. Cbl is colored pink, AdoH is colored red, and PLP is colored black. 5,6-LAM is unusual when compared to other AdoCbl-dependent mutases in that AdoCbl does not bind directly atop the center of the TIM barrel.

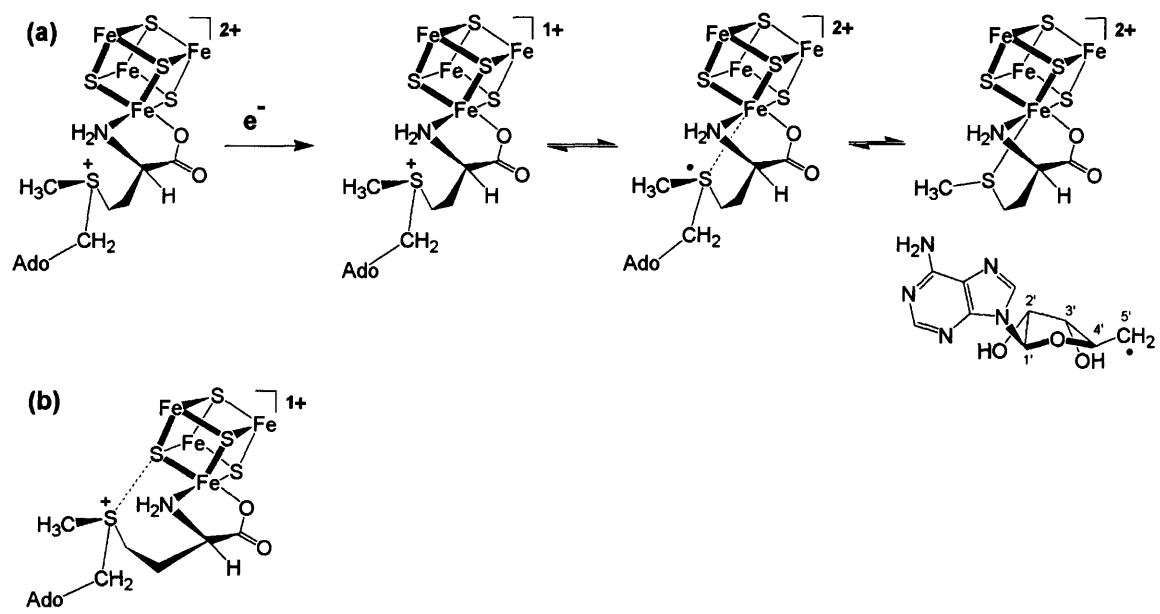


Figure. 1.14. Radical generation by the 4Fe-4S cluster and AdoMet in the AdoMet radical enzymes. **(a)** A model for radical generation, based on Frey and coworkers' spectroscopic studies of 2,3-LAM^{106,109}. **(b)** A model of AdoMet interacting with the reduced 4Fe-4S cluster of PFL activase, from Broderick and coworkers' pioneering ENDOR experiments^{125,126}.

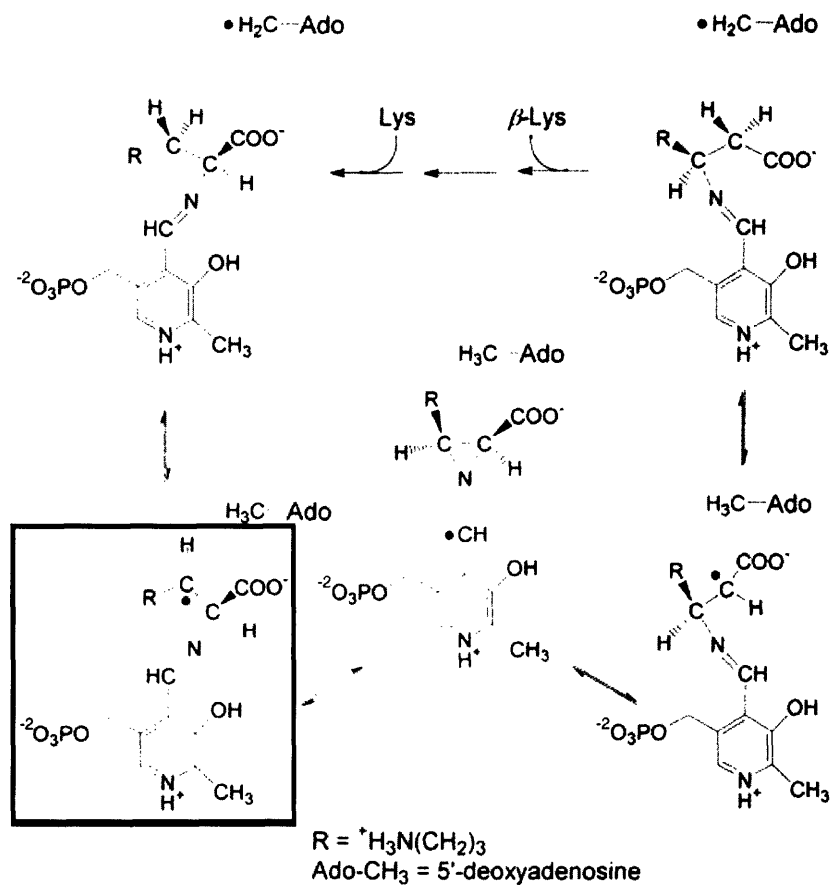


Figure 1.15. Mechanism proposed by Frey and coworkers for the 2,3-LAM reaction, modified from reference¹⁶⁸. The boxed intermediate has been observed by EPR and ESEEM spectroscopy and is kinetically competent¹¹³⁻¹¹⁶.



Figure 1.16. Crystal structure of BioB¹³⁷. Only one subunit of the BioB homodimer is shown. The structure is a major contribution to this thesis. Fe-S clusters are shown as spheres (Fe, brown; S, yellow), AdoMet (red) and substrate (DTB, black) are shown in ball-and-stick representations. The central β -sheet of the TIM barrel is highlighted in dark blue.



Figure 1.17. Crystal structure of HemN¹⁵⁷. The 4Fe-4S cluster is shown as spheres (Fe, brown; S, yellow). Two AdoMet molecules were observed in the structure; the one that chelates a unique Fe of the cluster is shown in red and the second molecule is shown in black. β -strands are colored dark blue.

1.9. References

1. Chanarin, I. Historical review: a history of pernicious anaemia. *Br. J. Haematol.* **111**, 407-415 (2000).
2. Minot, G.R. & Murphy, W.P. Treatment of pernicious anemia by special diet. *J. Am. Med. Assoc.* **14**, 470-476 (1926).
3. Rickes, E.L., Brink, N.G., Koniuszky, F.R., Wood, T.R. & Folkers, K. Crystalline Vitamin B₁₂. *Science* **107**, 396-397 (1948).
4. Lester-Smith, E. Purification of the anti-pernicious anaemia factor from liver. *Nature* **161**, 638-639 (1948).
5. Ledley, F.D. & Rosenblatt, D.S. Mutations in mut methylmalonic acidemia: clinical and enzymatic correlations. *Hum. Mutat.* **9**, 1-6 (1997).
6. Rosenblatt, D.S. & Fenton, W.A. in *The metabolic and molecular bases of inherited disease*. (eds. Scriver, C.R., Beaudet, A.L., Valle, D. & Sly, W.S.) 3897-3933 (McGraw-Hill, New York, 2001).
7. Barker, H.A., Weissbach, H. & Smyth, R.D. A coenzyme containing pseudovitamin B₁₂. *Proc. Natl. Acad. Sci.* **44**, 1093-1097 (1958).
8. Stadtman, E.R., Overath, P., Eggerer, H. & Lynen, F. The role of biotin and vitamin B₁₂ coenzyme in propionate metabolism. *Biochem. Biophys. Res. Commun.* **2**, 1-7 (1960).
9. Eggerer, H., Overath, P., Lynen, F. & Stadtman, E.R. On the mechanism of the cobamide coenzyme dependent isomerization of methylmalonyl CoA to succinyl CoA. *J. Am. Chem. Soc.* **82**, 2643-2644 (1960).
10. Hodgkin, D.C. et al. Structure of Vitamin B₁₂. *Nature* **178**, 64-66 (1956).
11. Lenhert, P.G. & Hodgkin, D.C. Structure of the 5,6-dimethylbenzimidazolylcobamide coenzyme. *Nature* **192**, 937-938 (1961).
12. Frey, P.A. & Abeles, R.H. The Role of the B₁₂ Coenzyme in the Conversion of 1,2-Propanediol to Propionaldehyde. *J. Biol. Chem.* **241**, 2732-2733 (1966).
13. Orme-Johnson, W.H., Beinert, H. & Blakley, R.L. Cobamides and ribonucleotide reduction. XII. The electron paramagnetic resonance spectrum of "active coenzyme B₁₂." *J. Biol. Chem.* **249**, 2338-2343 (1974).
14. Babior, B.M., Moss, T.H., Orme-Johnson, W.H. & Beinert, H. The mechanism of action of ethanolamine ammonia-lyase, a B-12-dependent enzyme. The participation of paramagnetic species in the catalytic deamination of 2-aminopropanol. *J. Biol. Chem.* **249**, 4537-4544 (1974).
15. Babior, B.M., Moss, T.H. & Gould, D.C. The mechanism of action of ethanolamine ammonia lyase, a B₁₂-dependent enzyme. A study of the reaction by electron spin resonance spectrometry. *J. Biol. Chem.* **247**, 4389-4392 (1972).
16. Banerjee, R. Radical peregrinations catalyzed by coenzyme B12-dependent enzymes. *Biochemistry* **40**, 6191-6198 (2001).
17. Banerjee, R. Radical carbon skeleton rearrangements: catalysis by coenzyme B12-dependent mutases. *Chem. Rev.* **103**, 2083-2094 (2003).
18. Banerjee, R. & Ragsdale, S.W. The many faces of vitamin B12: catalysis by cobalamin-dependent enzymes. *Annu. Rev. Biochem.* **72**, 209-247 (2003).
19. Frey, P.A. Radical Mechanisms of Enzymatic Catalysis. *Annu. Rev. Biochem.* **70**, 121-148 (2001).

20. Frey, P.A. & Reed, G.H. Radical Mechanisms in Adenosylmethionine- and Adenosylcobalamin-Dependent Enzymatic Reactions. *Arch. Biochem. Biophys.* **382**, 6-14 (2000).
21. Toraya, T. Enzymatic radical catalysis: coenzyme B₁₂-dependent diol dehydratase. *Chem. Rec.* **2**, 352-366 (2002).
22. Buckel, W. & Golding, B.T. Glutamate and 2-methyleneglutarate mutase: from microbial curiosities to paradigms for coenzyme B₁₂-dependent enzymes. *Chem. Soc. Rev.* **25**, 329-337 (1996).
23. Stubbe, J., Licht, S., Gerfen, G.J., Silva, D. & Booker, S.J. Adenosylcobalamin-dependent ribonucleotide reductases: still amazing but no longer confusing. in *Vitamin B₁₂ and B₁₂-proteins* (eds. Krautler, B., Arigoni, D. & Golding, B.T.) 321-331 (Wiley-VCH, Weinheim, 1998).
24. Moss, M. & Frey, P.A. The role of S-adenosylmethionine in the lysine 2,3-aminomutase reaction. *J. Biol. Chem.* **262**, 14859-14862 (1987).
25. Chirpich, T.P., Zappia, V., Costilow, R.N. & Barker, H.A. Lysine 2,3-aminomutase. Purification and properties of a pyridoxal phosphate and S-adenosylmethionine-activated enzyme. *J. Biol. Chem.* **245**, 1778-1789 (1970).
26. Stoner, G.L. & Eisenberg, M.A. Biosynthesis of 7, 8-diaminopelargonic acid from 7-keto-8-aminopelargonic acid and S-adenosyl-L-methionine. The kinetics of the reaction. *J. Biol. Chem.* **250**, 4037-4043 (1975).
27. Zhang, S., Sanyal, I., Bulboaca, G.H. & Rich, A. The gene for biotin synthase from *Saccharomyces cerevisiae*: cloning, sequencing, and complementation of *Escherichia coli* strains lacking biotin synthase. *Arch. Biochem. Biophys.* **309**, 29-35 (1994).
28. Baldet, P., Gerbling, H., Axiotis, S. & Douce, R. Biotin biosynthesis in higher plant cells. Identification of intermediates. *Eur. J. Biochem.* **217**, 479-485 (1993).
29. Sanyal, I., Cohen, G. & Flint, D.H. Biotin synthase: purification, characterization as a [2Fe-2S]cluster protein, and in vitro activity of the *Escherichia coli bioB* gene product. *Biochemistry* **33**(1994).
30. Escalletes, F., Florentin, D., Tse Sum Bui, B., Lesage, D. & Marquet, A. Biotin Synthase Mechanism: Evidence for Hydrogen Transfer from the Substrate into Deoxyadenosine. *J. Am. Chem. Soc.* **121**, 3571-3578 (1999).
31. Sofia, H.J., Chen, G., Hetzler, B.G., Reyes-Spindola, J.F. & Miller, N.E. Radical SAM, a novel protein superfamily linking unresolved steps in familiar biosynthetic pathways with radical mechanisms: functional characterization using new analysis and information visualization methods. *Nucleic Acids Res.* **29**, 1097-1106 (2001).
32. Beinert, H., Holm, R.H. & Munck, E. Iron-sulfur clusters: nature's modular, multipurpose structures. *Science* **277**, 653-659 (1997).
33. Huber, C. & Wachtershrauer, G. Activated acetic acid by carbon fixation on (Fe,Ni)S under primordial conditions. *Science* **276**, 245-247 (1997).
34. Huber, C. & Wachtershrauer, G. Peptides by activation of amino acids with CO on (Ni,Fe)S surfaces: implications for the origin of life. *Science* **281**, 670-672 (1998).
35. Scott, A.I. & Roessner, C.A. Biosynthesis of cobalamin (vitamin B₁₂). *Biochem. Soc. Trans.* **4**, 613-620 (2002).

36. Torrents, E., Aloy, P., Gibert, I. & Rodriguez-Trelles, F. Ribonucleotide Reductases: Divergent Evolution of an Ancient Enzyme. *J. Mol. Evol.* **55**, 138-152 (2002).
37. Reichard, P. The evolution of ribonucleotide reduction. *Trends Biochem. Sci.* **22**, 81-85 (1997).
38. Eschenmoser, A. Vitamin B₁₂: Experiments concerning the origin of its molecular structure. *Angew. Chem. Int. Ed.* **27**, 5-39 (1988).
39. Hesse, H. & Hoefgen, R. Molecular aspects of methionine biosynthesis. *Trends Plant. Sci.* **6**, 259-262 (2003).
40. Licht, S., Gerfen, G.J. & Stubbe, J. Thiyl Radicals in Ribonucleotide Reductases. *Science* **271**, 477-481 (1996).
41. Gerfen, G.J., Licht, S., Willems, J.-P., Hoffman, B.M. & Stubbe, J. electron paramagnetic resonance investigations of a kinetically competent intermediate formed in ribonucleotide reduction: evidence for a thiyl radical-Cob(II)alamin interaction. *J. Am. Chem. Soc.* **118**, 8192-8197 (1996).
42. Licht, S.S., Lawrence, C.C. & Stubbe, J. Thermodynamic and kinetic studies on carbon-cobalt bond homolysis by ribonucleoside triphosphate reductase: the importance of entropy in catalysis. *Biochemistry* **38**, 1234 (1999).
43. Brown, K.L. & Li, J. Activation parameters for the carbon-cobalt bond homolysis of coenzyme B₁₂ induced by the B₁₂-dependent ribonucleotide reductase from *Lactobacillus leichmannii*. *J. Am. Chem. Soc.* **120**, 9466-9474 (1998).
44. Cantoni, G.L. Methylation of nicotinamide with soluble enzyme system from rat liver. *J. Biol. Chem.* **189**, 203-216 (1951).
45. Chowdhury, S. & Banerjee, R. Thermodynamic and kinetic characterization of Co-C bond homolysis catalyzed by coenzyme B(12)-dependent methylmalonyl-CoA mutase. *Biochemistry* **39**, 7998-8006 (2000).
46. Marsh, E.N. & P., B.D. Coupling of cobalt-carbon bond homolysis and hydrogen atom abstraction in adenosylcobalamin-dependent glutamate mutase. *Biochemistry* **37**, 11864-11872 (1998).
47. Murzin, A.G., Brenner, S.E., Hubbard, T. & Chothia, C. SCOP: a structural classification of proteins database for the investigation of sequences and structures. *J. Mol. Biol.* **247**, 536-540 (1995).
48. Nagano, N., Orengo, C.A. & Thornton, J.M. One fold with many functions: The evolutionary relationships between TIM barrel families based on their sequences, structures and functions. *J. Mol. Biol.* **321**, 741-765 (2002).
49. Copley, R.R. & Bork, P. Homology among (β α)₈ barrels: Implications for the evolution of metabolic pathways. *J. Mol. Biol.* **303**, 627-641 (2000).
50. Hennig, M. et al. A TIM barrel protein without enzymatic activity? Crystal-structure of narbonin at 1.8 Å resolution. *FEBS Lett.* **306**, 80-84 (1992).
51. Drennan, C.L., Huang, S., Drummond, J.T., Matthews, R.G. & Ludwig, M.L. How a protein binds B₁₂: A 3.0 Å X-ray structure of B₁₂-binding domains of methionine synthase. *Science* **266**, 1669-1674 (1994).
52. Mancina, F. et al. How coenzyme B₁₂ radicals are generated: the crystal structure of methylmalonyl-coenzyme A mutase at 2 Å resolution. *Structure* **4**, 339-350 (1996).

53. Reitzer, R. et al. Glutamate mutase from *Clostridium cochlearium*: the structure of a coenzyme B₁₂-dependent enzyme provides new mechanistic insights. *Structure Fold. Des.* **7**, 891-902 (1999).
54. Chang, C.H. & Frey, P.A. Cloning, sequencing, heterologous expression, purification, and characterization of adenosylcobalamin-dependent D-lysine 5, 6-aminomutase from *Clostridium sticklandii*. *J. Biol. Chem.* **275**, 106-114 (2000).
55. Ratnatilleke, A., Vrijbloed, J.W. & Robinson, J.A. Cloning and sequencing of the coenzyme B(12)-binding domain of isobutyryl-CoA mutase from *Streptomyces cinnamonensis*, reconstitution of mutase activity, and characterization of the recombinant enzyme produced in *Escherichia coli*. *J. Biol. Chem.* **274**, 31679-31685 (1999).
56. Beatrix, B., Zelder, O., Liner, D. & Buckel, W. Cloning, sequencing and expression of the gene encoding the coenzyme B₁₂-dependent 2-methyleneglutarate mutase from *Clostridium barkeri* in *Escherichia coli*. *Eur. J. Biochem.* **221**, 101-109 (1994).
57. Chen, H.P., Wu, S.H., Lin, Y.L., Chen, C.M. & Tsay, S.S. Cloning, sequencing, heterologous expression, purification, and characterization of adenosylcobalamin-dependent D-ornithine aminomutase from *Clostridium sticklandii*. *J. Biol. Chem.* **276**, 44744-44750 (2001).
58. Masuda, J., Shibata, N., Morimoto, Y., Toraya, T. & Yasuoka, N. How a protein generates a catalytic radical from coenzyme B₁₂: X-ray structure of a diol-dehydratase-adeninylpentylcobalamin complex. *Structure Fold. Des.* **8**, 775 (2000).
59. Abend, A. et al. Ethanolamine ammonia-lyase has a "base-on" binding mode for coenzyme B₁₂. *Arch. Biochem. Biophys.* **370**, 138-141 (1999).
60. Sintchak, M.D., Arjara, G., Kellog, B.A., Stubbe, J. & Drennan, C.L. The crystal structure of class II ribonucleotide reductase reveals how an allosterically regulated monomer mimics a dimer. *Nat. Struct. Biol.*, 293-300 (2002).
61. Borths, E.L., Locher, K.P., Lee, A.T. & Rees, D.C. The structure of *Escherichia coli* BtuF and binding to its cognate ATP binding cassette transporter. *Proc. Natl. Acad. Sci.* **99**, 16642-16647 (2002).
62. Bauer, C.B. et al. Three-dimensional structure of ATP:corrinoid adenosyltransferase from *Salmonella typhimurium* in its free state, complexed with MgATP, or complexed with hydroxycobalamin and MgATP. *Biochemistry* **40**, 361-374 (2001).
63. Ouyang, L., Rulis, P., Ching, W.Y., Nardin, G. & Randaccio, L. Accurate redetermination of the X-ray structure and electronic bonding in adenosylcobalamin. *Inorg. Chem.* **43**, 1235-1241 (2004).
64. Ng, F.T.T. & Rempel, G.L. Ligand effects on transition metal-alkyl bond dissociation energies. *J. Am. Chem. Soc.* **104**, 621-623 (1982).
65. Geno, M.K. & Halpern, J. Why does nature not use the porphyrin ligand in vitamin B₁₂? *J. Am. Chem. Soc.* **109**, 1238-1240 (1987).
66. Champloy, F. et al. EXAFS data indicate a "normal" axial cobalt-nitrogen bond of the organo-B₁₂ cofactor in the two coenzyme B₁₂-dependent enzymes glutamate mutase and 2-methyleneglutarate mutase. *J. Am. Chem. Soc.* **121**, 11780-11789 (1999).

67. Scheuring, E., Padmakumar, R., Banerjee, R. & Chance, M.R. Extended X-ray absorption fine structure analysis of coenzyme B₁₂ bound to methylmalonyl-coenzyme A mutase using global mapping techniques. *J. Am. Chem. Soc.* **119**, 12192-12200 (1997).
68. Mancina, F. & Evans, P.R. Conformational changes on substrate binding to methylmalonyl CoA mutase and new insights into the free radical mechanism. *Structure* **6**, 711-720 (1998).
69. Smith, D.M., Golding, B.T. & Random, L. Understanding the mechanism of B₁₂-dependent methylmalonyl-CoA mutase: partial proton transfer in action. *J. Am. Chem. Soc.* **121**, 9388-9399 (1999).
70. Maiti, N., Widjaja, L. & Banerjee, R. Proton transfer from histidine 244 may facilitate the 1,2 rearrangement reaction in coenzyme B(12)-dependent methylmalonyl-CoA mutase. *J. Biol. Chem.* **274**, 32733-32737 (1999).
71. Thoma, N.H., Evans, P.R. & Leadlay, P.F. Protection of radical intermediates at the active site of adenosylcobalamin-dependent methylmalonyl-CoA mutase. *Biochemistry* **39**, 9213-9221 (2000).
72. Mancina, F., Smith, G.A. & Evans, P.R. Crystal structure of substrate complexes of methylmalonyl-CoA mutase. *Biochemistry* **25**, 7999-8005 (1999).
73. Vlasie, M.D. & Banerjee, R. Tyrosine 89 accelerates Co-carbon bond homolysis in methylmalonyl-CoA mutase. *J. Am. Chem. Soc.* **125**, 5431-5435 (2003).
74. Lee, H.A.J. & Abeles, R.H. Purification and properties of dioldehydrase, and enzyme requiring a cobamide coenzyme. *J. Biol. Chem.* **238**, 2367-2373 (1963).
75. Toraya, T. Radical catalysis in coenzyme B₁₂-dependent isomerization (eliminating) reactions. *Chem. Rev.* **103**, 2095-2127 (2003).
76. Shibata, N. et al. A new mode of B₁₂ binding and the direct participation of a potassium ion in enzyme catalysis: X-ray structure of diol dehydratase. *Structure* **7**, 997-1008 (1999).
77. Liao, D.-I., Dotson, G., Turner, I.J., Reiss, L. & Emptage, M. Crystal structure of substrate free form of glycerol dehydratase. *J. Inorg. Biochem.* **93**, 84-91 (2003).
78. Shibata, N., Masuda, J., Morimoto, Y., Yasuoka, N. & Toraya, T. Substrate-induced conformational change of a coenzyme B₁₂-dependent enzyme: crystal structure of the substrate-free form of diol dehydratase. *Biochemistry* **41**, 12607-12617 (2002).
79. Barker, H.A., Smyth, R.D., Wilson, R.M. & Weissbach, H. The purification and properties of β-methylaspartase. *J. Biol. Chem.* **234**, 320-328 (1959).
80. Gruber, K., Reitzer, R. & Kratky, G. Radical Shuttling in a Protein: Ribose Pseudorotation Controls Alkyl-Radical Transfer in the Coenzyme B(12) Dependent Enzyme Glutamate Mutase. *Angew. Chem. Int. Ed.* **40**, 3377-3380 (2001).
81. Bothe, H. et al. Identification of the 4-glutamyl radical as an intermediate in the carbon skeleton rearrangement catalyzed by coenzyme B₁₂-dependent glutamate mutase from *Clostridium cochlearium*. *Biochemistry* **37**, 4105-4113 (1998).
82. Hoffman, B., Konrat, R., Bothe, H., Buckel, W. & Krautler, B. Structure and dynamics of the B₁₂-binding subunit of glutamate mutase from *Clostridium cochlearium*. *Eur. J. Biochem.* **263**, 178-188 (1999).

83. Tollinger, M., Konrat, R., Hilbert, B.H., Marsh, E.N. & Krautler, B. How a protein prepares for B₁₂ binding: structure and dynamics of the B₁₂-binding subunit of glutamate mutase from *Clostridium tetanomorphum*. *Structure* **6**, 1021-1033 (1998).
84. Hoffman, B. et al. A protein pre-organized to trap the nucleotide moiety of coenzyme B₁₂: refined solution structure of the B₁₂-binding subunit of glutamate mutase from *Clostridium tetanomorphum*. *Chembiochem* **2**, 643-655 (2001).
85. Tollinger, M. et al. The B₁₂-binding subunit of glutamate mutase from *Clostridium tetanomorphum* traps the nucleotide moiety of coenzyme B₁₂. *J. Mol. Biol.* **309**(2001).
86. Booker, S.J., Licht, S., Broderick, J.B. & Stubbe, J. Coenzyme B₁₂-dependent ribonucleotide reductase: evidence for the participation of five cysteine residues in ribonucleotide reduction. *Biochemistry* **33**(1994).
87. Holmgren. Thioredoxin. *Annu. Rev. Biochem.* **54**, 205-235 (1985).
88. Abeles, R.H. & Beck, W.S. The mechanism of action of cobamide coenzyme in the ribonucleotide reductase reaction. *J. Biol. Chem.* **242**, 3589-3593 (1967).
89. Hogenkamp, H.P., Ghambeer, R.K., Brownson, C., Blakley, R.L. & Vitols, E. Cobamides and ribonucleotide reduction. VI. Enzyme-catalyzed hydrogen exchange between water and deoxyadenosylcobalamin. *J. Biol. Chem.* **243**, 799-808 (1968).
90. Licht, S.S., Booker, S.J. & Stubbe, J. Studies on the catalysis of carbon-cobalt bond homolysis by ribonucleoside triphosphate reductase: evidence for concerted carbon-cobalt bond homolysis and thiyl radical formation. *Biochemistry* **38**, 1221-1233 (1999).
91. Lawrence, C.C., Gerfen, G.J., Samano, V., Nitsche, R. & Robins, M.J. Binding of Cob(II)alamin to the adenosylcobalamin-dependent ribonucleotide reductase from *Lactobacillus leichmannii*. Identification of dimethylbenzimidazole as the axial ligand. *J. Biol. Chem.* **274**(1999).
92. Jordan, A. & Reichard, P. Ribonucleotide reductases. *Annu. Rev. Biochem.* **67**, 71-98 (1998).
93. Tamao, Y. & Blakley, R.L. Direct spectrophotometric observation of an intermediate formed from deoxyadenosylcobalamin in ribonucleotide reduction. *Biochemistry* **12**, 24-34 (1973).
94. Uhlin, U. & Eklund, H. Structure of ribonucleotide reductase protein R1. *Nature* **370**(1994).
95. Logan, D.T., Andersson, J., Sjoberg, B.M. & Nordlund, P. A glycy radical site in the crystal structure of a class III ribonucleotide reductase. *Science* **283**, 1499-1504 (1999).
96. Baker, J.J., van der Drift, C. & Stadtman, T.C. Purification and properties of β-lysine mutase, a pyridoxal phosphate and B₁₂ coenzyme dependent enzyme. *Biochemistry* **12**, 1054-1063 (1973).
97. Stadtman, T.C. Anaerobic degradation of lysine. II. Cofactor requirements and properties of the soluble enzyme system. *J. Biol. Chem.* **238**, 2766-2773 (1963).
98. Stadtman, T.C. & Renz, P. The B₁₂-coenzyme dependent step in lysine fermentation: the migration of an amino group from carbon 6 to carbon 5 forming 3,5-diaminohexanoate. *Fed. Proc.* **26**, 343 (1967).

99. Dekker, E.E. & Barker, H.A. Identification and Cobamide Coenzyme-dependent Formation of 3,5-Diaminohexanoic Acid, and Intermediate in Lysine Fermentation. *J. Biol. Chem.* **243**, 3232-3237 (1968).
100. Morley, C.G.D. & Stadtman, T.C. Studies on the fermentation of D- α -Lysine. Purification and properties of an adenosine triphosphate regulated B₁₂-coenzyme-dependent D- α -Lysine mutase complex from *Clostridium sticklandii*. *Biochemistry* **9**, 1970 (1970).
101. Morley, C.G.D. & Stadtman, T.C. The role of pyridoxal phosphate in the B₁₂ coenzyme-dependent D- α -Lysine mutase reaction. *Biochemistry* **11**, 600-605 (1972).
102. Barker, H.A., Kahn, J.M. & Hedrick, L. Pathway of lysine degradation in *Fusobacterium nucleatum*. *J. Bact.* **152**, 201-207 (1982).
103. Tang, K.H., Chang, C.H. & Frey, P.A. Electron transfer in the substrate-dependent suicide inactivation of Lysine 5,6-Aminomutase. *Biochemistry* **40**, 5190-5199 (2001).
104. Danen, W.C. & West, C.T. An electron spin resonance investigation of the 1-Aziridylcarbinyl and related free radicals. *J. Am. Chem. Soc.* **96**, 2447-2453 (1973).
105. Song, K.B. & Frey, P.A. Molecular properties of lysine-2,3-aminomutase. *J. Biol. Chem.* **266**, 7651-7655 (1991).
106. Coper, N.J., Booker, S.J., Ruzicka, F., Frey, P.A. & Scott, R.A. Direct FeS cluster involvement in generation of a radical in lysine 2,3-aminomutase. *Biochemistry* **39**, 15668-15673 (2000).
107. Baraniak, J., Moss, M.L. & Frey, P.A. Lysine 2,3-aminomutase. Support for a mechanism of hydrogen transfer involving S-adenosylmethionine. *J. Biol. Chem.* **264**, 1357-1360 (1989).
108. Moss, M.L. & Frey, P.A. Activation of lysine 2,3-aminomutase by S-adenosylmethionine. *J. Biol. Chem.* **265**, 18112-18115 (1990).
109. Chen, D., Walsby, C.J., Hoffman, B.M. & Frey, P.A. Coordination and mechanism of reversible cleavage of S-adenosylmethionine by the [4Fe-4S] center in lysine 2,3-aminomutase. *J. Am. Chem. Soc.* **125**, 11788-11789 (2003).
110. Petrovich, R.M., Ruzicka, F.J., Reed, G.H. & Frey, P.A. Characterization of iron-sulfur clusters in lysine 2,3-aminomutase by electron paramagnetic resonance spectroscopy. *Biochemistry* **31**, 10774-10781 (1992).
111. Lieder, K.W., Booker, S.J., Ruzicka, F.J., Beinert, H. & Reed, G.H. S-Adenosylmethionine-dependent reduction of lysine 2,3-aminomutase and observation of the catalytically functional iron-sulfur centers by electron paramagnetic resonance. *Biochemistry* **37**, 2578-2585 (1998).
112. Han, O. & Frey, P.A. Chemical model for the pyridoxal 5'-phosphate dependent lysine aminomutases. *J. Am. Chem. Soc.* **112**, 8982-8983 (1990).
113. Ballinger, M.D., Frey, P.A. & Reed, G.H. Structure of a substrate radical intermediate in the reaction of lysine 2,3-aminomutase. *Biochemistry* **31**, 10782-10789 (1992).
114. Ballinger, M.D., Frey, P.A., Reed, G.H. & LoBrutto, R. Pulsed electron paramagnetic resonance studies of the lysine 2,3-aminomutase substrate radical:

- evidence for participation of pyridoxal 5'-phosphate in a radical rearrangement. *Biochemistry* **34**, 10086-10093 (1995).
115. Ballinger, M.D., Reed, G.H. & Frey, P.A. An organic radical in the lysine 2,3-aminomutase reaction. *Biochemistry* **31**, 949-953 (1992).
 116. Chang, C.H., Ballinger, M.D., Reed, G.H. & Frey, P.A. Lysine 2,3-Aminomutase: Rapid Mix-Freeze-Quench Electron Paramagnetic Resonance Studies Establishing the Kinetic Competence of a Substrate-Based Radical Intermediate. *Biochemistry* **35**, 11081-11084 (1996).
 117. Knappe, J. & Schmitt, T. A novel reaction of S-adenosyl-L-methionine correlated with the activation of pyruvate formate-lyase. *Biochem. Biophys. Res. Commun.* **23**, 1110-1117 (1976).
 118. Knappe, J., Blaschkowski, H.P., Grobner, P. & Schmitt, T. Pyruvate formate-lyase of *Escherichia coli*: the acetyl-enzyme intermediate. *Eur. J. Biochem.* **50**, 253-263 (1974).
 119. Knappe, J. et al. Pyruvate formate-lyase reaction in *Escherichia coli*. The enzymatic system converting an inactive form of the lyase into the catalytically active enzyme. *Eur. J. Biochem.* **11**, 316-327 (1969).
 120. Broderick, J.B. et al. Pyruvate formate-lyase activating enzyme is an iron-sulfur protein. *J. Am. Chem. Soc.* **119**, 7396-7397 (1997).
 121. Kulzer, R., Pils, T., Kappl, R., Huttermann, J. & Knappe, J. Reconstitution and characterization of the polynuclear iron-sulfur cluster in pyruvate formate-lyase-activating enzyme. Molecular properties of the holoenzyme form. *J. Biol. Chem.* **273**, 4897-4903 (1998).
 122. Henshaw, T.F., Cheek, J. & Broderick, J.B. The [4Fe-4S]¹⁺ cluster of pyruvate formate-lyase activating enzyme generates the glycyl radical on pyruvate formate-lyase: EPR-detected single turnover. *J. Am. Chem. Soc.* **122**, 8331-8332 (2000).
 123. Conradt, H., Hohmann-Berger, M., Hohmann, H.P., Blaschkowski, H.P. & Knappe, J. Pyruvate formate-lyase (inactive form) and pyruvate formate-lyase activating enzyme of *Escherichia coli*: isolation and structural properties. *Arch. Biochem. Biophys.* **228**, 133-142 (1984).
 124. Frey, M., Rothe, M., Wagner, A.F.V. & Knappe, J. Adenosylmethionine-dependent synthesis of the glycyl radical in pyruvate formate-lyase by abstraction of the glycine C-2 pro-S hydrogen atom. Studies of [²H]glycine-substituted enzyme and peptides homologous to the glycine 734 site. *J. Biol. Chem.* **269**, 12432-12437 (1994).
 125. Krebs, C., Broderick, W.E., Henshaw, T.F., Broderick, J.B. & Huynh, B.H. Coordination of adenosylmethionine to a unique iron site of the [4Fe-4S] of pyruvate formate-lyase activating enzyme: A mossbauer spectroscopic study. *J. Am. Chem. Soc.* **124**, 912-913 (2001).
 126. Walsby, C.J., Ortillo, D., Broderick, W.E., Broderick, J.B. & Hoffman, B.M. An anchoring role for FeS clusters: chelation of the amino acid moiety of S-adenosylmethionine to the unique iron site of the [4Fe-4S] cluster of pyruvate formate-lyase activating enzyme. *J. Am. Chem. Soc.* **124**, 11270-11271 (2002).
 127. Fontecave, M., Eliasson, R. & Reichard, P. Oxygen-sensitive ribonucleoside triphosphate reductase is present in anaerobic *Escherichia coli*. *Proc. Natl. Acad. Sci.* **86**, 2147-2151 (1989).

128. Harder, J., Eliason, R., Pontis, E., Ballinger, M.D. & Reichard, P. Activation of the anaerobic ribonucleotide reductase from *Escherichia coli* by S-adenosylmethionine. *J. Biol. Chem.* **267**, 25548-25552 (1992).
129. Ollagnier, S. et al. Activation of the anaerobic ribonucleotide reductase from *Escherichia coli*. The essential role of the iron-sulfur center for S-adenosylmethionine reduction. *J. Biol. Chem.* **272**, 24216-24223 (1997).
130. Padovani, D., Thomas, F., Trautwein, A.X., Mulliez, E. & Fontecave, M. Activation of class III ribonucleotide reductase from *E. coli*. The electron transfer from the iron-sulfur center to S-adenosylmethionine. *Biochemistry* **40**, 6713-6719 (2001).
131. Tamarit, J., Mulliez, E., Meier, C., Trautwein, A.X. & Fontecave, M. The anaerobic ribonucleotide reductase from *Escherichia coli*. The small protein is an activating enzyme containing a [4Fe-4S](2+) center. *J. Biol. Chem.* **274**, 31291-31296 (1999).
132. Tamarit, J. et al. The activating component of the anaerobic ribonucleotide reductase from *Escherichia coli*. An iron-sulfur center with only three cysteines. *J. Biol. Chem.* **275**, 15669-15675 (2000).
133. Mulliez, E., Padovani, D., Atta, M., Alcouffe, C. & Fontecave, M. Activation of class III ribonucleotide reductase by flavodoxin: A protein radical-driven electron transfer to the iron-sulfur center. *Biochemistry* **40**, 3730-3736 (2001).
134. Ohsawa, I. et al. Cloning of the biotin synthetase gene from *Bacillus sphaericus* and expression in *Escherichia coli* and Bacilli. *Gene* **80**, 39-48 (1989).
135. Mejean, A. et al. Highly purified biotin synthase can transform dethiobiotin into biotin in the absence of any other protein, in the presence of photoreduced deazaflavin. *Biochem. Biophys. Res. Commun.* **217**, 1231-1237 (1995).
136. Ugulava, N.B., Gibney, B.R. & Jarrett, J.T. Biotin synthase contains two distinct iron-sulfur cluster binding sites: chemical and spectroelectrochemical analysis of iron-sulfur interconversions. *Biochemistry* **40**, 8343-8351 (2001).
137. Berkovitch, F., Nicolet, Y., Wan, J.T., Jarrett, J.T. & Drennan, C.L. Crystal structure of biotin synthase, an S-adenosylmethionine-dependent radical enzyme. *Science* **303**, 76-79 (2004).
138. Coper, M.M. et al. The [4Fe-4S]²⁺ cluster in reconstituted biotin synthase binds S-adenosylmethionine. *J. Am. Chem. Soc.* **124**, 14006-14007 (2002).
139. Coper, M.M. et al. Structural studies of the interaction of S-adenosylmethionine with the [4Fe-4S] clusters in biotin synthase and pyruvate formate-lyase activating enzyme. *Protein Sci.* **12**, 1573-1577 (2003).
140. Tse Sum Bui, B. et al. Fate of the (2Fe-2S)²⁺ cluster of *Escherichia coli* biotin synthase during reaction: a Mossbauer characterization. *Biochemistry* **42**, 8791-8798 (2003).
141. Ugulava, N.B., Sacanell, C.J. & Jarrett, J.T. Spectroscopic Changes during a Single Turnover of Biotin Synthase: Destruction of a [2Fe-2S] Cluster Accompanies Sulfur Insertion. *Biochemistry* **40**, 8352-8358 (2001).
142. Tse Sum Bui, B. et al. Biotin synthase mechanism: on the origin of sulphur. *FEBS Lett.* **440**, 226-230 (1998).

143. Jameson, G.N., Cosper, M.M., Hernandez, H.L., Johnson, M.K. & Huynh, B.H. Role of the [2Fe-2S] cluster in recombinant *Escherichia coli* biotin synthase. *Biochemistry* **43**, 2022-2031 (2004).
144. Ollagnier-de Choudens, S., Mulliez, E. & Fontecave, M. The PLP-dependent biotin synthase from *Escherichia coli*: mechanistic studies. *FEBS Lett.* **532**, 465-468 (2002).
145. Ollagnier-de Choudens, S., Mulliez, E., Hewiston, K.S. & Fontecave, M. Biotin synthase is a pyridoxal phosphate-dependent cysteine desulfurase. *Biochemistry* **41**, 9145-9152 (2002).
146. Picciocchi, A., Douce, R. & Alban, C. Biochemical characterization of the Arabidopsis biotin synthase reaction. The importance of mitochondria in biotin synthesis. *Plant Physiol.* **127**, 1224-1233 (2001).
147. Reed, L.J. A trail of research from lipoic acid to alpha-keto acid dehydrogenase complexes. *J. Biol. Chem.* **276**, 38329-38336 (2001).
148. Zhao, X., Miller, J.R., Jiang, Y., Marletta, M.A. & Cronan, J.E. Assembly of the covalent linkage between lipoic acid and its cognate enzymes. *Chem. Biol.* **10**, 1293-1302 (2003).
149. Cicchillo, R.M. et al. Lipoyl synthase requires two equivalents of S-adenosyl-L-methionine to synthesize one equivalent of lipoic acid. *Biochemistry* **43**, 6378-6386 (2004).
150. Miller, J.R. et al. *Escherichia coli* LipA is a lipoyl synthase: in vitro biosynthesis of lipoylated pyruvate dehydrogenase complex from octanoyl-acyl carrier protein. *Biochemistry* **39**, 15166-15178 (2000).
151. Cicchillo, R.M. et al. *Escherichia coli* lipoyl synthase binds two distinct [4Fe-4S] clusters per polypeptide. *Biochemistry* **ASAP**(2004).
152. Trainor, D.A., Parry, R.J. & Gitterman, A. Biotin Biosynthesis. 2. Stereochemistry of Sulfur Introduction at C-4 of Dethiobiotin. *J. Am. Chem. Soc.* **102**, 1467-1468 (1980).
153. Keithly, J.H. & Nadler, K.D. Protoporphyrin formation in *Rhizobium japonicum*. *J. Bact.* **154**, 838-845 (1983).
154. Poulson, R. & Polglase, W.J. Aerobic and anaerobic coproporphyrinogenase activities in extracts from *Saccharomyces cerevisiae*. Purification and characterization. *J. Biol. Chem.* **249**, 6367-6371 (1974).
155. Tait, G.H. Coproporphyrinogenase activity in extracts from *Rhodospseudomonas spheroides*. *Biochem. Biophys. Res. Commun.* **37**, 116-122 (1969).
156. Layer, G., Verfurth, K., Mahlitz, E. & Jahn, D. Oxygen-independent coproporphyrinogen-III oxidase HemN from *Escherichia coli*. *J. Biol. Chem.* **277**, 34136-34142 (2002).
157. Layer, G., Moser, J., Heinz, D.W., Jahn, D. & Schubert, W.D. Crystal structure of coproporphyrinogen III oxidase reveals cofactor geometry of Radical SAM enzymes. *EMBO J.* **22**, 6214-6224 (2003).
158. Marsh, E.N. & Drennan, C.L. Adenosylcobalamin-dependent isomerases: new insights into structure and mechanism. *Curr. Opin. Chem. Biol.* **5**, 499-505 (2001).
159. Iwata-Reuyl, D. Biosynthesis of the 7-deazaguanosine hypermodified nucleosides of transfer RNA. *Bioorg. Chem.* **31**, 24-43 (2003).

160. O'Hagan, D., Schaffrath, C., Cobb, S.L., Hamilton, J.T. & Murphy, C.D. Biosynthesis of an organofluorine molecule. *Nature* **416**, 279 (2002).
161. White, M.F., Vasquez, J., Yang, S.F. & Kirsch, J.F. Expression of apple 1-aminocyclopropane-1-carboxylate synthase in *Escherichia coli*: kinetic characterization of wild-type and active-site mutant forms. *Proc. Natl. Acad. Sci.* **91**, 12428-12432 (1994).
162. Val, D.L. & Cronan, J.E.J. In vivo evidence that S-adenosylmethionine and fatty acid synthesis intermediates are the substrates for the LuxI family of autoinducer synthases. *J. Bact.* **10**, 2644-2651 (1998).
163. Nishimura, S., Taya, Y., Kuchino, Y. & Oashi, Z. Enzymatic synthesis of 3-(3-amino-3-carboxypropyl)uridine in *Escherichia coli* phenylalanine transfer RNA: transfer of the 3-amino-acid-3-carboxypropyl group from S-adenosylmethionine. *Biochem. Biophys. Res. Commun.* **57**, 702-708 (1974).
164. Tabor, C.W. & Tabor, H. Polyamines. *Annu. Rev. Biochem.* **53**, 749-790 (1984).
165. Taylor, F.R. & Cronan, J.E.J. Cyclopropane fatty acid synthase of *Escherichia coli*. Stabilization, purification, and interaction with phospholipid vesicles. *Biochemistry* **18**, 3292-3300 (1979).
166. Fontecave, M., Atta, M. & Mulliez, E. S-adenosylmethionine: nothing goes to waste. *Trends Biochem. Sci.* **29**, 243-249 (2004).
167. DeLano, W.L. The PyMOL Molecular Graphics System. (<http://pymol.sourceforge.net>).
168. Chen, D. & Frey, P.A. Identification of lysine 346 as a functionally important residue for pyridoxal 5'-phosphate binding and catalysis in lysine 2, 3-aminomutase from *Bacillus subtilis*. *Biochemistry* **40**, 596-602 (2001).

Chapter 2

Preliminary crystallographic characterization of biotin synthase

Abbreviations:

AdoMet
ASU
BioB
DTB
PEG
Tris

S-adenosyl-L-methionine
Asymmetric unit
Biotin synthase
Dethiobiotin
Polyethylene glycol
Tris(hydroxymethyl)aminomethane

The determination of the structure of BioB was a two year-long collaboration with the laboratory of J.T. Jarrett at the University of Pennsylvania Department of Biochemistry and Biophysics. Producing good quality crystals of BioB proved to be a challenging process, requiring approximately 15 months of experimentation to finally obtain 3.4 Å resolution data. Table 2.1 summarizes developments in the crystallization, and the basic analysis of the structure of BioB. Only one preparation of BioB ever crystallized in my hands, and I am convinced that something unique about that purification led to crystallization. The crystallization of BioB by hanging drop vapor diffusion methods was unusual in several ways which warrant the attention provided by this chapter.

2.1. Protein purification, Fe-S cluster reconstitution, and addition of substrates

Recombinant histidine-tagged *Escherichia coli* BioB was purified from *E. coli* and the Fe-S clusters were anaerobically reconstituted in the Jarrett laboratory as previously described^{1,2}. Additionally, purified AdoMet was produced in the Jarrett laboratory and used in the crystallization process. Dethiobiotin (DTB) and all other reagents used in crystallization were purchased from Sigma. The protein solution contained 20 mg/mL BioB, 25 mM Tris hydrochloride, pH 8.0, and a four-fold molar excess of AdoMet and of DTB. Protein solutions and all other crystallization materials were handled in a Coy anaerobic chamber, under an atmosphere of 5% H₂ / 95% Ar.

2.2. Crystallization and preliminary analysis

Crystallization experiments were carried out in a Coy anaerobic chamber at room temperature, under an atmosphere of 95% Ar, 5% H₂. To ensure anaerobiosis, the

chamber contains palladium catalysts mounted on fan systems, which react with H₂ gas and scrub any O₂ that may be present in the chamber. All solutions used in crystallization were thoroughly purged with Ar before transfer into the anaerobic chamber. Crystallization trays, pipet tips, and all other supplies and apparatus were subjected to rounds of vacuum and pressurized Ar in order to exchange any adsorbed oxygen before being transferred to the anaerobic chamber. PEG solutions, cofactors, and other light-sensitive reagents were kept in a dark box in the anaerobic chamber.

Table 2.2 shows a list of crystallization screens, commercially available from Hampton Research Corp., that were used in combination with various crystallization methods in an attempt to crystallize BioB. Initial crystallization experiments were done in glass capillary tubes (Kimble Products KIMAX-51, 1.5 x 90 mm), using the microbatch method. For these experiments, 3 μ L of protein (20 mg/mL BioB, 25 mM Tris pH 8.0) were mixed with an equal volume of precipitant solution and deposited in a capillary, a 6 μ L reservoir of precipitant solution was deposited opposite the protein/precipitant mixture, with a small space separating the two liquid plugs, and the capillary was then sealed with wax. These experiments did not produce protein crystals of observable size. Due to the difficulties and large amounts of protein that are associated with microbatch crystallization, this method was soon abandoned in favor of a somewhat unconventional hanging drop vapor diffusion method described below.

Typically, the hanging drop vapor diffusion method involves a small amount of protein, which is placed on a siliconized glass cover slip, mixed with precipitant solution, and

sealed over a 0.5-1.0 mL well of precipitant solution. The hanging drop method has the tremendous advantage of requiring far less protein (1 μL or less) per crystallization trial than the microbatch method, while suffering from the disadvantage of requiring far more precipitant solution, which must be degassed before introduction to the anaerobic chamber. The degassing step adds a degree of uncertainty to the experiment, since degassing likely results in a change in concentration of the solution.

Rather than degassing larger volumes of each component of each screen to use as well solutions, a solution of 2.5 M $(\text{NH}_4)_2\text{SO}_4$ was used as a standard well solution, in place of precipitant solution. The use of ammonium sulfate as well solution was a common practice, before the availability of commercial crystallization screens. For the purposes of anaerobic crystallization, this method allows the investigator to reclaim the time that it would take to degas larger volumes of precipitant solutions, but presents disadvantages as well. For instance, small amounts of volatile ammonia may evolve from aqueous $(\text{NH}_4)_2\text{SO}_4$, diffuse into the hanging drop, and change its pH over the course of the experiment³. Likewise, if the precipitant solution contains volatile components, their concentrations would be expected to fall as diffusion from the hanging drop to the well solution proceeds. Nevertheless, it was assumed that the salt-equilibrated hanging drop method would be useful in screening a large number of precipitant solutions. In later experiments, the potential problem of ammonia volatility was eliminated by using 2.5 M NaCl instead of a solution of $(\text{NH}_4)_2\text{SO}_4$. For a given precipitant solution, wells containing the NaCl solution generally produced fewer and better quality crystals than wells containing $(\text{NH}_4)_2\text{SO}_4$.

The salt-equilibrated hanging drops were set up as follows: 1 μ L of protein (20 mg/mL BioB, 25 mM Tris pH 8.0) was mixed with 1 μ L of precipitant solution (see Table 2.2) on a siliconized cover slip. The cover slip was placed over a well solution of NaCl or $(\text{NH}_4)_2\text{SO}_4$. Trays were set up and stored in the Coy anaerobic chamber at room temperature. Approximately two weeks into the salt-equilibrated hanging drop experiments, small yellow-brown crystals were observed to grow in crystallization condition BioB1 (Table 2.1). Interestingly, BioB forms a very heavy brown precipitate within an hour of mixing protein with precipitant solution, indicating a relatively rapid phase transition of the enzyme under these crystallization conditions. The small crystals appeared to grow from this precipitate. Unfortunately, these crystals were too small to manipulate, even with a 0.05 mm nylon cryoloop. It was assumed, for reasons discussed above, that the salt-equilibrated hanging drop method would add an extra layer of complications to the crystallization experiment, so efforts to reproduce these crystals and to screen around this condition were undertaken using the conventional method. During the course of two weeks, no crystals were observed to grow when the well solution was replaced with precipitant solution. The salt-equilibrated method was then redeployed, resulting in the successful reproduction of the initial crystals. Screening around the original condition (by varying the salt concentration and the molecular weight and concentration of the PEGs used) resulted in a slightly better crystallization condition BioB2 (Table 2.1). The crystals grown in condition BioB2 were slightly larger and thus more intensely brown. As in the original crystallization condition, a heavy brown precipitate was observed to form several minutes after mixing the precipitant and protein solutions, and crystals appeared to grow out of this precipitate. Attempts to lessen the

precipitation by decreasing the concentration of PEG resulted in failure to produce crystals, suggesting once again that precipitate formation is part of the pathway to crystal growth. The growth of protein crystals out of precipitate is a common phenomenon in macromolecular crystallography⁴.

The crystallization seemed to be extremely sensitive to motion disturbances. Crystallization trays that were not handled for two weeks after the experiment was started produced fewer, crystals which were large enough to manipulate with a 0.05 mm cryoloop. These crystals were used in macro- and micro-seeding experiments. However, these seeding experiments failed to produce larger crystals.

At this point, crystals grown in condition BioB2 were characterized by SDS-PAGE (Fig. 2.1). Interestingly, lane 3 of Fig. 2.1 contains two distinct bands, one at ~39 KDa and a second band at ~36 KDa, instead of one expected single band at ~40 KDa (BioB is a homodimer of ~80 kDa). The ~36 KDa band is due to a problem with C-terminal proteolysis that has now been corrected (J. Jarrett, personal communication). Proteolysis was occurring at the C-terminal end of the protein just after the last alpha-helix of the TIM barrel, and although this gel suggests that approximately half of the protein in the crystals should have the last 31 residues, no electron density is observed for these residues in either molecule in the structure. It is unclear what the function of this C-terminal region is, since proteolyzed protein shows no reduction in activity compared to the wild-type enzyme (J. Jarrett, personal communication). It is also not clear whether proteolysis is an important factor in crystallizing BioB, since the C-terminus of the

crystallographic model does not participate in lattice contacts (Fig. 2.2). However, crystallization of C-terminal truncated BioB is probably worth pursuing in order to obtain higher resolution crystallographic data, since disordered regions of proteins can prevent the formation of tight lattice contacts.

Crystals produced by condition BioB2 did not diffract synchrotron source X-rays when cryoprotected and tested for diffraction at 100K. Likewise, no diffraction was observed when crystals were mounted in capillaries and tested using a rotating copper anode generator. Attempts were made to improve the crystal quality using detergents and crystallization additives. Each of Hampton Detergent Screens 1, 2, and 3 was used to supplement condition BioB2 in crystallization experiments. Due to the surfactant properties of detergents, the sitting drop vapor diffusion method was used, in which protein and precipitant solution are mixed and placed in a small reservoir above the well solution. Like the successful hanging drop experiments, the sitting drops were also salt-equilibrated. Addition of detergents to condition BioB2 had a deleterious effect on the crystallization, and detergents were generally excluded from further crystallization experiments. A small molecule additive screen was designed with the hope that additives might improve the crystallization. The additive screen, whose formulations are shown in Table 2.3, included salts, polymers, metals, organic solvents, amino acids, sugars, reductants, cofactors, polyamines, etc. Through screening with additives, it was observed that substantially larger crystals (Fig. 2.3a) are grown in condition BioB2 supplemented with 100 mM glycine and titrated to pH ~6.5 (condition BioB3, Table 2.1). As before, these crystals appeared only after a heavy brown precipitate was observed.

Cryo-cooled crystals grown in condition BioB3 diffracted Cu K_{α} source X-rays, albeit weakly to $\sim 10\text{-}11$ Å resolution (Fig. 2.4). Though the resolution is quite low, the diffraction quality is good, with no evident problems due to cryo-protection or multiple lattices. Cryo-cooling was accomplished inside the anaerobic chamber by first soaking the crystal in condition BioB3 supplemented with 20% v/v glycerol for several seconds, and then plunging the crystal into liquid nitrogen. 50% v/v glycerol was carefully prepared by degassing for 24 hours in a round-bottom flask with stirring. To ensure that cryo-protection was not damaging the crystals, a crystal was transferred from the crystallization drop to a quartz capillary anaerobically, and then tested for diffraction at room temperature. Crystals tested in this manner produced weak or no discernable diffraction. A further test was done to see if the resolution limit could be improved by cryo-cooling crystals in a gaseous stream of nitrogen at 100 K. This method takes advantage of the transient oxygen stability of BioB in the presence of its substrates⁵, and seemed to produce better-quality diffraction than freezing in liquid nitrogen. Cryo-cooling in the cold stream was adopted as the standard method of cryo-protecting BioB crystals.

The best crystals grown in condition BioB3 appeared 1 month after the crystallization experiment was set up, and required that the crystallization tray not be handled during the duration of the experiment. Such crystals diffracted synchrotron source X-rays to afford data to 5.5 Å resolution (Table 2.4). Data were processed with the programs DENZO and SCALEPACK⁶. While these data were not of high enough resolution to allow us to solve the structure, the data were useful for the purposes of beginning the characterization of

the crystals. Crystals are trigonal (P321, P3₁21, or P3₂21), with a=b=155.3 Å, c= 91.3 Å. Unfortunately, no data were collected along (00l), and it was thus impossible to properly identify a 3₁ or 3₂screw axis at this time. Given the dimensions of the unit cell and the molecular weight of BioB, a solvent content of ~53% (corresponding to a Matthews coefficient⁷ of $V_m=2.65 \text{ \AA}^3/\text{Da}$ and 3 molecules per ASU) or ~69% (corresponding to $V_m=3.98 \text{ \AA}^3/\text{Da}$ and 2 molecules per ASU) was expected. Since BioB is a homodimer and the crystals diffract to low resolution, we suspected that the solvent content was indeed 69%, and this turned out to be correct. Data collected at the Fe absorption peak wavelength was processed with DENZO and SCALEPACK⁶, and SOLVE⁸ was used to search for Fe sites in the possible space groups. In (P3₁21, P3₂21), four Fe sites were identified (Fig. 2.6), consistent with expected set of two 4Fe-4S and two 2Fe-2S clusters per BioB dimer². Spacegroup P3₁21 and the sites that were located turned out to be correct (see below), illustrating the value of low resolution (5.5 Å) data in preliminary crystal characterization.

To improve upon the 5.5 Å resolution limit, the crystallization of BioB was revisited. Upon re-examination of the conventional hanging-drop crystallization experiments, small, irregularly shaped crystals were observed to grow in condition BioB4. Based on previous results, it was inferred that the addition of glycine to the precipitant and the use of the salt-equilibrated hanging drop method might produce better crystals. Condition BioB4 was optimized to give condition BioB5, consisting of 0.1 M Tris hydrochloride, 0.1 M glycine, 0.2 M MgCl₂, 20% w/v polyethylene glycol 1000, which was titrated to a final pH of ~6.5. Once again, trays were set up in a Coy anaerobic chamber at room

temperature, with 1 μ L of protein (20 mg/mL BioB, 25 mM Tris pH 8.0) added to 1 μ L of precipitant solution on a siliconized cover slip, and equilibrated over a well containing 0.5 mL 2.5 M NaCl. Crystals grown in condition BioB5 (Fig. 2.3b) were the largest BioB crystals obtained to date and diffracted synchrotron source X-rays to 3.4 \AA resolution (Table 2.5). These crystals belong to space group $P3_121$ (six ASUs), with 2 molecules per ASU ($Z=12$) and $a = b = 155.69 \text{ \AA}$, $c = 90.88 \text{ \AA}$, $V=1,908,412 \text{ \AA}^3$. Systematic absences distinguished ($P3_121$, $P3_221$) from $p321$, and $P3_121$ was differentiated from $P3_221$ by inspection of α helices.

As with previous crystallization conditions, extensive macro- and micro- seeding experiments under condition BioB5 failed to produce larger or better-quality crystals, and crystals always appeared several days to weeks after the formation of a heavy brown precipitate in the crystallization drop. Using Tris that was buffered at pH 7.0 (instead of titrating the final precipitant solution to pH ~ 6.5) resulted in smaller crystals that diffracted relatively poorly, suggesting that Tris is serving as an additive rather than as an effective buffer in condition BioB5. Data collected from crystals grown in condition BioB5 allowed us to solve the structure of BioB. The protein's intrinsic Fe cofactors were used to phase the structure by multiwavelength anomalous dispersion (MAD) methods, as described in chapter 3.

2.3. Tables

Table 2.1. Timeline of BioB crystallization.

Date	Development	Crystallization condition	Precipitant formulation	Well solution (0.5 mL, 2.5 M)
Jul. 2001	Small crystals	BioB1	0.2 M KCl 0.01 M MgCl ₂ 0.05 M Na-Cacodylate pH 6.5, 10% w/v PEG 4000	(NH ₄) ₂ SO ₄
Sep. 2001	Crystals large enough to manipulate	BioB2	0.2 M MgCl ₂ 0.1 M Na-Cacodylate pH 6.5 20% w/v PEG 1000	NaCl
Nov. 2001	~11 Å diffraction (Cu K _α radiation)	BioB3	0.2 M MgCl ₂ 0.1 M Na-Cacodylate pH 6.5 0.1 M glycine 20% w/v PEG 1000	NaCl
Jan. 2002	5.5 Å data (synchrotron radiation), location of two putative Fe-S cluster sites per BioB monomer	BioB3		NaCl
	Crystals observed in previous conventional hanging drop experiments	BioB4	0.2 M MgCl ₂ 0.1 M Tris-HCl pH 7.0 12% w/v PEG 3000	NaCl
Aug. 2002	3.7 Å data (synchrotron radiation)	BioB5	0.1 M Tris-HCl 0.1 M glycine 0.2 M MgCl ₂ 20% w/v PEG 1000 final pH ~6.5	NaCl
Sep. 2002	3.4 Å data (synchrotron radiation)	BioB5		NaCl

Table 2.2. Hampton Research screens used to find BioB crystallization conditions.

Screen	Microbatch capillaries	Conventional hanging drop	(NH ₄) ₂ SO ₄ -equilibrated hanging drop	NaCl-equilibrated hanging drop
<i>Sparse-matrix</i>				
Crystal Screen	Tried	Tried	Tried	Tried
Crystal Screen 2	Tried	Tried	Tried	Tried
Crystal Screen Cryo	Tried	Tried	Tried	Tried
Crystal Screen Lite	Tried	Tried	Tried	Tried
PEG/Ion screen	Tried	Tried	Tried	Tried
Natrix	Tried	Tried	Tried	Tried
MembFac	Tried	Tried	Tried	Tried
<i>Grid screens</i>				
Grid Screen (NH ₄) ₂ SO ₄	Not Tried	Tried	Not Tried	Not Tried
Grid Screen PEG 6000	Not Tried	Tried	Tried	Tried
Grid Screen MPD	Not Tried	Tried	Tried	Tried
Grid Screen PEG/LiCl	Not Tried	Tried	Not Tried	Not Tried
Grid Screen NaCl	Not Tried	Tried	Not Tried	Not Tried

For each screen listed, one or more crystallization methods were used in an attempt to crystallize BioB. For crystallization drops that were equilibrated against either (NH₄)₂SO₄ or NaCl wells, the well solution was 2.5 M.

Table 2.3. Additives used to optimize BioB crystallization conditions.

#	Additive	Stock Conc.	Unit Conc.	#	Additive	Stock Conc.	Unit Conc.
1	CaCl ₂	0.1	M	41	NaFormate	1.0	M
2	MnCl ₂	0.1	M	42	NaH ₂ PO ₄	1.0	M
3	ZnCl ₂	0.01	M	43	D-Sucrose	30	% w/v
4	Ethylene Glycol	30	% v/v	44	NaKTartarate*4H ₂ O	1.0	M
5	Glycerol	30	% v/v	45	D-Sorbitol	30	% w/v
6	MPD	30	% v/v	46	Dioxane	30	% v/v
7	PEG 400	50	% v/v	47	Na ₂ EDTA	0.1	M
8	Urea	0.1	M	48	CsCl	1.0	M
9	Ethanol	30	% v/v	49	KSCN	1.0	M
10	Isopropanol	30	% v/v	50	NaOAc	1.0	M
11	Methanol	30	% v/v	51	NaCitrate	1.0	M
12	(NH ₄) ₂ SO ₄	1.0	M	52	BaCl ₂	0.1	M
13	KCl	1.0	M	53	PEG 3000	30	% w/v
14	LiCl	1.0	M	54	PEG 5000 MME	30	% w/v
15	NaCl	2.0	M	55	PEG 20,000	30	% w/v
16	CH ₃ CN	40	% v/v	56	Jeffamine M 600 pH 7.0	50	% v/v
17	Acetone	40	% v/v	57	L-Lysine	1.0	M
18	DTT	0.1	M	58	L-Arginine	1.0	M
19	CdCl ₂	0.1	M	59	Dextran Sulfate	0.15	% w/v
20	CoCl ₂	0.1	M	60	Decanedioic acid	Sat'd soln.	
21	Saturated FeCl ₂	10	% v/v	61	6-Aminocaproic Acid	1.0	M
22	SrCl ₂	0.1	M	62	1,6-Diaminohexane	1.0	M
23	NiCl ₂	0.1	M	63	1,8-Diaminooctane	Sat'd soln.	
24	CuSo ₄	0.1	M	64	1,5-Diaminopentane	0.5	M
25	Spermine	0.1	M	65	Azelaic acid	Sat'd soln.	
26	Spermidine•3HCl	0.1	M	66	(Glycyl) ₂ -glycine	0.3	M
27	Octyl Glucoside (n-Octyl-β-D-Glucoside)	0.245	M	67	(Glycyl) ₂ -glycine	0.3	M
28	LDAO (Lauryldimethylamine Oxide)	0.02	M	68	(Glycyl) ₃ -glycine	0.1	M
29	Dimethylsulfoxide	30	% v/v	69	1,10-Diaminodecane	Sat'd soln.	
30	Glutathione (reduced)	0.025	M	69	Palmitic acid	Sat'd soln.	
31	Glycine	1.0	M	70	L-Methionine	1	M
32	Mg(OAc) ₂	0.1	M	71	L-Serine	1	M
33	D-Glucose	20	% w/v	72	L-Threonine	1	M
34	Guanidine•HCl	1.0	M	73	L-Glutamate	1	M
35	Hexaaminocobalt(III)Trichloride	0.1	M	74	L-Glutamine	1	M
36	Na ₂ Malonate	1.0	M	75	L-Aspartate	1	M
37	Li ₂ SO ₄	1.0	M	76	Hexadecyltrimethylammonium bromide	0.01	M
38	KI	1.0	M	77	Adenine	0.01	M
39	Beta alanine	0.1	M	78	Biotin	0.01	M
40	NaBr	1.0	M	79	Pyridoxal 5'-phosphate	0.01	M

Table 2.4. Data collected from a single crystal grown in condition BioB3.

	Remote	Fe Peak
Wavelength (Å)	1.2	1.736
Exposure time (s)	60	80
Oscillation range (deg)	1	1
Resolution (Å)	30-5.5	30-5.5
$R_{\text{sym}}^{1,2}$ (%)	6.7 (30.3)	8 (41.6)
Unique reflections	4025 ³	7584
Redundancy	6.3	3.2
$I/\sigma(I)^2$	11.2 (5.14)	7.5 (2.27)
Completeness (%) ²	95.0 (95.5)	95.8 (93.8)

Data were collected at Beamline 9-2, Stanford Synchrotron Radiation Laboratory, at 100 K. ¹ $R_{\text{sym}} = \sum_{hkl} \sum_i [|I_i(hkl) - \langle I(hkl) \rangle|] / \sum_{hkl} \langle I(hkl) \rangle$, where $I_i(hkl)$ is the i th measured diffraction intensity (no σ cutoff) and $\langle I(hkl) \rangle$ is the mean intensity of the miller index (hkl). ²Values for the highest resolution bins are in parentheses. ³For this wavelength, Friedel pairs were merged during data processing.

Table 2.5. Data collected from crystals grown in condition BioB5 and used to solve the structure of BioB.

Wave-length (Å)	Resolution range (Å)	Unique reflections	Redundancy	Completeness (%) ¹	$I/\sigma(I)$ ¹	R_{sym} ^{1,2}
1.30000	100 - 3.7	26,018	3.4	99.5 (100.0)	11.8 (2.3)	6.7 (37.5)
1.73827	100 - 4.1	19,002	3.1	98.3 (99.7)	14.6 (1.9)	6.4 (29.7)
1.74150	100 - 4.5	14,030	2.8	97.1 (95.7)	14.0 (2.6)	8.2 (36.7)
1.10000 ³	100 - 3.4	17,465	5.4	98.1 (87.9)	15.8 (3.8)	6.6 (25.9)

Data were collected at 100 K, using an inverse beam geometry, at the Advanced Light Source beamline 5.0.2 (1.30000Å, 1.73827Å, and 1.74150Å wavelengths) and the National Synchrotron Light Source beamline X25 (1.10000Å wavelength), both equipped with a charge-coupled device detector (Area Detector Systems Corp). Data were processed and scaled with DENZO⁶, SCALEPACK⁶, and XDS⁹. ¹Values for the highest resolution bins are in parentheses. ² $R_{\text{sym}} = \sum_{hkl} \sum_i [|I_i(hkl) - \langle I(hkl) \rangle|] / \sum_{hkl} \langle I(hkl) \rangle$, where $I_i(hkl)$ is the i th measured diffraction intensity (no σ cutoff) and $\langle I(hkl) \rangle$ is the mean intensity of the miller index (hkl). ³For this wavelength, Friedel pairs were merged during data processing.

2.4. Figures

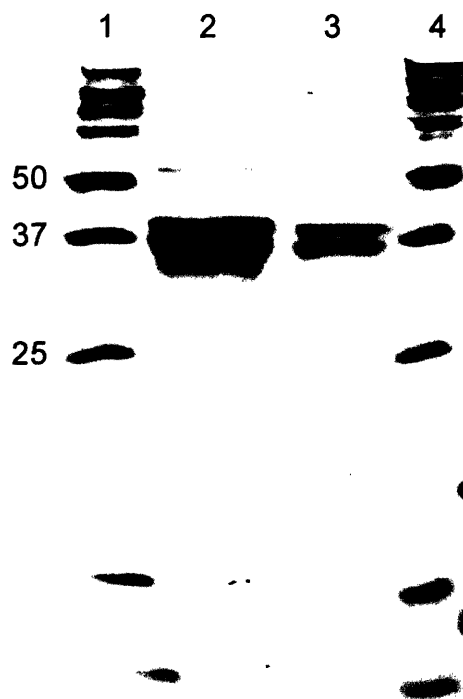


Figure 2.1. SDS-PAGE analysis of BioB crystals grown in condition BioB2. A sample of the crystallization drop (lane 2) was run on a 15% polyacrylamide gel alongside BioB crystals that were first washed with fresh precipitant solution and then dissolved in distilled water (lane 3). 50, 37, and 25 kDa molecular weight markers (lanes 1 and 4) are labeled.

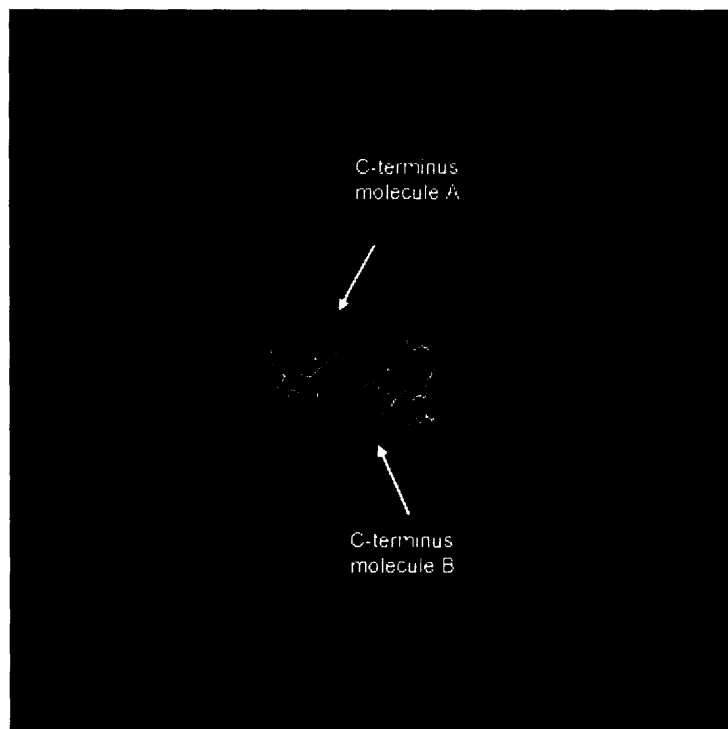


Figure 2.2. Lattice contacts in the final structure of BioB, showing the last observable residue in both molecules in the ASU (each molecule is depicted as an alpha carbon trace). The model is truncated at residue 315 since no electron density was observed for the last 31 residues of the protein. Symmetry related molecules are show in shades of pink, purple, and red. The C-termini do not participate in lattice contacts.

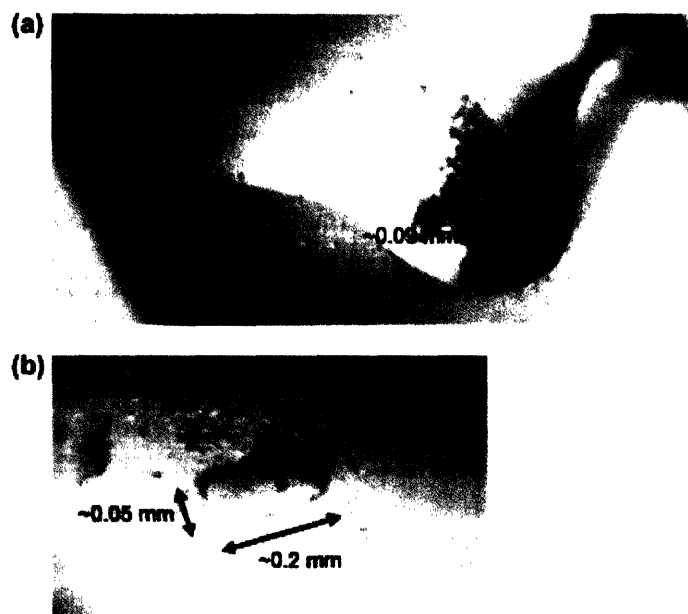


Figure 2.3. BioB crystals. **(a)** Crystals grown in condition BioB3 were transferred to a capillary to check for diffraction at room temperature. The crystals measured less than 10 microns in the largest dimension. The heavy brown precipitate, characteristic of all BioB crystallizations, is prominent in this image. **(b)** Crystals grown in condition BioB5. Crystals appeared as bloated hexagonal rods with a maximal radius of ~50 microns and a maximal length of ~200 microns. Such crystals produced the data used to solve the structure.

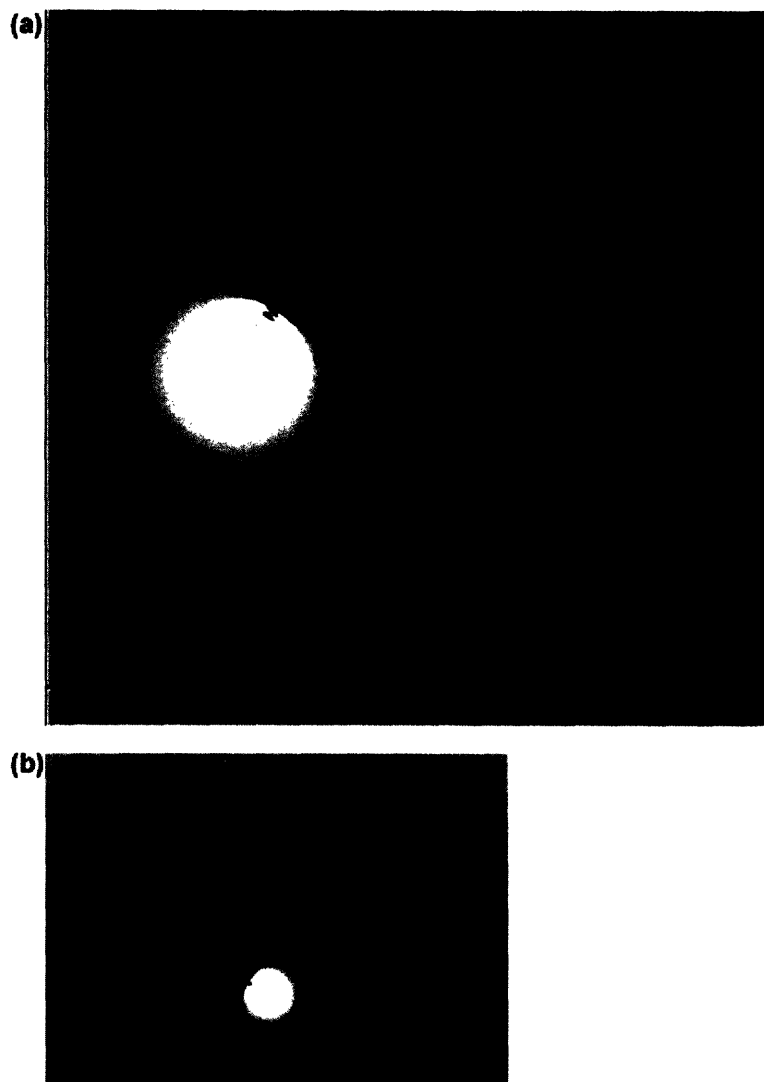


Figure 2.4. First diffraction from a BioB crystal. **(a)** Crystals grown in condition BioB3 were cryoprotected by briefly soaking in precipitant solution supplemented with 20% v/v glycerol, followed by plunging into liquid nitrogen in the anaerobic chamber. The diffraction limit is $\sim 10\text{-}11$ Å when tested with $\text{Cu } K_{\alpha}$ radiation. **(b)** zoomed-out view of the image in part a.

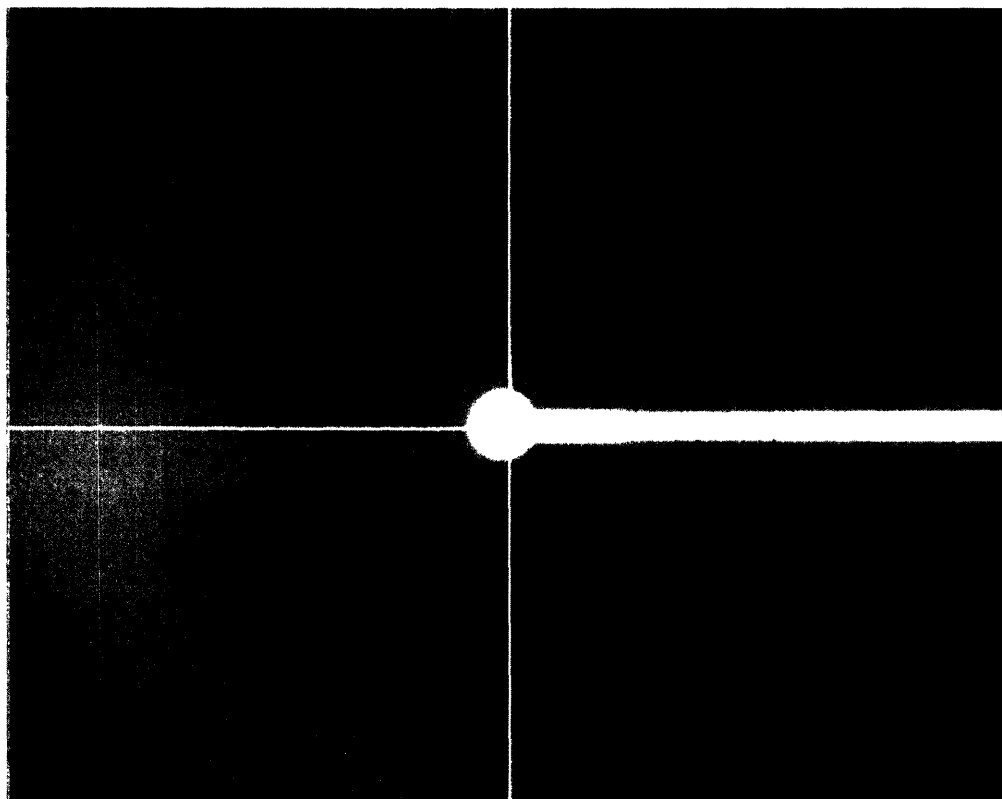


Figure 2.5. 5.5 Å data from crystals grown in condition BioB3. Data were collected at SSRL beamline 9-2. Though the resolution is low, the diffraction quality is generally good.

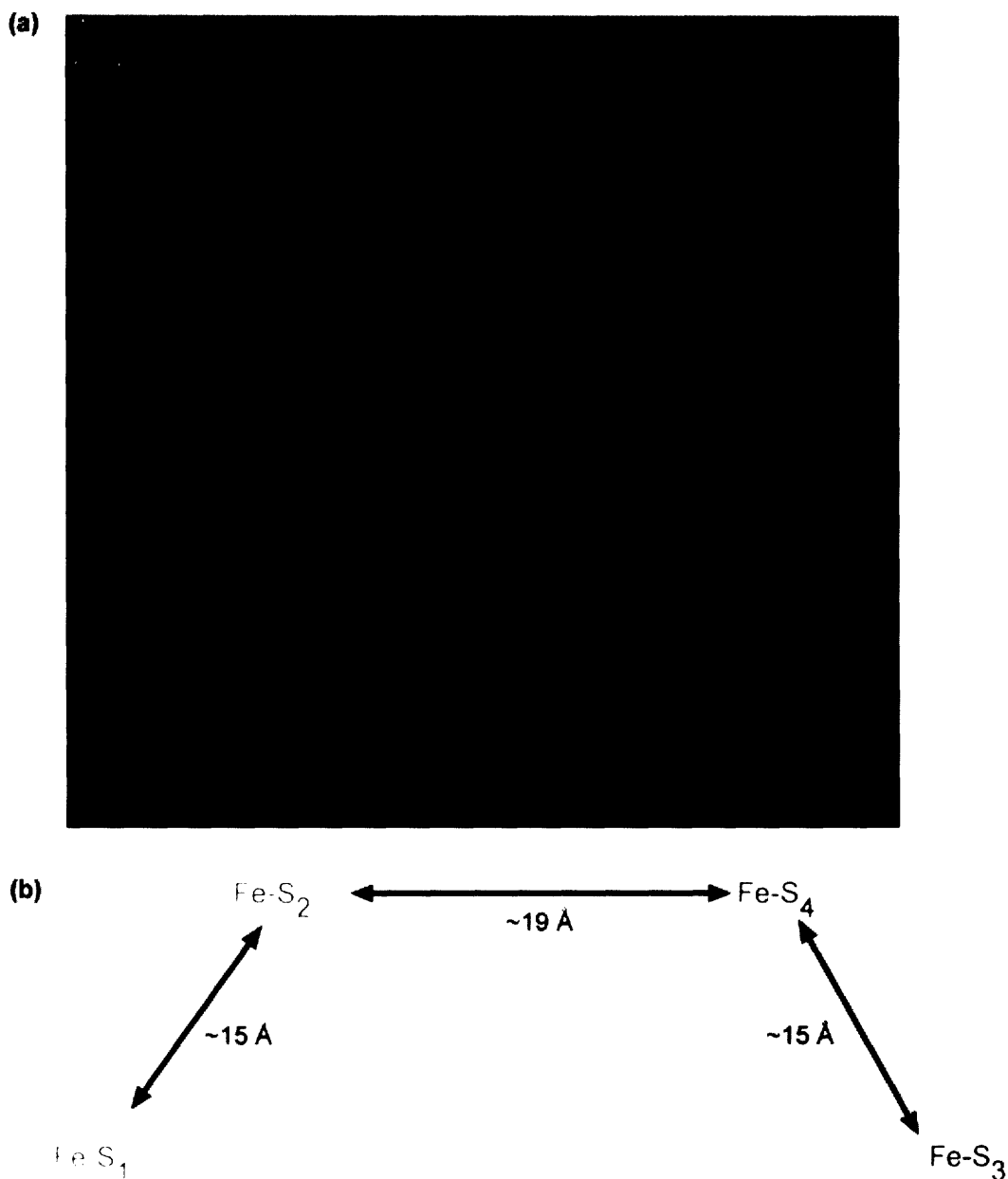


Figure 2.6. Location of putative Fe sites in BioB. (a) Data collected from crystals grown in condition BioB3 at the Fe absorption peak wavelength were used to locate putative Fe-S clusters in unit cell. The unit cell is visualized parallel to the *c* axis. This number and arrangement of Fe-S sites is consistent with a structure that reasonably fills the unit cell and has sensible lattice contacts. (b) Diagram showing the cluster sites in the asymmetric unit, showing intercluster distances.

2.5. References

1. Ugulava, N.B., Gibney, B.R. & Jarrett, J.T. Iron-Sulfur cluster Interconversion in Biotin Synthase: Dissociation and Reassociation of Iron during Conversion of [2Fe-2S] to [4Fe-4S] Clusters. *Biochemistry* **39**, 5206-5214 (2000).
2. Ugulava, N.B., Gibney, B.R. & Jarrett, J.T. Biotin synthase contains two distinct iron-sulfur cluster binding sites: chemical and spectroelectrochemical analysis of iron-sulfur interconversions. *Biochemistry* **40**, 8343-8351 (2001).
3. Seinfeld, J.H. & Pandis, S.N. *Atmospheric Chemistry and Physics*, 1326 (John Wiley and Sons, New York, 1998).
4. <http://xray.bmc.uu.se/~terese/crystallization/tutorials/tutorial2.html>.
5. Ugulava, N.B., Frederick, K.K. & Jarrett, J.T. Control of Adenosylmethionine-Dependent Radical Generation in Biotin Synthase: A Kinetic and Thermodynamic Analysis of Substrate Binding to Active and Inactive Forms of BioB. *Biochemistry* **42**, 2708-2719 (2003).
6. Otwinowski, Z. & Minor, W. Processing of X-ray diffraction data collected in oscillation mode. *Methods Enzymol.* **276**, 307-326 (1997).
7. Matthews, B.W. Solvent content of protein crystals. *J. Mol. Biol.* **33**, 491-497 (1968).
8. Terwilliger, T.C. & Berendzen, J. Automated structure solution for MIR and MAD. *Acta. Cryst.* **D55**, 849-861 (1999).
9. Kabsch, W. Automatic processing of rotation diffraction data from crystals of initially unknown symmetry and cell constants. *J. Appl. Cryst.* **26**, 795-800 (1993).

Chapter 3

Crystal structure of biotin synthase

Abbreviations:

2,3-LAM	Lysine 2,3-aminomutase
Ado•	5'-deoxyadenosyl radical
AdoCbl	Adenosylcobalamin, coenzyme B ₁₂
AdoH	5'-deoxyadenosine
AdoMet	<i>S</i> -adenosyl-L-methionine
ASU	Asymmetric unit
BioB	Biotin synthase
DTB	Dethiobiotin
FNR	Flavodoxin/NADPH oxidoreductase
HemN	Coproporphyrinogen III oxidase
MAD	Multiwavelength anomalous dispersion
NADPH	Reduced nicotinamide adenine dinucleotide phosphate
NCS	Non-crystallographic symmetry
PFL	Pyruvate formate-lyase
PLP	Pyridoxal 5'-phosphate
SAM	<i>S</i> -adenosyl-L-methionine
TIM	Triosephosphate isomerase
Tris	Tris(hydroxyethyl)aminoethane

3.1. Introduction

Biotin synthase (BioB) catalyzes the final step in the biotin (vitamin B₈) biosynthetic pathway, the conversion of dethiobiotin (DTB) to biotin. This remarkable reaction requires the insertion of a sulfur atom between non-activated carbons C6 and C9 of DTB (Fig. 3.1). BioB contains unusual iron-sulfur clusters that play a role in sulfur insertion through an AdoMet-dependent radical-based mechanism. Like all AdoMet radical enzymes, BioB contains a conserved CxxxCxxC sequence motif that coordinates an essential redox-active 4Fe-4S cluster, with AdoMet coordinating a unique Fe of this cluster¹⁻⁵. The crystal structure of BioB in complex with AdoMet and DTB is presented in this chapter. This work begins to address the disputed cofactor content of BioB, the two hypothetical mechanisms for the BioB reaction, and AdoMet binding by the AdoMet radical enzymes. The structure also suggests an evolutionary relationship between the AdoMet- and AdoCbl-dependent radical enzymes, which is discussed in further detail in chapter 5. A modified version of this chapter was published in January 2004⁶.

In the reaction catalyzed by BioB, there is general agreement that Ado• generated from AdoMet oxidizes DTB, as demonstrated by Marquet and coworkers⁷, but the number and types of Fe-S clusters and other cofactors involved in the reaction have been a subject of controversy⁸⁻¹⁵. Protein preparation-dependent cofactor differences have led to two mechanistic proposals for the method of sulfur insertion in BioB. The “hybrid cluster model”, put forth by Jarrett and coworkers¹⁶, involves the use of a 2Fe-2S cluster as the immediate sulfur donor for biotin (Fig. 3.2a), and is consistent with Marquet’s pioneering

^{34}S isotopic labeling studies¹⁷ and with the observed destruction of a 2Fe-2S cluster that accompanies BioB turnover^{16,18}. The hybrid-cluster model of Jarrett and coworkers lead to a proposal which requires two molecules of AdoMet and two reducing equivalents (Fig. 3.2a). The stoichiometry of AdoMet and the sulfur source in this mechanism are both consistent with initial studies from the Marquet laboratory^{17,19}, but conflict with studies from Fontecave and coworkers^{11,20}. The proposal of Fontecave and coworkers is based on the activity of BioB from which the 2Fe-2S cluster has been removed, and suggests that S is provided from an enzyme-bound persulfide, generated via an intrinsic pyridoxal-5'-phosphate (PLP) -dependent cysteine desulfurase activity^{11,20} (Fig. 3.2b). Recently, Johnson and coworkers have obtained evidence that BioB does not bind PLP²¹, casting doubt on the intrinsic cysteine desulfurase activity proposed by Fontecave's group^{11,20}. Spectroscopic data from the Johnson and Huynh groups support the presence of two distinct Fe-S clusters in BioB, a 4Fe-4S cluster and a 2Fe-2S cluster^{14,16,21,22}. These studies are consistent with sulfur donation from the 2Fe-2S cluster to DTB and destruction of the 2Fe-2S cluster (the hybrid cluster model), but, in contrast to Jarrett and coworkers, the destruction of the 2Fe-2S cluster was found to be faster than the formation of biotin²². The mechanism proposed by Jarrett and coworkers can still account for the results from the laboratories of Johnson and Huynh, but the kinetic analysis does not exclude additional steps between the 2Fe-2S cluster destruction and formation of biotin. Our results, presented below, also favor a mechanism that invokes a role for a 2Fe-2S cluster over a mechanism that involves PLP. Irrespective of whether BioB preparations contain a 2Fe-2S cluster or PLP, assay mixtures produce one or fewer turnovers per monomer, over the course of several minutes to hours, although BioB from *Arabidopsis*

is reported to catalyze >2 turnovers per hour (Table 3.1). Due to low enzymatic activity, it has been suggested that BioB is either subject to strong product inhibition by AdoH²⁰, or that it may be a "suicide enzyme," i.e. a stoichiometric reactant rather than a true catalyst.

3.2. Materials and methods

The crystallization of BioB was discussed in detail in chapter 2. This section describes crystallographic methods that were used to arrive at the final model of BioB.

The experimental electron density map was calculated using the phase information derived from four Fe sites in the asymmetric unit (ASU), corresponding to one 4Fe-4S clusters and one 2Fe-2S clusters for each of the two molecules in the ASU. The program SOLVE²³ was used to refine the sites and to calculate the experimental electron density map. The non-crystallographic symmetry (NCS) operator that relates the two molecules in the ASU was found using the program LSQKAB²⁴, after manually placing α helices into the density corresponding to both molecules in the ASU. The experimental electron density map, calculated to 3.7 Å resolution, was subjected to solvent flattening and twofold NCS averaging using DM²⁵, which resulted in an electron density map of high-enough quality to distinguish the 2Fe-2S cluster from the 4Fe-4S cluster of the BioB monomer, and to model the clusters in their respective densities (Fig. 3.3). Using SOLVE²³, the coordinates of the twelve Fe atoms in the ASU (4 Fe for each of two 4Fe-4S clusters + 2 Fe for each of two 2Fe-2S clusters) were refined and used to calculate phases. The electron density map that resulted was subjected to solvent flattening and twofold NCS averaging, giving the map that was used to build the initial model (Fig. 3.4). After several rounds of iterative model building using the program O²⁶, refinement of the model with CNS²⁷, and rebuilding of the model into sigma-A weighted, phase-combined electron density maps, the resolution of the experimental map was extended to 3.4 Å (using the programs SIGMAA, SFALL, and FFT from the CCP4 package²⁸), and

solvent flattening and twofold NCS averaging were performed again. Toward the end of the model building process, electron density maps with coefficients of $2|F_o|-|F_c|$ and $|F_o|-|F_c|$ and phases calculated from the model were used, along with the phase-extended experimental electron density map.

The model was refined against 3.4 Å data using the program CNS²⁷, to a final $R = 25.6\%$ and $R_{free} = 30.0\%$ on F (Table 3.2). Early in the refinement, strict NCS constraints were applied to the two molecules in the ASU; these were relaxed to moderate restraints (with a weight of 400) during the last few rounds of refinement. The refined structure of the dimeric enzyme contains residues 4-315 (molecule A) and 3-315 (molecule B), two DTB, two AdoMet, two Fe₄S₄ clusters, two Fe₂S₂ clusters, and one Tris molecule. There is no electron density for the N-terminal histidine tag, the first 2 or 3 residues at the N-terminus, and the last 31 residues at the C-terminus in either molecule.

The final model has 99.3% of all residues residing in the allowed region of the Ramachandran plot (Fig. 3.5), with 79.8% (molecule A) and 79.8% (molecule B) in the most favored region, 18.3% (molecule A) and 17.9% (molecule B) in the additional allowed regions, 1.5% (molecule A) and 1.5% (molecule B) in generously allowed regions, and 0.7% (molecule A) and 0.5% (molecule B) in disallowed regions, as calculated by PROCHECK²⁹. One of the residues in the disallowed regions, Asn311, is at the conformationally flexible C-terminus. The other residue, Asp 155, is in position to interact with the ribose moiety of AdoMet, and therefore its unusual geometry is likely to

be functionally significant. The equivalent residue in HemN, another AdoMet radical enzyme, also has disallowed Ramachandran angles³⁰.

3.3. Results

3.3.1. Overall structure and the location of Fe-S clusters

The fold of each subunit of the BioB homodimer is a TIM barrel, with two additional helices at the N-terminus and a disordered region at the C-terminus (Figs. 3.6a, 3.7a and b). The arrangement of the two TIM barrels allows access to the bottom and to the top of both subunits, forming an elongated structure (Figs. 3.6a and 3.8). BioB joins at least 26 other protein superfamilies incorporating TIM barrel architecture³¹ and four AdoCbl-dependent enzymes that use this fold for catalysis of radical-based chemistry (see chapter 1). However, to the best of our knowledge, this is the first example of Fe-S clusters bound within and on top of a TIM barrel.

A 4Fe-4S cluster is located at the C-terminal end of the TIM barrel, far (~30 Å) from the dimer interface, and a 2Fe-2S cluster is located deep inside of the barrel, ~25 Å from the C-terminal end (Fig. 3.6a, 3.7a and b). The active site, containing AdoMet and DTB, is situated between these two clusters (Figs. 3.6a and b, Fig. 3.7a and b). This Fe-S cluster arrangement suggests an explanation for the reported differences in Fe-S cluster content of BioB; a surface Fe-S cluster may be more readily lost and reconstituted than a deeply buried cluster. The 2Fe-2S cluster is observed by Mössbauer spectroscopy^{8,32} in whole cells containing recombinant BioB, and is always retained in the initial purified protein^{9,12,13,15,33}. Treatment of BioB with strong chemical reductants and metal chelators, followed by Fe reconstitution, yields a 2Fe-2S-depleted form of BioB, with an

intact 4Fe-4S cluster^{9,10,14,34,35}. Reconstituted protein not subjected to a reduction or chelation step (such as used in this study) contains both a 4Fe-4S and a 2Fe-2S cluster^{8,14,15,21}.

The lattice packing of BioB crystals is shown in Fig. 3.9. Each BioB subunit contacts three neighboring subunits of neighboring ASUs. The interaction between subunits of neighboring ASUs is sparse and does not suggest a physiological docking surface for other proteins, such as flavodoxin.

3.3.2. A PLP binding site is not observed in the structure

With respect to the proposal that PLP is a cofactor in BioB^{11,20}, we did not add PLP during protein purification or crystallization and do not find it in our structure. Additionally, the structure does not reveal an obvious binding site for PLP. Indeed, cysteine desulfurases typically bind PLP *via* an imine linkage to a Lys residue, and all Lys residues, including the one highly conserved Lys (K49 in BioB) are found at the surface of the protein (Fig. 3.10), far from the putative site of a cysteine persulfide¹¹ and the observed DTB binding site. Furthermore, no obvious phosphate-binding site can be found in the structure. In accord with studies from the Jarrett^{14,16}, Marquet^{17,36}, and Johnson and Huynh^{21,22} groups, and in contrast to results from Fontecave and coworkers^{11,20}, this X-ray structure analysis favors a mechanism that invokes a role for an 2Fe-2S cluster over one that requires PLP.

3.3.3. *The novel 2Fe-2S cluster of BioB*

The 2Fe-2S cluster of BioB is unique both in terms of its coordination by β -strand residues in the core of a TIM barrel (Figs. 3.6a and b, 3.7a and b, 3.10), as well as in terms of the identity of the amino acid ligands: C97, C128, C188, and R260, (Figs. 3.6b, 3.11a-c, 3.12a-g). All four of these residues are conserved, and the assignment of the fourth ligand as Arg is unambiguous, even at the moderate resolution of this structure; the amino acid sequence of the TIM barrel has been fully assigned with no breaks or gaps, and the shape of the omit electron density at position 260 is completely consistent with an Arg sidechain (Fig. 3.11b). Our ligand assignment is consistent with Johnson and coworkers' spectroscopic observation of incomplete cysteinyl ligation for the 2Fe-2S cluster^{9,21}. The assignment of an Arg ligand to a metal is unprecedented in biology, although guanidine and guanidine-like species have been observed to ligate metals in small molecules (Fig. 3.13a-e and Table 3.3; discussed below).

3.3.4. *The 4Fe-4S cluster and AdoMet*

Proteins are classified as members of the AdoMet radical superfamily based on the presence of the sequence motif CxxxCxxC (C53, C57, and C60 for BioB)¹. This motif is contained in a 28-residue loop extending from β -strand 1 to helix 1 of the TIM barrel, and the three cysteines coordinate three of the four irons of the 4Fe-4S cluster, as expected from mutagenesis studies^{33,37} (Fig. 3.11a). AdoMet is the fourth ligand to the cluster and binds as an N/O chelate to a unique Fe position, through the AdoMet amino group nitrogen and carboxyl group oxygen (Fig. 3.11a, Table 3.4).

This binding mode is consistent with spectroscopic results for PFL activase^{2,3}, and is likely to be common to AdoMet radical proteins, since spectral changes associated with AdoMet binding have been reported for several family members³⁸⁻⁴⁰. In a report published at the same time as the BioB structure, Schubert and coworkers noted the same mode of AdoMet binding in the crystal structure of HemN³⁰, another AdoMet radical enzyme. Also consistent with spectroscopic data on BioB and PFL activase^{3,41}, the sulfonium of AdoMet does not appear to be a ligand to Fe and is ~4.0 Å away from the nearest cluster Fe.

Interestingly, BioB is the only known AdoMet-binding TIM barrel^{31,42}. AdoMet is bound to BioB in an extended conformation, stretching across the top of the barrel, such that contacts are made to AdoMet by residues in or following β -strands 1, 2, and 4-6 (Fig. 3.6b, Table 3.5). The net result of these interactions is that AdoMet is completely buried from solvent and appears to be ideally positioned for both electron transfer from the 4Fe-4S cluster and for hydrogen atom abstraction from DTB (discussed below).

Some contacts to AdoMet are made by residues that are homologous across several AdoMet radical enzymes. For example, I192, which makes a van der Waal contact to AdoMet (Fig. 3.11a), is part of a short sequence motif (192-IxGxxE-196) that is located near the AdoMet binding site. This sequence corresponds to MxGxxE in LipA, VxGxxD in PFL activase, LxGxxD in 2,3-LAM, etc. (Fig. 3.14). Additionally, almost all sequenced AdoMet radical enzymes have an aromatic residue at the penultimate position

of the CxxxCxxC sequence. In BioB, this is residue Y59, which forms π -stacking interactions with the adenine ring of AdoMet. Other contacts to AdoMet are made by D155, which hydrogen bonds to the 2' and 3' -OH groups of the ribose ring, R173, which forms a salt bridge with the AdoMet carboxylate, and N153, which hydrogen bonds to both AdoMet and DTB.

3.3.5. *The methionyl moiety*

In our structure, the adenine and ribose moieties of AdoMet fit the electron density well, whereas the broad electron density of the methionyl moiety indicates some ambiguity in the exact location of the sulfonium (Fig. 3.11a). The electron density may suggest that we have a combination of cleaved and uncleaved AdoMet, presumably resulting from radiolytic reduction due to long exposures of the crystal to synchrotron radiation. Alternatively, the breadth of the methionine might be explained by racemization at the sulfonium of AdoMet, which is well documented⁴³. A racemic mixture of (*S,S*)-AdoMet (which is not found in biological systems⁴⁴) and (*R,S*)-AdoMet is observed in the crystal structure of HemN³⁰. A more detailed analysis of the methionyl moiety awaits the availability of higher resolution data.

3.3.6. *The dethiobiotin binding site*

The enzyme preparation used for crystallization has DTB bound⁴⁵, and we observe electron density in the active site that fits this substrate (Fig. 3.11c). DTB binds in the core of the TIM barrel, between the 2Fe-2S cluster and AdoMet. In contrast to the reported stoichiometry of bound substrates⁴⁵, we find one DTB and one AdoMet in each

BioB subunit. This discrepancy is currently under investigation. DTB binding to BioB requires the presence of AdoMet⁴⁵, and we find that DTB makes substantial van der Waal contacts with AdoMet, covering 50% of its surface. These interactions include the stacking of the carboxylate tail against the AdoMet adenine and the stacking of the DTB ureido ring with the AdoMet ribose. DTB makes a series of contacts with protein as well (Table 3.6), the most important of which is the bidentate interaction with N222 that may play a role in orienting DTB for hydrogen atom abstraction. Finally, the DTB carboxylate interacts with the backbone amides of T292 and T293, as well as the side chain of T292 (Fig. 3.15). Interactions with these residues could serve to close a loop over the top of the barrel upon DTB binding, helping to seal the barrel for the radical-mediated reaction that follows.

3.4. Discussion

3.4.1. Arginine as an Fe ligand

The assignment of an Arg ligand to a metal is unprecedented in biology, although guanidine species have been observed or proposed to ligate Co^{III}, Os^{III}, Pt^{II}, Ni^{II}, and Zn^{II} in small molecules in aqueous solution at pH ~3.5 - 10⁴⁶⁻⁴⁹ (Fig. 3.13, Table 3.3). In BioB, the metal-nitrogen distance (~2.3-2.4 Å) is longer than those observed in the small molecule crystal structures (1.94 - 2.07 Å, Table 3.3). However, at our current resolution limit of 3.4 Å, any discussion of Fe-N distance is premature. It has been predicted that Arg could serve as a metal ligand in a protein environment where the Arg sidechain were uncharged⁴⁸, and in BioB, R260 has an unusual environment that should indeed alter its pK_a. It is buried in the center of a TIM barrel and has a high number of potential hydrogen-bonding partners (S43, S218, S283, and R95, Fig. 3.11b). The conservation of Arg as an Fe-S cluster ligand in BioB, rather than the more common Cys or His residues, is peculiar and suggests an important role for this residue in modulating the properties of the cluster or in facilitating catalysis. The choice of metal ligands may be important for preserving charge neutrality within the core of the (α/β)₈ barrel, since one common mechanism of Fe-S cluster redox modulation by backbone-NH-to-S hydrogen bonds is not possible with this structural motif. All surrounding main-chain amides are involved in hydrogen bonding between the β-strands of the barrel and can not interact with the cluster. Thus, the ligands and neighboring sidechains are likely to play a significant role in redox modulation, and an Arg (or His) ligand would be a better choice than Cys in terms of reducing the overall net negative charge of this buried cluster. The use of Arg,

rather than His, is more difficult to explain. In part, the answer may be structural, in that the long length of the Arg side-chain allows for a barrel that is less compact and able to fit both substrates. However, R260 may be conserved as a ligand to the 2Fe-2S cluster for catalytic rather than structural reasons. During turnover of BioB, the 2Fe-2S cluster is destroyed as one S is transferred into biotin^{16,17,36}. In our structure, the R260 side-chain could rearrange to bridge the two Fe atoms and facilitate the proposed S transfer. Our knowledge of how Fe-S clusters are assembled in biological systems is still in its infancy, and it will be interesting to discover if any of the features observed in the BioB structure are mimicked in proteins involved in cluster assembly.

3.4.2. Structural insight into the reaction catalyzed by BioB

Although the elucidation of a detailed enzyme mechanism awaits further biochemical studies, the structure does provide insight into key steps of the BioB reaction. The observed cooperativity of substrate binding⁴⁵ can be explained by the extensive interaction between AdoMet and DTB (described in section 3.3.6), and by the interaction of both substrates with N153. With respect to radical generation, the electron transfer from flavodoxin to the 4Fe-4S cluster is made possible by the binding of the cluster close to the protein surface (~6-7 Å). The subsequent electron transfer from the 4Fe-4S cluster to the AdoMet sulfonium is facilitated by direct O/N coordination of the AdoMet to Fe, thereby restraining the position of the sulfonium to the proximity of the 4Fe-4S cluster. The resulting formation of Ado• is likely coupled to hydrogen atom abstraction from C9 of DTB, and we find that DTB is positioned accordingly, with C9 ~3.9 Å away from the 5' carbon of AdoMet. Closure of the biotin thiophane ring requires the abstraction of a

second hydrogen atom from C6 of DTB. Deuterium transfer from of the C6 position of (²H)DTB has demonstrated that a second Ado• is likely also responsible for this second hydrogen atom abstraction⁷, although the requirement for two equivalents of AdoMet has recently been disputed²⁰. In our structure, C6 of DTB is positioned ~4.1 Å from the 5' carbon position of AdoMet, suggesting that Ado• also accomplishes the second hydrogen atom abstraction. Exactly how structural changes of the enzyme facilitate the release of AdoH and Met and the binding of a second AdoMet molecule remains to be determined. The rearrangements involved in this process will likely involve the movement of loops at the C-terminal end of the TIM barrel.

The sulfur insertion step is the most controversial part of the mechanism of BioB. The structure analysis shows that the 2Fe-2S cluster is ideally positioned to play a role in sulfur insertion. The closest bridging S of the 2Fe-2S cluster is only 4.6 Å away from C9 of DTB, a position which is consistent with transfer of this sulfur to biotin as suggested by results from ³⁴S-labeling experiments¹⁷ and the observation of 2Fe-2S cluster degradation during turnover^{16,18,22}.

3.4.3. Questions arising from the structure of BioB

If the *in vivo* sulfur source for biotin is the 2Fe-2S cluster, is BioB a “suicide enzyme”, capable of performing only a single turnover because of the destruction of the 2Fe-2S cluster? Only two biotin-requiring proteins are present in *E. coli*: acetyl-CoA carboxylase and the bifunctional biotin operon repressor/holocarboxylase synthetase (BirA)⁵⁰. Therefore, a single turnover of multiple BioB proteins may provide enough biotin for the

life-cycle of *E. coli*. Alternatively, the 2Fe-2S cluster may be rebuilt after each turnover by cysteine desulfurases and iron-sulfur cluster assembly proteins, conferring true catalytic capability to BioB. Although the 2Fe-2S cluster is buried, the movement of R95 and/or Y149 could open access to the 2Fe-2S cluster from the bottom of the barrel. Thus, the cluster may be destroyed from the top of the TIM barrel and rebuilt from the bottom. It would not be unexpected to find that BioB requires proteins and other components to restore its activity after turnover. The requirement of chaperones and reactivases to repair inactivated AdoCbl-dependent radical enzymes is well documented⁵¹.

3.5. Tables

Table 3.1. Maximal BioB activity						
<i>Cofactor content</i>			Source	Mol biotin produced/ mol BioB monomer	Time (h)	Reference
2Fe-2S	4Fe-4S	PLP				
1	1	0	<i>E. coli</i>	1	4	16
1	1	0	<i>E. coli</i>	1	24	22
0	1	1	<i>E. coli</i>	1	4	20
ND ¹	ND ¹	ND ¹	<i>Arabidopsis</i>	7	6	52

¹Not determined

Table 3.2. BioB Data collection and refinement statistics

Wavelength (Å)	Resolution range (Å)	Unique reflections	Redundancy	Completeness (%)	I/sigma(I)	R_{sym}^1
1.30000	100 - 3.7	26,018	3.4	99.5 (100.0)	11.8 (2.3)	6.7 (37.5)
1.73827	100 - 4.1	19,002	3.1	98.3 (99.7)	14.6 (1.9)	6.4 (29.7)
1.74150	100 - 4.5	14,030	2.8	97.1 (95.7)	14.0 (2.6)	8.2 (36.7)
1.100001 ²	100 - 3.4	17,465	5.4	98.1 (87.9)	15.79 (3.78)	6.6 (25.9)
Non-hydrogen atoms in ASU				4,984		
Resolution range (Å)				44.5 - 3.4		
Number of reflections (working set / test set)				16,222 / 1242		
$R_{\text{work}} (\%)^2$				25.6		
$R_{\text{free}} (\%)$				30.0		
RMS deviations of protein from ideal geometry						
Bonds (Å)				0.009		
Angles (°)				2.3		
				Molecule A	Molecule B	
Overall B (Å ²) (all atoms)				87.8	93.3	
Group B (Å ²)						
AdoMet						
Methionine				130.5	146.3	
Ribose				84.6	84.6	
Adenine				68.3	88.6	
Dethiobiotin				47.4	61.8	
4Fe-4S				50.8	71.0	
2Fe-2S				35.7	43.0	

Values in parentheses are for the highest-resolution shell. $^1R_{\text{sym}} = [\sum_{hkl} \sum_i |I_i(hkl) - \langle I(hkl) \rangle|] / \sum_{hkl} \sum_i I_i(hkl)$ for hkl independent reflections and i observations of a given reflection, with no σ cutoff. $\langle I(hkl) \rangle$ is the mean intensity of the miller index (hkl). ²For this wavelength, Friedel pairs were merged during data processing. $^3R_{\text{work}} = \sum_{hkl} ||F_o(hkl)| - |F_c(hkl)|| / \sum_{hkl} |F_o(hkl)|$. No σ cutoff was used in the refinement. $R_{\text{free}} = R_{\text{work}}$ for a test set of reflections not included in refinement.

Table 3.3. Metal-nitrogen (guanidine) distances from crystallographic structures of metal-guanidine complexes.

Metal (M)	N-M distance (Å)	Reference
Pt ^{II}	2.06	39
Pt ^{II}	2.07	39
Pt ^{II}	2.018	40
Co ^{III}	1.94	39
Zn ^{II}	1.95	38
Fe ^{III}	~2.3-2.4	This work

Table 3.4. Fe-S cluster-ligand distances¹.

Atom	Contacting residue	Contacting atom	distance (Å)
2Fe-2S			
Fe1	Cys 188	SG	2.3
	Arg 260	NH1	~2.3-2.4
Fe2	Cys 97	SG	2.2
	Cys 128	SG	2.2
4Fe-4S			
Fe1	Cys 57	SG	2.2
Fe2	AdoMet	O	~3.2
	AdoMet	N	~2.4
Fe3	Cys 60	SG	2.2
Fe4	Cys 53	SG	2.2

¹At our current resolution limit of 3.4 Å, distances are not precisely known.

Table 3.5. Electrostatic interactions and potential hydrogen bonds between BioB and AdoMet¹.

AdoMet Atom	Contacting residue	Contacting atom	distance (Å)
Methionine			
OXT	Arg 173	NH2	2.8
O	Arg 173	NH2	3.2
N	Ala 100	O	3.2
N	Trp 102	O	3.5
Ribose			
O3*	Asn 153	ND2	3.5
O3*	Asp 155	OD1	3.5
O2*	Asn 153	ND2	3.5
O2*	Asp 155	OD1	2.8
Adenine			
N1	Val 225	N	2.9
N6	Val 225	O	3.2
	Tyr 59	O	3.3

¹At our current resolution limit of 3.4 Å, distances are not precisely known.

Table 3.6. Potential hydrogen bonds between BioB and DTB¹.

DTB Atom	Contacting residue	Contacting atom	distance (Å)
Carboxylate			
OI2	Thr 292	N	3.1
OI2	Thr 292	OG1	2.8
OI2	Thr 293	N	3.0
Ureido ring			
O	Asn 222	ND2	2.9
O	Asn 153	ND2	3.7
N1	Asn 151	OD1	3.7
N2	Asn 222	OD1	2.8

¹At our current resolution limit of 3.4 Å, distances are not precisely known.

3.6. Figures

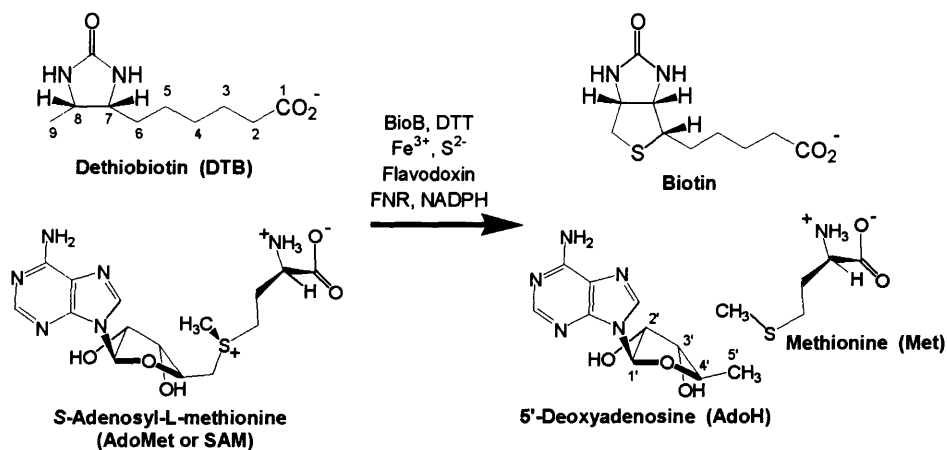


Figure 3.1. Overall reaction of BioB. BioB reconstituted anaerobically with Fe³⁺ and S²⁻ in the presence of DTT requires flavodoxin, flavodoxin/NADPH oxidoreductase (FNR), and NADPH to convert DTB to biotin. Numbering schemes for DTB and AdoH are shown. The number of equivalents of AdoMet required for the reaction is disputed (see text).

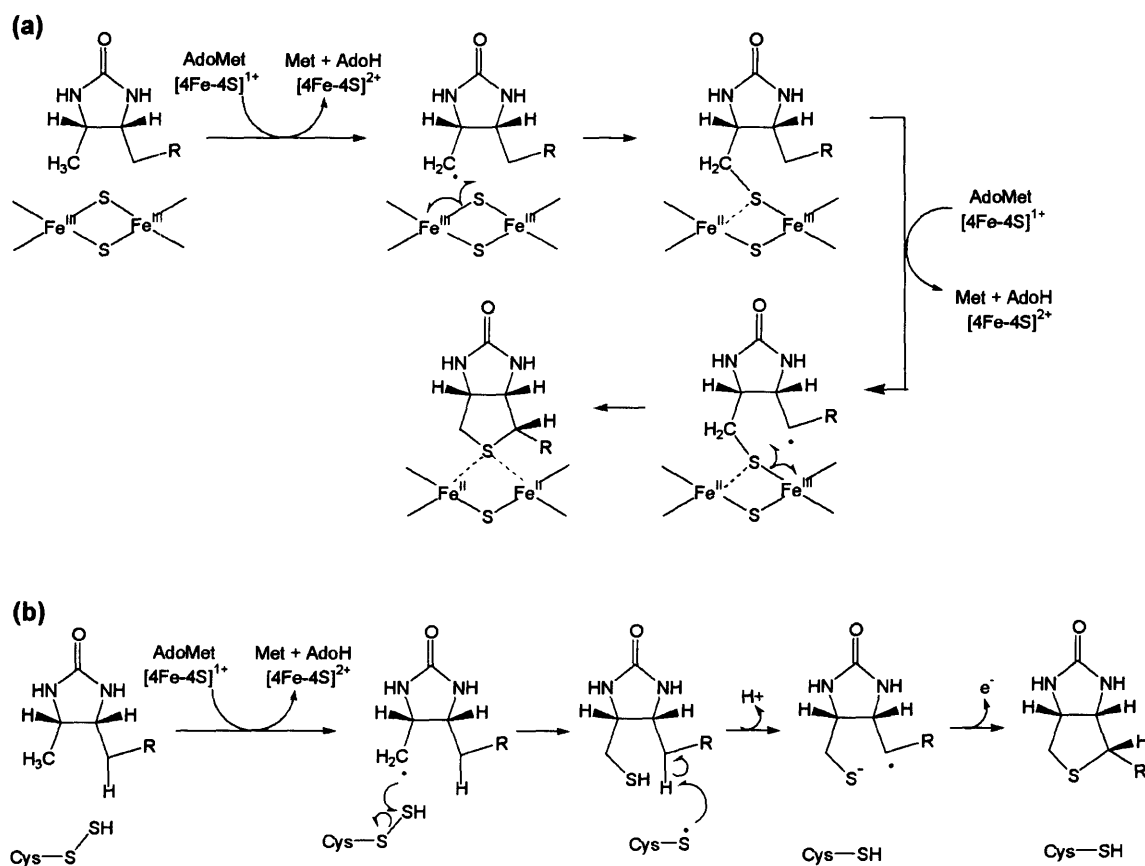


Figure 3.2. Mechanisms proposed for the BioB reaction. **(a)** Mechanism put forth by Jarrett and coworkers¹⁶, which requires two equivalents of AdoMet and a 2Fe-2S cluster that is intrinsic to BioB. **(b)** Mechanism proposed by Fontecave and coworkers, which requires one equivalent of AdoMet, a Cys persulfide generated from one equivalent of Cys by a PLP-dependent Cys desulfurase activity of BioB, the presence of a thiyl radical, and an external electron acceptor²⁰.

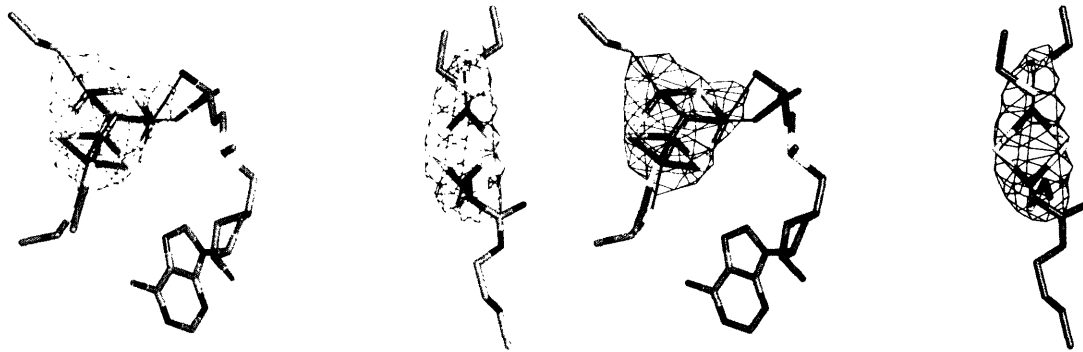


Figure 3.3. Stereo figure showing the electron density of the Fe-S clusters of BioB. The map shown is the experimental map, after solvent flattening and two-fold NCS averaging, at 3.7 Å resolution. The map is contoured around the clusters at 3.0 σ . All of the cluster ligands (see text) are shown. The atomic coloring scheme is: grey, C; red, O; blue, N; yellow, S; brown, Fe.

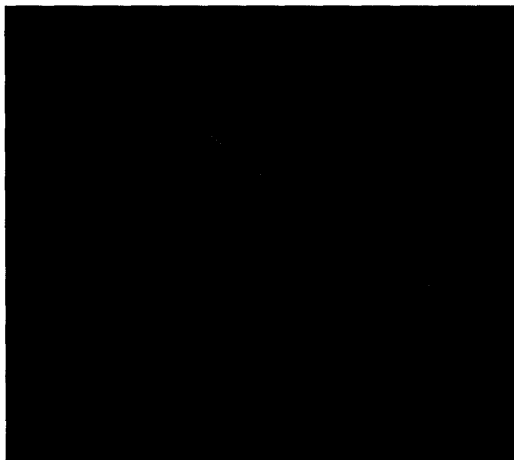


Figure 3.4. Solvent flattened, two-fold NCS-averaged experimental electron density of Trp 7, contoured at 1 σ . This electron density map (3.7 Å resolution) was used to build the initial model. Figure prepared with O²⁶.

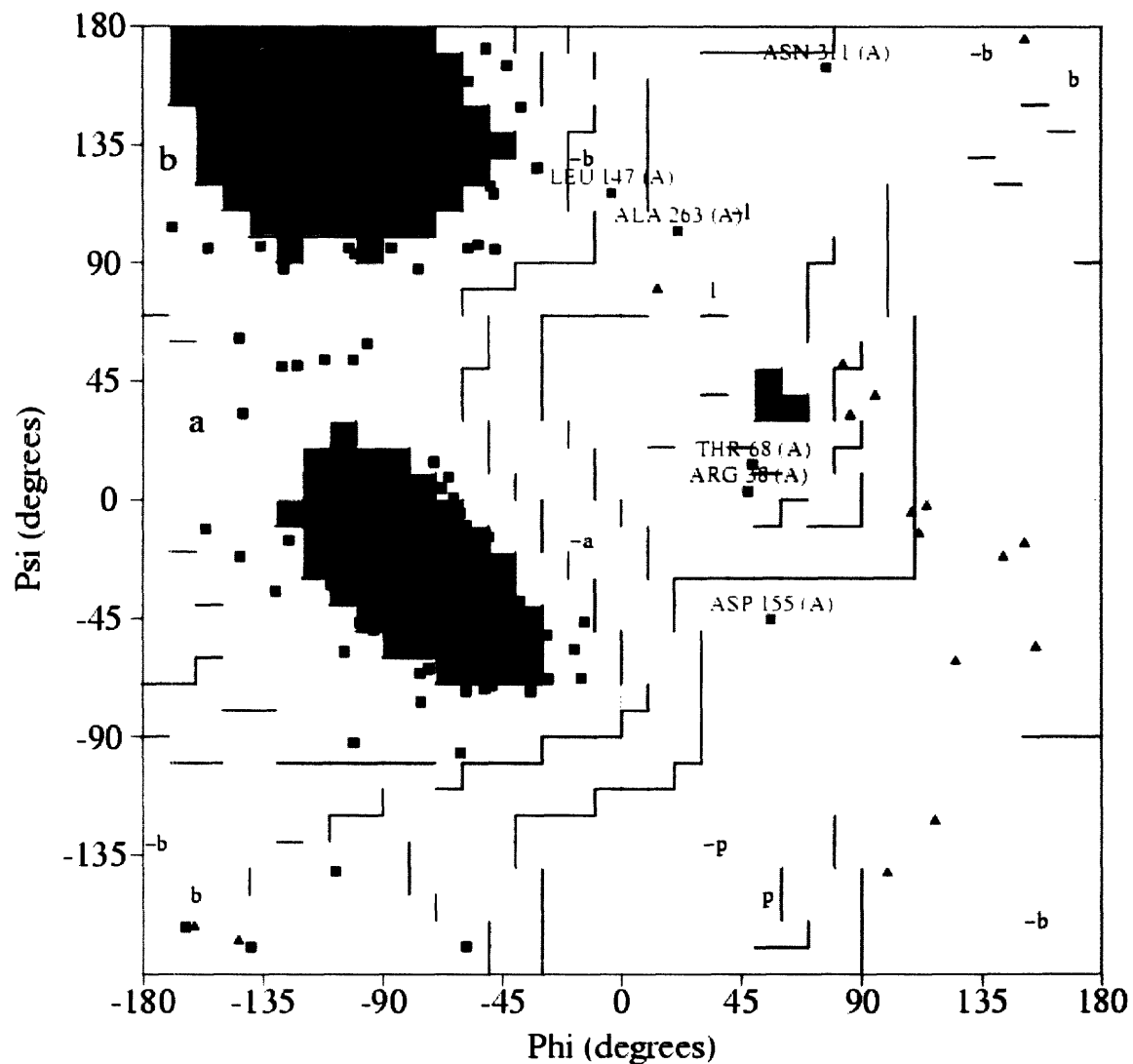


Figure 3.5. Ramachandran plot of the BioB monomer. The plot is colored as follows: red, most favored regions; yellow, additional allowed regions; light yellow, generously allowed regions; white, disallowed regions. Glycine residues are shown as triangles. Figure made using PROCHECK²⁹.

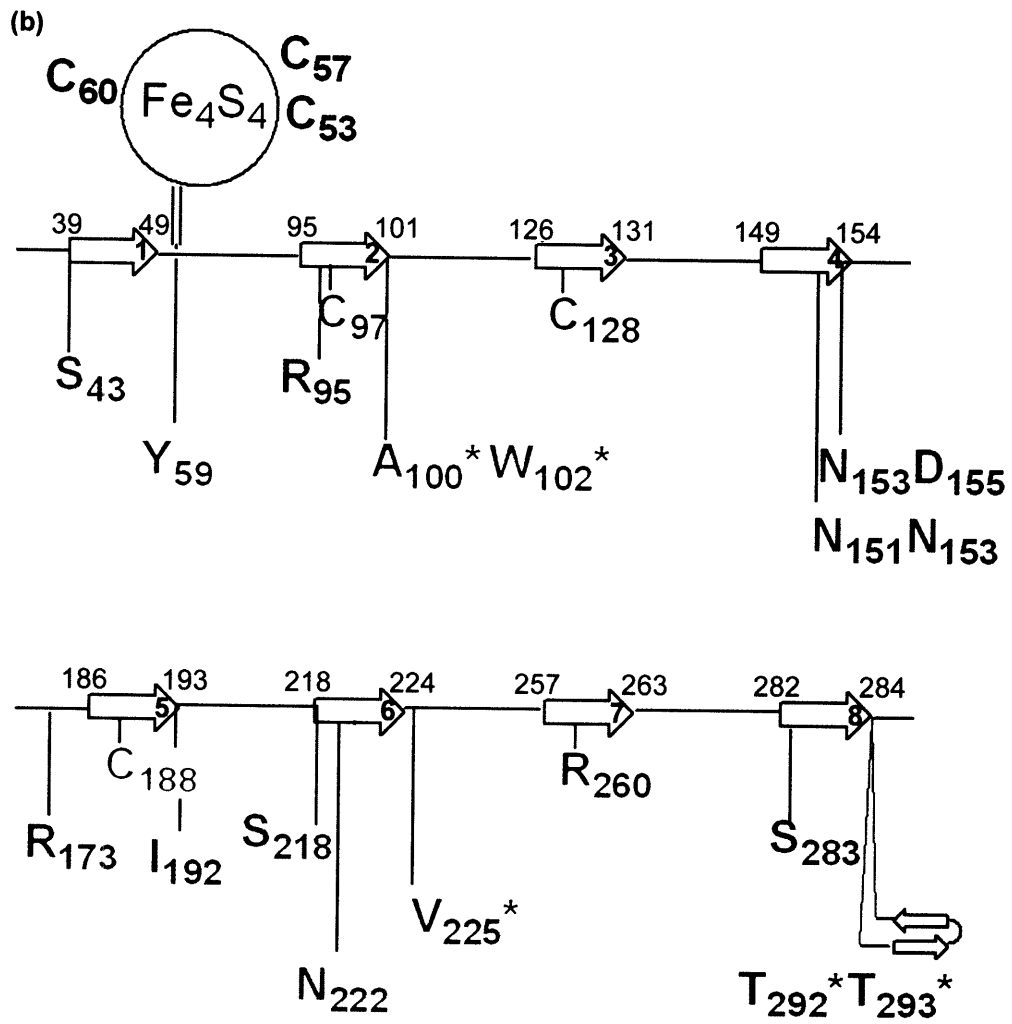
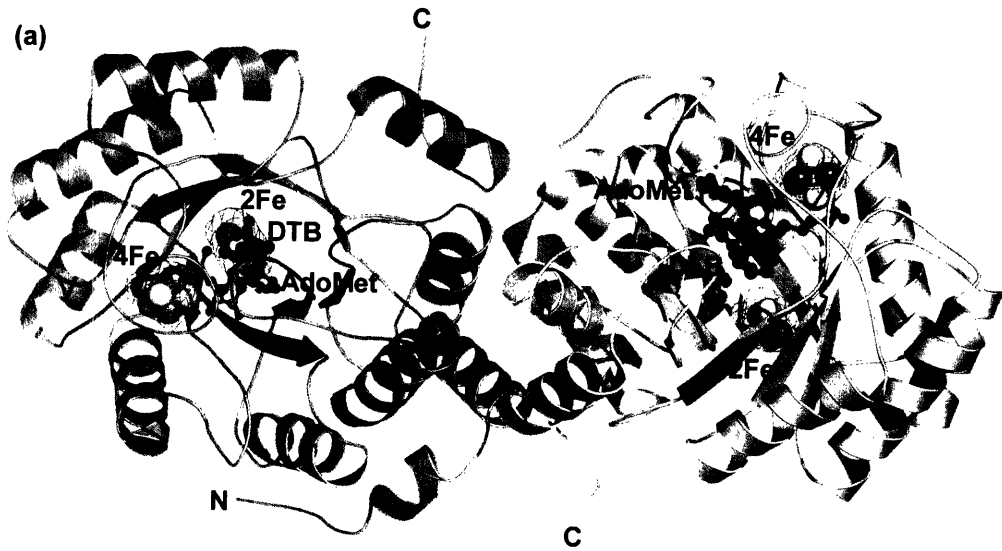


Figure 3.6. Overall structure of BioB. **(a)** Structure of the BioB dimer. BioB exists as a homodimer in solution¹². We find two possible dimeric relationships between BioB monomers in the crystal. The dimer shown here buries 17.6% of the monomer surface area (13,249 Å², see Fig. 3.8) and is likely to be physiologically relevant. An anomalous Fourier electron density map, calculated with data collected at the Fe absorption peak wavelength (1.73827 Å) and phases from the polypeptide portion of the model, is contoured at 3 σ in green mesh. These electron density peaks represent the positions of the four Fe-S clusters in this dimeric structure. There are no other features of similar size in the electron density map. The Fe-S cluster atoms are shown as large spheres, with brown Fe atoms and yellow S atoms. We observe one AdoMet (red) and one DTB (black) per subunit. All cartoon and ball-and-stick figures were prepared with PyMOL⁵³, unless otherwise noted. **(b)** Topology diagram of the BioB TIM barrel showing the location of important residues with respect to the β -strands (shown as arrows, numbered 1-8). The numbers above and to the left of each β -strand correspond to the N-terminal residue of that strand; those above and to the right of the beta strands correspond to the C-terminal residue. Ligands to the 4Fe-4S cluster are in black, ligands to the 2Fe-2S cluster are in red, and residues that contact the 2Fe-2S cluster ligand R260 are in green. AdoMet contacts (blue) include A100, W102, and R173, which hydrogen bond to the amino acid moiety; D155 and N153, which hydrogen bond to the ribose hydroxyl groups; Y59 and I192 which stack against the adenine ring; and V225 which forms backbone hydrogen bonds to the adenine ring. Residues in position to hydrogen bond to DTB (brown) include N151, N153, and N222, which contact the DTB ureido ring, T292 and T293, which contact the carboxylate tail. Asterisks (*) denote main-chain interactions.

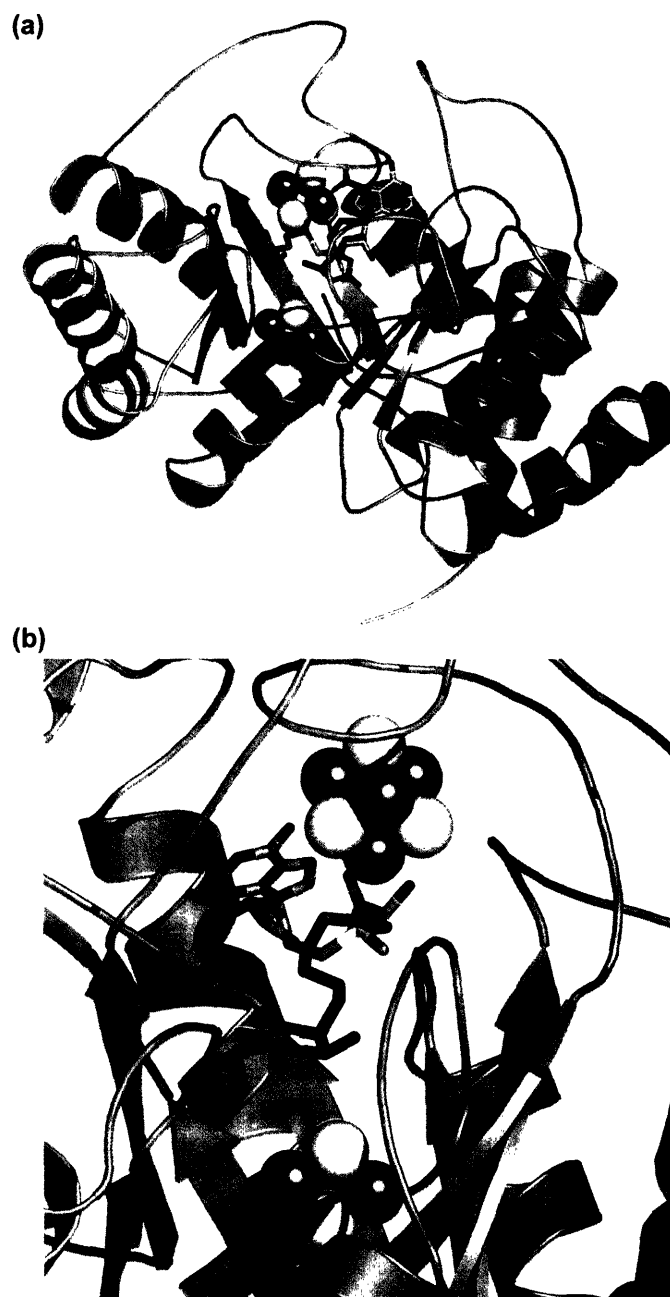


Figure 3.7. The BioB monomer. **(a)** Structure of the BioB monomer. The color scheme is: red, O; blue, N; yellow, S, brown, Fe. AdoMet carbon atoms are grey; DTB carbons are black. **(b)** A view of the active site.

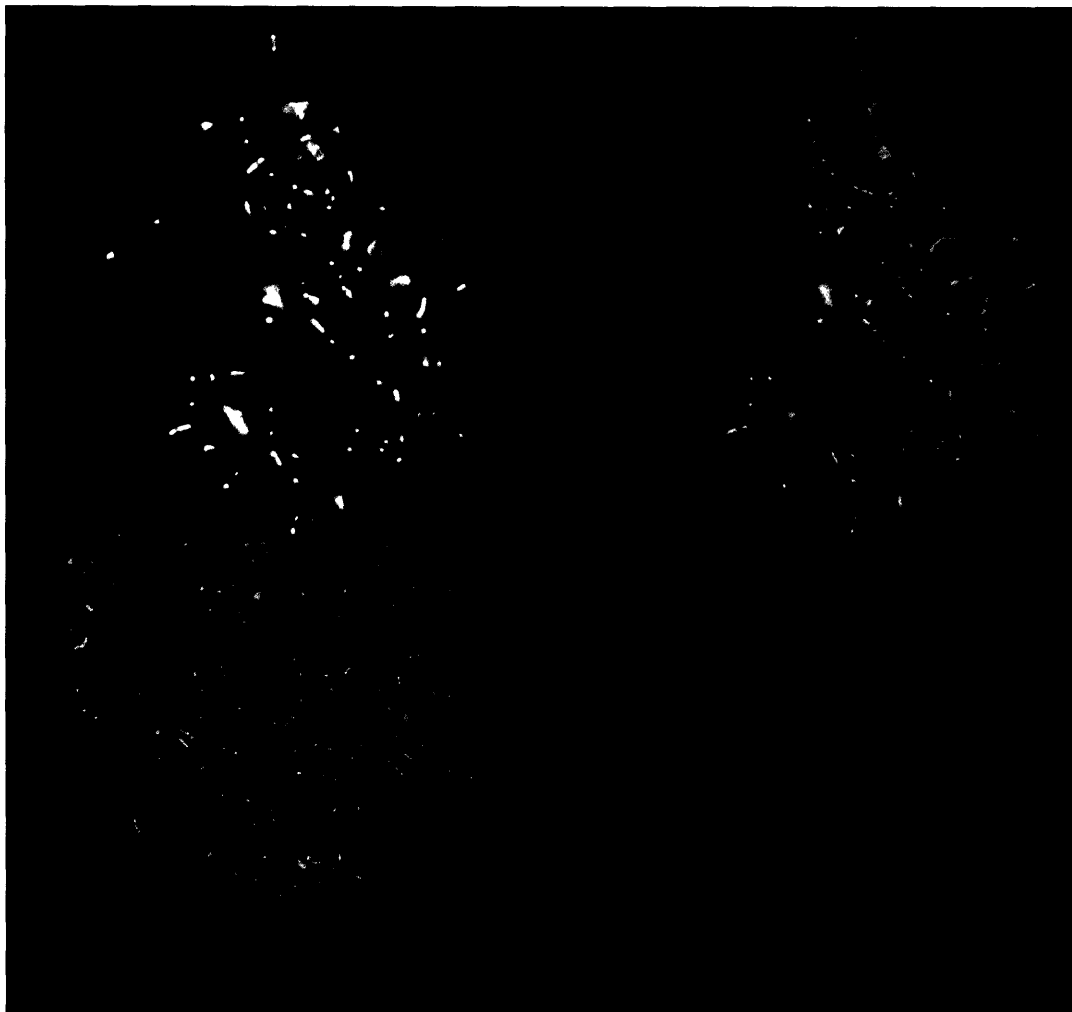


Figure 3.8. Space filling model of BioB. Stereo figure showing the two subunits of BioB, colored in red and blue.

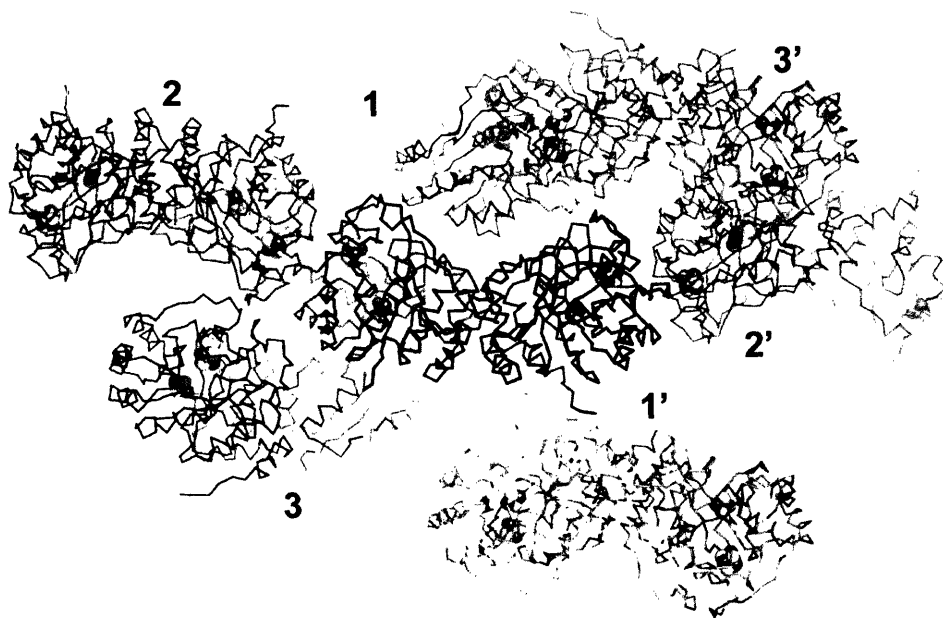


Figure 3.9. Lattice packing in BioB crystals. Each BioB homodimer is shown in a different color and drawn as an alpha carbon trace. Fe-S clusters are shown in brown (Fe) and yellow (S). The BioB homodimer contacts six neighboring molecules in the crystal. One of the BioB subunits, shown here in black, contacts a portion of homodimers 1, 2, and 3; the other subunit, also shown in black, contacts a portion of homodimers 1', 2', and 3'.

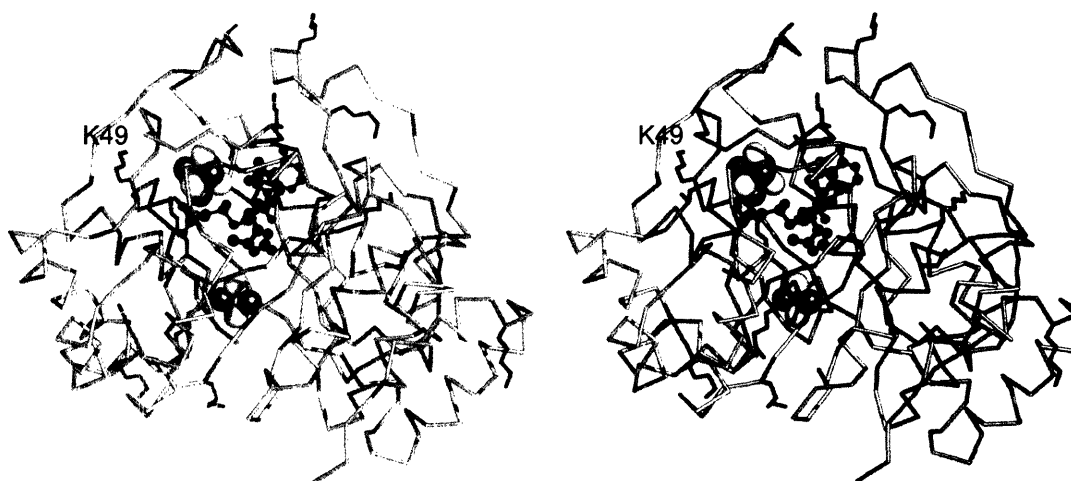


Figure 3.10. Stereo alpha carbon trace of a single BioB subunit, showing the locations of all Lys residues in the structure. The coloring scheme is the same as that of Fig. 3.3a, but Lys sidechains are colored in purple (C) and dark blue (N ϵ). In some cases, the Lys sidechain was truncated due to poor electron density. K49, the only highly conserved Lys residue in BioB, is labeled. All Lys residues are solvent-accessible and far-removed from the active site.

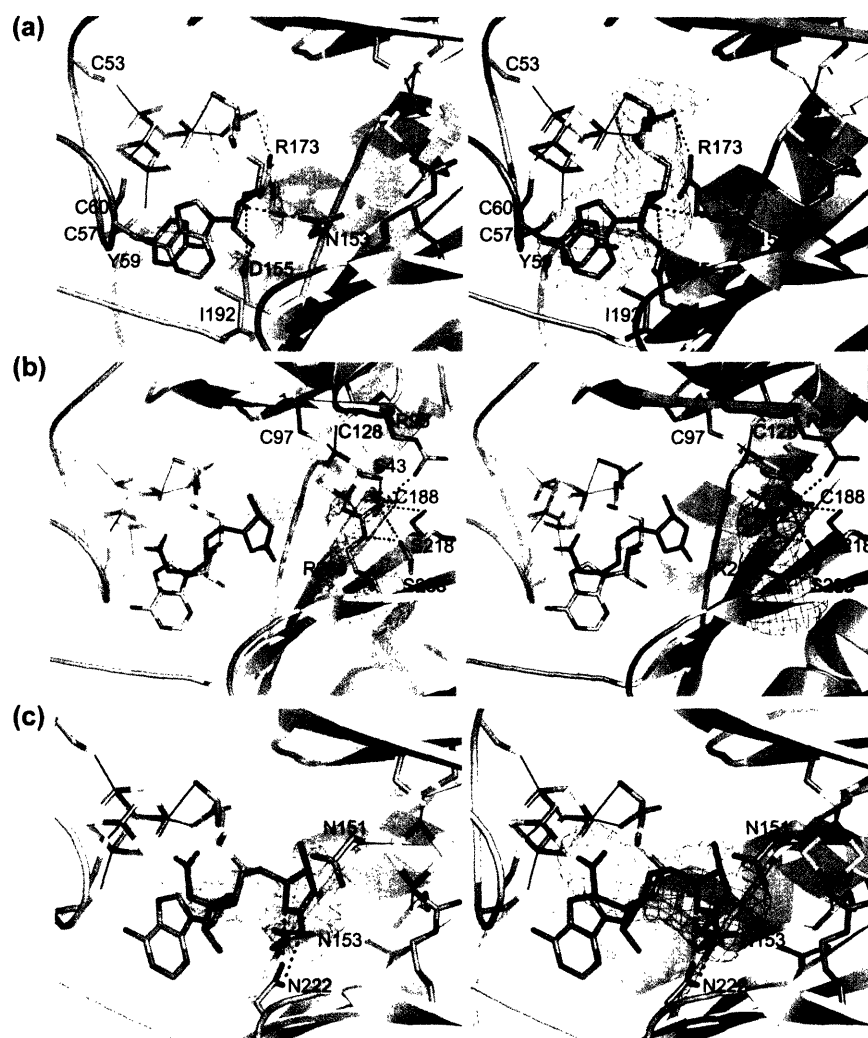


Figure 3.11. The BioB active site. **(a)** Stereo view of the 4Fe-4S cluster with AdoMet bound. Conserved side-chain contacts between BioB and AdoMet are indicated, and AdoMet is shown in a simulated annealing omit map contoured at 4.5σ (orange). DTB is omitted for clarity. The coloring scheme is: grey, C; red, O; blue, N; yellow, S, brown, Fe. **(b)** Stereo view of the active site, focusing on the 2Fe-2S cluster and its ligands. The unusual R260 ligand is shown in a simulated annealing omit map contoured at 4.5σ . In addition to the 2Fe-2S cluster, R260 interacts with S43, S218, S283, and R95. Also shown are the positions of the 4Fe-4S cluster, AdoMet, and DTB with respect to the 2Fe-2S cluster. **(c)** Stereo view of DTB interacting with AdoMet and conserved residues N222, N151, and N153 in the active site. Potential hydrogen bonds between N222 and DTB are drawn as dashed lines. The stacking of the carboxylate tail of DTB and the adenine ring of AdoMet is visible in this orientation, although contacts of the DTB carboxylate to T292 and T293 are not (Fig. 3.15). DTB is shown in a simulated annealing omit map contoured at 4.0σ .

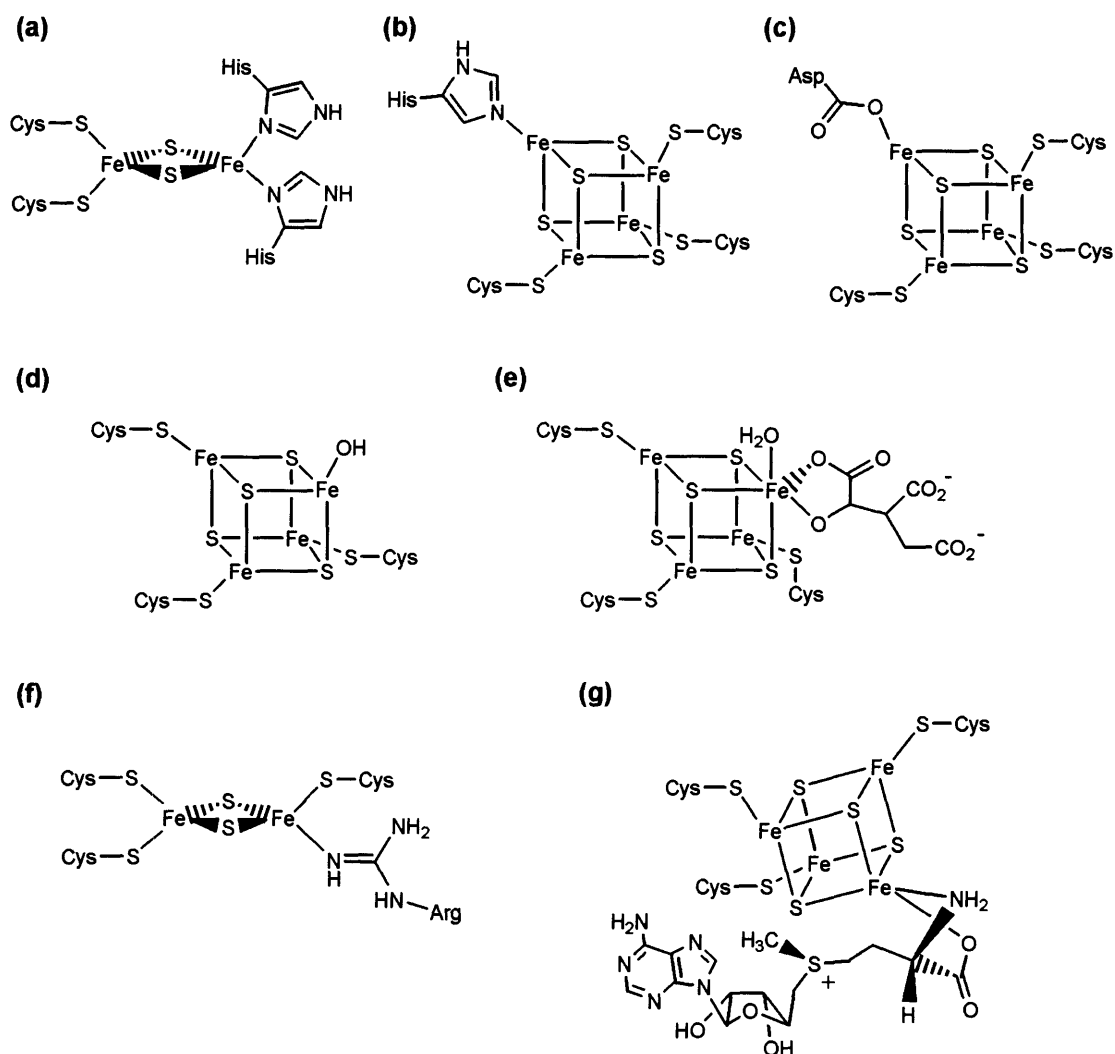


Figure 3.12. 2Fe-2S and 4Fe-4S clusters with incomplete cysteinyl ligation. (a) The Rieske protein 2Fe-2S cluster⁵⁴ (b) 4Fe-4S cluster of the Fe-only hydrogenase from *C. pasteurianum*. (c) 4Fe-4S cluster of the ferredoxin from *P. furiosus*⁵⁵. (d) and (e) 4Fe-4S cluster of aconitase in the resting state and with product bound, respectively^{55,56}. (f) 2Fe-2S cluster from BioB, as determined in this study. The protonation of the Arg sidechain is inferred by analogy to small molecule metal-guanidine complexes (see Fig. 3.13), but the true protonation state remains in question. (g) 4Fe-4S cluster from BioB, also from this study.

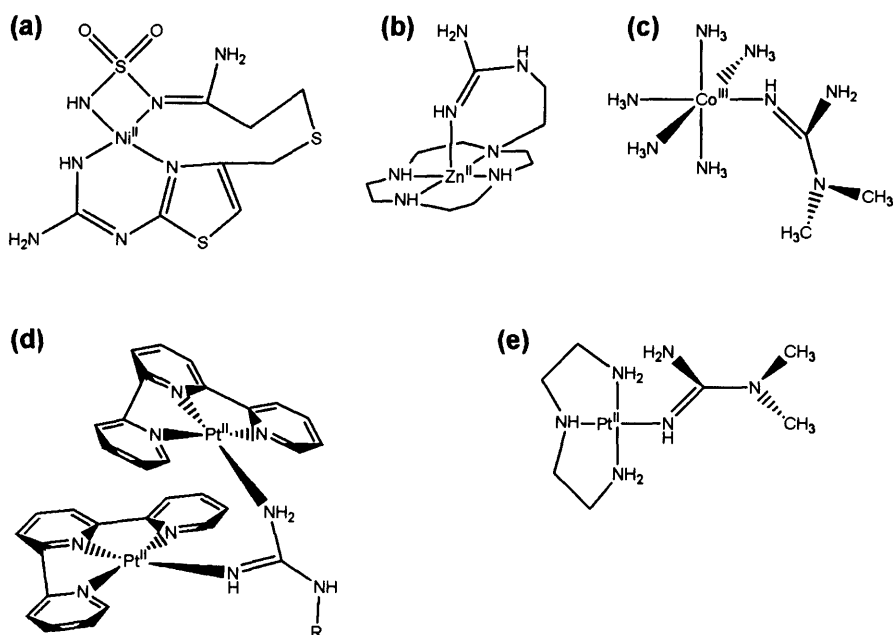


Figure 3.13. Structures of aqueous metal complexes with guanidine or guanidine-like ligands. (a) Structure of a Ni^{II}-famotidine complex, proposed from spectroscopic studies⁴⁶. (b) Crystallographic structure of a Zn^{II} complex with a guanidine ligand⁴⁷. (c) Crystallographic structure of a Co^{III} complex with a guanidine ligand⁴⁸. (d) and (e) Crystallographic structures of Pt^{II} complexes with guanidine ligands^{48,49}.

BioB	53-CPEDCK YC	192- IVGLGE
LipA	94-CTRRC FC	217- MVGLGE
KamA	125-CSMYCR HC	262- LRGVND
PflA	30-CLMRCL YC	171- VPGWSD

Figure 3.14. Conservation of residues across the AdoMet radical enzymes. Enzymes are denoted by their corresponding gene names (BioB, *E. coli* biotin synthase; LipA, *E. coli* lipoyl synthase; KamA, *C. subterminale* lysine 2,3-aminomutase; PflA, *E. coli* PFL activase). Absolutely conserved residues, including the CxxxCxxC motif that ligates the 4Fe-4S cluster, are shown in bold red typeface. Bold black typeface denotes similar residues. Y59 in BioB, which forms π -stacking interactions with AdoMet, corresponds to an aromatic residue in the other enzymes. I192 forms van der Waal contacts to AdoMet and corresponds to a hydrophobic residue in the other enzymes.

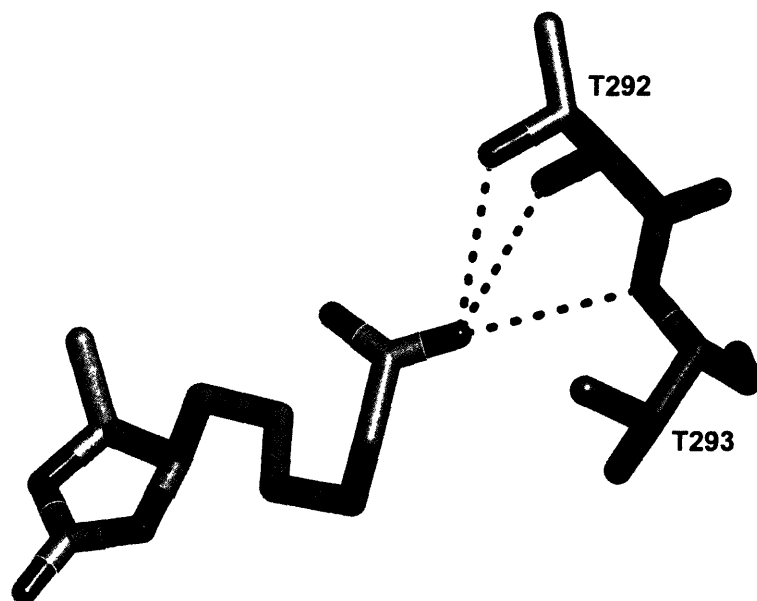


Figure 3.15. The carboxylate tail of DTB interacting with residues T292 and T293. These two residues are part of the loop that follows β strand 8 of the TIM barrel. The coloring scheme is: grey, C; blue, N; red, O.

3.7. References

1. Sofia, H.J., Chen, G., Hetzler, B.G., Reyes-Spindola, J.F. & Miller, N.E. Radical SAM, a novel protein superfamily linking unresolved steps in familiar biosynthetic pathways with radical mechanisms: functional characterization using new analysis and information visualization methods. *Nucleic Acids Res.* **29**, 1097-1106 (2001).
2. Krebs, C., Broderick, W.E., Henshaw, T.F., Broderick, J.B. & Huynh, B.H. Coordination of adenosylmethionine to a unique iron site of the [4Fe-4S] of pyruvate formate-lyase activating enzyme: A mossbauer spectroscopic study. *Journal of the American Chemical Society* **124**, 912-913 (2001).
3. Walsby, C.J., Ortillo, D., Broderick, W.E., Broderick, J.B. & Hoffman, B.M. An anchoring role for FeS clusters: chelation of the amino acid moiety of *S*-adenosylmethionine to the unique iron site of the [4Fe-4S] cluster of pyruvate formate-lyase activating enzyme. *Journal of the American Chemical Society* **124**, 11270-11271 (2002).
4. Coper, M.M. et al. The [4Fe-4S]²⁺ cluster in reconstituted biotin synthase binds *S*-adenosylmethionine. *Journal of the American Chemical Society* **124**, 14006-14007 (2002).
5. Chen, D., Walsby, C.J., Hoffman, B.M. & Frey, P.A. Coordination and mechanism of reversible cleavage of *S*-adenosylmethionine by the [4Fe-4S] center in lysine 2,3-aminomutase. *Journal of the American Chemical Society* **125**, 11788-11789 (2003).
6. Berkovitch, F., Nicolet, Y., Wan, J.T., Jarrett, J.T. & Drennan, C.L. Crystal structure of biotin synthase, an *S*-adenosylmethionine-dependent radical enzyme. *Science* **303**, 76-79 (2004).
7. Escalletes, F., Florentin, D., Tse Sum Bui, B., Lesage, D. & Marquet, A. Biotin Synthase Mechanism: Evidence for Hydrogen Transfer from the Substrate into Deoxyadenosine. *Journal of the American Chemical Society* **121**, 3571-3578 (1999).
8. Benda, R. et al. Iron-Sulfur Clusters of Biotin Synthase In Vivo: A Mossbauer Study. *Biochemistry* **41**, 15000-15006 (2002).
9. Duin, E.C. et al. [2Fe-2S] to [4Fe-4S] cluster conversion in *Escherichia coli* biotin synthase. *Biochemistry* **36**, 11811-11820 (1997).
10. Ollagnier-de Choudens, S. et al. Iron-sulfur center of biotin synthase and lipoate synthase. *Biochemistry* **39**, 4165-4173 (2000).
11. Ollagnier-de Choudens, S., Mulliez, E., Hewiston, K.S. & Fontecave, M. Biotin synthase is a pyridoxal phosphate-dependent cysteine desulfurase. *Biochemistry* **41**, 9145-9152 (2002).
12. Sanyal, I., Cohen, G. & Flint, D.H. Biotin synthase: purification, characterization as a [2Fe-2S] cluster protein, and in vitro activity of the *Escherichia coli bioB* gene product. *Biochemistry* **33**(1994).
13. Tse Sum Bui, B., Florentin, D., Marquet, A., Benda, R. & Trautwein, A.X. Mossbauer studies of *Escherichia coli* biotin synthase: evidence for reversible

- interconversion between $[2\text{Fe-2S}]^{2+}$ and $[4\text{Fe-4S}]^{2+}$ clusters. *Federation of European Biochemical Societies Letters* **459**, 411-414 (1999).
14. Ugulava, N.B., Gibney, B.R. & Jarrett, J.T. Biotin synthase contains two distinct iron-sulfur cluster binding sites: chemical and spectroelectrochemical analysis of iron-sulfur interconversions. *Biochemistry* **40**, 8343-8351 (2001).
 15. Ugulava, N.B., Surerus, K.K. & Jarrett, J.T. Evidence from Mossbauer spectroscopy for distinct $[2\text{Fe-2S}](2+)$ and $[4\text{Fe-4S}](2+)$ cluster binding sites in biotin synthase from *Escherichia coli*. *J. Am. Chem. Soc.* **124**, 9050-1 (2002).
 16. Ugulava, N.B., Sacanell, C.J. & Jarrett, J.T. Spectroscopic Changes during a Single Turnover of Biotin Synthase: Destruction of a $[2\text{Fe-2S}]$ Cluster Accompanies Sulfur Insertion. *Biochemistry* **40**, 8352-8358 (2001).
 17. Tse Sum Bui, B. et al. Biotin synthase mechanism: on the origin of sulphur. *Federation of European Biochemical Societies Letters* **440**, 226-230 (1998).
 18. Tse Sum Bui, B. et al. Fate of the $(2\text{Fe-2S})^{2+}$ Cluster of *Escherichia coli* Biotin Synthase during Reaction: A Mössbauer Characterization. *Biochemistry* **42**, 8791-8798 (2003).
 19. Florentin, D., Bui, B.T., Marquet, A., Ohshiro, T. & Izumi, Y. On the mechanism of biotin synthase of *Bacillus sphaericus*. *Comptes Rendus de L Academie des Sciences Serie III - Sciences de la Vie* **317**, 485-488 (1994).
 20. Ollagnier-de Choudens, S., Mulliez, E. & Fontecave, M. The PLP-dependent biotin synthase from *Escherichia coli*: mechanistic studies. *Federation of European Biochemical Societies Letters* **532**, 465-468 (2002).
 21. Cospers, M.M. et al. Characterization of the cofactor composition of *Escherichia coli* biotin synthase. *Biochemistry* **43**, 2007-2021 (2004).
 22. Jameson, G.N., Cospers, M.M., Hernandez, H.L., Johnson, M.K. & Huynh, B.H. Role of the $[2\text{Fe-2S}]$ cluster in recombinant *Escherichia coli* biotin synthase. *Biochemistry* **43**, 2022-2031 (2004).
 23. Terwilliger, T.C. & Berendzen, J. Automated structure solution for MIR and MAD. *Acta Crystallographica* **D55**, 849-861 (1999).
 24. Kabsch, W. A solution for the best rotation to relate two sets of vectors. *Acta Crystallographica* **A32**, 922-923 (1976).
 25. Cowtan, K.D. & Zhang, K.Y.J. Density modification for macromolecular phase improvement. *Progress in Biophysics and Molecular Biology* **72**, 245-270 (1999).
 26. Jones, T.A., Zou, J.-Y., Cowan, S.W. & Kjeldgaard, M. Improved methods for building protein models in electron density maps and the location of errors in these models. *Acta Crystallographica* **A47**, 110-119 (1991).
 27. Brunger, A.T. et al. Crystallography & NMR system: A new software suite for macromolecular structure determination. *Acta Crystallographica* **D55**, 905-921 (1998).
 28. Collaborative Computational Project Number 4. The CCP4 suite: programs for protein crystallography. *Acta Crystallographica* **D50**, 760-763 (1994).
 29. Laskowski, R.A., MacArthur, M.W., Moss, D.S. & Thornton, J.M. PROCHECK: a program to check the stereochemical quality of protein structures. *Journal of Applied Crystallography* **26**, 283-291 (1993).
 30. Layer, G., Moser, J., Heinz, D.W., Jahn, D. & Schubert, W.D. Crystal structure of coproporphyrinogen III oxidase reveals cofactor geometry of Radical SAM

- enzymes. *European Molecular Biology Organization Journal* **22**, 6214-6224 (2003).
31. Murzin, A.G., Brenner, S.E., Hubbard, T. & Chothia, C. SCOP: a structural classification of proteins database for the investigation of sequences and structures. *Journal of Molecular Biology* **247**, 536-540 (1995).
 32. Cospers, M.M., Jameson, G.N.L., Eidsness, M.K., Huynh, B.H. & Johnson, M.K. Recombinant *Escherichia coli* biotin synthase is a [2Fe-2S]²⁺ protein in whole cells. *Federation of European Biochemical Societies Letters* **529**, 332-336 (2002).
 33. Hewitson, K.S., Baldwin, J.E., Shaw, N.M. & Roach, P.L. Mutagenesis of the proposed iron-sulfur cluster binding ligands in *Escherichia coli* biotin synthase. *Federation of European Biochemical Societies Letters* **466**, 372-376 (2000).
 34. Ollagnier-de Choudens, S., Sanakis, Y., Hewitson, K.S., Roach, P. & Munck, E. Reductive cleavage of *S*-Adenosylmethionine by biotin synthase from *Escherichia coli*. *Journal of Biological Chemistry* **277**, 13449-13454 (2002).
 35. Ugulava, N.B., Gibney, B.R. & Jarrett, J.T. Iron-Sulfur cluster Interconversion in Biotin Synthase: Dissociation and Reassociation of Iron during Conversion of [2Fe-2S] to [4Fe-4S] Clusters. *Biochemistry* **39**, 5206-5214 (2000).
 36. Tse Sum Bui, B. et al. Fate of the (2Fe-2S)²⁺ cluster of *Escherichia coli* biotin synthase during reaction: a Mossbauer characterization. *Biochemistry* **42**, 8791-8798 (2003).
 37. Hewitson, K.S. et al. The iron-sulfur center of biotin synthase: site-directed mutants. *Journal of Biological Inorganic Chemistry* **7**, 83-93 (2002).
 38. Cospers, M.M. et al. The [4Fe-4S]₂⁺ cluster in reconstituted biotin synthase binds *S*-adenosyl-L-methionine. *J. Am. Chem. Soc.* **124**, 14006-14007 (2002).
 39. Liu, A. & Graslund, A. Electron paramagnetic resonance evidence for a novel interconversion of [3Fe-4S](+) and [4Fe-4S](+) clusters with endogenous iron and sulfide in anaerobic ribonucleotide reductase activase in vitro. *J. Biol. Chem.* **275**, 12367-73 (2000).
 40. Padovani, D., Thomas, F., Trautwein, A.X., Mulliez, E. & Fontecave, M. Activation of class III ribonucleotide reductase from *E. coli*. The electron transfer from the iron-sulfur center to *S*-adenosylmethionine. *Biochemistry* **40**, 6713-9 (2001).
 41. Cospers, M.M. et al. Structural studies of the interaction of *S*-adenosylmethionine with the [4Fe-4S] clusters in biotin synthase and pyruvate formate-lyase activating enzyme. *Protein Science* **12**, 1573-1577 (2003).
 42. Schubert, H.L., Blumenthal, R.M. & Cheng, X. Many paths to methyltransfer: a chronicle of convergence. *Trends in Biochemical Sciences* **28**, 329-335 (2003).
 43. Hoffman, J.L. Chromatographic analysis of the chiral and covalent instability of *S*-adenosyl-L-methionine. *Biochemistry* **25**, 4444-4449 (1986).
 44. de la Haba, G., Jamieson, G.A., Harvey Mudd, S. & Richards, H.H. *S*-adenosylmethionine: the relation of configuration at the sulfonium center to enzymatic reactivity. *Journal of the American Chemical Society* **81**, 3975-3980 (1959).
 45. Ugulava, N.B., Frederick, K.K. & Jarrett, J.T. Control of Adenosylmethionine-Dependent Radical Generation in Biotin Synthase: A Kinetic and Thermodynamic

- Analysis of Substrate Binding to Active and Inactive Forms of BioB. *Biochemistry* **42**, 2708-2719 (2003).
46. Baranska, M., Gumienna-Kontecka, E., Kozlowski, H. & Proniewicz, L.M. A study on the nickel(II)-famotidine complexes. *Journal of Inorganic Biochemistry* **92**, 112-120 (2002).
 47. Aoki, S., Iwaida, K., Hanamoto, N., Shiro, M. & Kimura, E. Guanidine is a Zn²⁺-binding ligand at neutral pH in aqueous solution. *Journal of the American Chemical Society* **124**, 5256-5257 (2002).
 48. Fairlie, D.P. et al. Models for Arginine-Metal Binding. Synthesis of Guanidine and Urea Ligands through Amination and Hydration of a Cyanamide Ligand Bound to Platinum (II), Osmium (III), and Cobalt (III). *Inorganic Chemistry* **36**, 1020-1028 (1997).
 49. Ratilla, E.M.A., Scott, B.K., Moxness, M.S. & Kostic, N.M. Terminal and new bridging coordination of methylguanidine, arginine, and canavanine to platinum(II). The first crystallographic study of bonding between a transition metal and a guanidine ligand. *Inorganic Chemistry* **29**, 918-926 (1990).
 50. Wilson, K.P., Shewchuk, L.M., Brennan, R.G., Otsuka, A.J. & Matthews, B.W. *Escherichia coli* biotin holoenzyme synthetase/bio repressor crystal structure delineates the biotin- and DNA-binding domains. *Proceedings of the National Academy of Sciences* **89**, 9257-9261 (1992).
 51. Toraya, T. Radical catalysis in coenzyme B₁₂-dependent isomerization (eliminating) reactions. *Chemical Reviews* **103**, 2095-2127 (2003).
 52. Picciocchi, A., Douce, R. & Alban, C. Biochemical characterization of the Arabidopsis biotin synthase reaction. The importance of mitochondria in biotin synthesis. *Plant Physiol.* **127**, 1224-1233 (2001).
 53. DeLano, W.L. The PyMOL Molecular Graphics System. (2002).
 54. Colbert, C.L., Coutre, M.M., Eltis, L.D. & Bolin, J.T. A cluster exposed: structure of the Rieske ferredoxin from biphenyl dioxygenase and the redox properties of Rieske Fe-S proteins. *Structure* **8**, 1267-1278 (2000).
 55. Zhou, Z.H. & Adams, M.W.W. Site-directed mutations of the 4Fe-ferredoxin from the hyperthermophilic archaeon *Pyrococcus furiosus*: role of the cluster-coordinating aspartate in physiological electron transfer reactions. *Biochemistry* **36**, 10892-10900 (1997).
 56. Zheng, L., Kennedy, M.C., Beinert, H. & Zalkin, H. Mutational analysis of active site residues in pig heart aconitase. *Journal of Biological Chemistry* **267**, 7895-7903 (1992).

Chapter 4

Crystal structure of lysine 5,6-aminomutase

Abbreviations:

2.3-LAM	Lysine 2,3-aminomutase
5,6-LAM	Lysine 5,6-aminomutase
Ado•	5'-deoxyadenosyl radical
AdoCbl	Adenosylcobalamin, Coenzyme B ₁₂
AdoH	5'-deoxyadenosine
AdoMet	S-adenosyl-L-methionine
Cbl	Cobalamin
CNCbl	Cyanocobalamin, Vitamin B ₁₂
CoA	Coenzyme A
Cob(II)	Cob(II)alamin
DMB	Dimethylbenzimidazole
GM	Glutamate mutase
MCM	Methylmalonyl coenzyme A mutase
MS	Methylcobalamin-dependent methionine synthase
PEG	Polyethylene glycol
SAD	Single-wavelength anomalous dispersion
SeMet	Selenomethionine
OAM	Ornithine aminomutase
PLP	Pyridoxal 5'-phosphate
TIM	Triosephosphate isomerase

Introduction

Lysine 5,6-aminomutase (5,6-LAM) is an enzyme in the bacterial lysine fermentation pathway¹. The enzyme catalyzes the interconversion of DL-lysine or of β -L-lysine to 2,5-diaminohexanoate or to 3,5-diaminohexanoate, respectively (Fig. 4.1). The crystal structure of 5,6-LAM, a major contribution to this thesis, was determined in collaboration with the laboratory of P. A. Frey at the University of Wisconsin at Madison. We present a crystal structure of a substrate-free holoenzyme form of 5,6-LAM from *Clostridium sticklandii*, which is the first structure of an enzyme that utilizes both adenosylcobalamin (AdoCbl) and pyridoxal 5'-phosphate (PLP) cofactors. The structure reveals that AdoCbl is bound by a Rossmann-like domain, and that PLP, which is tethered to the B₁₂-binding domain via its imine linkage, is bound in the putative active site, at the top of a triosephosphate isomerase (TIM) barrel domain. Thus, 5,6-LAM joins a group of three other AdoCbl-dependent radical enzymes (glutamate mutase [GM], Methylmalonyl-CoA mutase [MCM], and diol dehydratase, see chapter 1)²⁻⁴ and one adenosylmethionine (AdoMet) -dependent radical enzyme (biotin synthase, see chapter 3)⁵ in utilizing the TIM barrel fold to sequester substrates that form free-radical intermediates. Our structure is unique among all PLP-dependent enzymes, in that the imine linkage is provided by a Rossmann-like domain. Strikingly, in the pre-catalytic, substrate-free conformation captured in our structure, the PLP and AdoCbl cofactors are separated by a distance of $\sim 25\text{\AA}$, suggesting that a gross conformational change occurs upon substrate binding. The work presented in this chapter is in press at the Proceedings of the National Academy of Sciences⁶.

AdoCbl-dependent isomerases are often present in catabolic pathways and can serve to rearrange the substrate's carbon skeleton and/or functional groups for further degradation. One such pathway that operates in several bacterial species is the fermentation of lysine to yield acetate. Interestingly, the lysine fermentation pathway contains two analogous enzymes: 5,6-LAM, which is AdoCbl-dependent^{7,8}, and lysine 2,3-aminomutase (2,3-LAM), which is an AdoMet-dependent radical enzyme⁹⁻¹¹. Both enzymes require PLP^{9,12} in addition to AdoCbl or AdoMet, and both catalyze a 1,2 amino group shift with concomitant H atom migration (Fig. 4.1). In 5,6-LAM, AdoCbl is the source of the transient 5'-deoxyadenosyl radical (Ado●), whereas in 2,3-LAM, Ado● is produced from AdoMet coordinated to the unique iron of a 4Fe-4S cluster, and an exogenous electron. The exogenous electron is transferred first into the $[4\text{Fe-4S}]^{2+}$ cluster and then into AdoMet, cleaving AdoMet to give methionine and the transient Ado●. Because of the similarity of their reactions, their requirement for PLP, and their common substrates, 5,6-LAM may be thought of as the AdoCbl-dependent counterpart of the AdoMet-dependent 2,3-LAM. Studies on both 2,3-LAM and 5,6-LAM have allowed Frey and coworkers to propose a general mechanism for these reactions (Fig. 4.2a). For both 5,6-LAM and 2,3-LAM, radical propagation from Ado● to the substrate-PLP covalent complex (known as the external aldimine) initiates the isomerization, and both reaction mechanisms are likely to involve analogous intermediates.

The role of PLP in the aminomutase reaction is not completely clear. The 5,6-LAM mechanism proposed by Frey and coworkers is consistent with computational studies conducted by Random's laboratory, which suggest that the role of PLP in the AdoCbl-

dependent aminomutases is to provide a conjugated π system to stabilize the rearranging radical species^{13,14}. This hypothesis is consistent with model chemistry, wherein an imine with an aromatic substituent undergoes a 1,2-imino shift under radical generating conditions¹⁵ (Fig. 4.3a). Significantly, the rearrangement of the aziridylcarbinyl radical, which is the simplest model for the 5,6-LAM reaction, takes place at cryogenic temperatures, despite the absence of an aromatic substituent¹⁶ (Fig. 4.3b), indicating that PLP is not necessary for the rearrangement to occur.

All AdoMet- or AdoCbl-dependent radical enzymes rely on Ado• for catalysis, yet the formation of this highly oxidative intermediate must be controlled in order to prevent aberrant reactions. C-Co bond homolysis and the transient formation of Ado• is triggered by substrate binding in the AdoCbl dependent enzymes MCM¹⁷, GM^{18,19}, and diol dehydratase²⁰, while effector binding triggers the C-Co bond homolysis in the AdoCbl-dependent ribonucleotide reductase²¹ (see chapter 1). How substrates or effectors afford a 10¹²-fold rate acceleration of Co-C bond cleavage in AdoCbl-dependent enzymes is a question that has intrigued scientists for decades. The crystal structure of 5,6-LAM suggests a novel role for PLP in locking the enzyme into its resting-state conformation, keeping AdoCbl out of the active site in the absence of substrate and preventing radical-based protein damage. This will be discussed in detail below.

4.2. Materials and methods

4.2.1. Protein preparation

Selenomethionine (SeMet)-incorporated 5,6-LAM from *Clostridium sticklandii* was purified and reconstituted with PLP in the Frey laboratory. A plasmid *KamDE* containing the genes encoding both β and α subunits of 5,6-LAM was used to transform *E. coli* B834 (DE3) cells. Ten mL of an overnight culture was used to inoculate 1 L of SeMet media, prepared according Budisa and coworkers²² with the omission of L-cysteine and addition of 5 μ M pyridoxal hydrochloride. The culture was grown for 16 hours at 37 °C. The yield was 25 g wet cells from 10 L minimal media. The SeMet recombinant protein was purified by the procedure of Chang and Frey²³ without the gel filtration chromatography step.

4.2.2. Storage, handling, and crystallization of protein samples, and crystal cryoprotection

Protein was stored at -80 °C and handled on ice during crystallization. All solutions containing AdoCbl (including protein solutions) were formulated and handled in a dark room under dim red light.

Crystals were grown using hanging drop vapor diffusion techniques at room temperature in a dark room, under dim red light. Crystals were manipulated in the dark room until after cryo-cooling. Five crystal forms were obtained, as detailed in Fig. 4.4. Of these crystals, only one crystal form (form 1, Fig. 4.4a) produces data adequate to solve the structure. Protein and precipitant solutions (Fig. 4.4) were mixed in a 1:1 ratio, with drop

sizes of 2 μL total, and equilibrated over 0.5 mL of precipitant solution. Form 1 crystals (those used to solve the structure) were cryoprotected, within 48 hours after their initial appearance, by quickly soaking in precipitant solution with 20% glycerol added and plunging into liquid nitrogen.

4.2.3. *Crystal properties, phasing, model building, and refinement*

Crystals belong to space group $P3_121$, with one $\alpha\beta$ heterodimer per asymmetric unit, for a total of 6 $\alpha\beta$ heterodimers in the unit cell ($Z=6$), and $a = b = 99.7 \text{ \AA}$, $c = 168.8 \text{ \AA}$. The unit cell volume $V = 1,453,093 \text{ \AA}^3$. Data were collected at the Argonne National Laboratory beamline NE-CAT 8-BM, equipped with a charge-coupled device detector (Area Detector Systems Corp.). Data were processed and scaled with DENZO and SCALEPACK²⁴.

A single set of data, collected at the Se absorption peak wavelength (0.97918 \AA), was used to solve the structure by anomalous dispersion methods^{25,26} (Table 4.1). Twenty-nine Se atoms and the Co atom of AdoCbl were located and refined with SOLVE²⁷, with a mean figure of merit of 0.40 to 3.0 \AA resolution. The experimental electron density map was subjected to solvent-flattening with RESOLVE²⁷, resulting in a good-quality map that allowed us to begin model building (Fig. 4.5). The space group, $P3_121$, was distinguished from $P3_221$ by inspection of α helices, which are right-handed.

Iterative rounds of model building in XFIT²⁸ and refinement in CNS²⁹ resulted in the final model at 2.8 \AA resolution. The refined structure contains all 516 residues of the α

subunit (chain A), residues 24-84 and 102-261 of the β subunit (chain B), one AdoCbl molecule, and one PLP molecule (as the imine adduct to K144 β). A simulated annealing composite omit map was used to validate the final structure. There is no electron density for the histidine tag, residues 1-23 β , 85-101 β , or 262 β . The final model has all residues residing in the allowed regions of the Ramachandran plot (87.7% in the most favored regions, 11% in additionally allowed regions, and 1.3% in generously allowed regions), as calculated by PROCHECK³⁰ (Fig. 4.6).

4.3. Results

4.3.1. Overall structure

5,6-LAM is an $\alpha_2\beta_2$ tetramer³¹ that can be thought of as a dimer of $\alpha\beta$ units (Fig. 4.7). In the crystal, the asymmetric unit contains one $\alpha\beta$ dimer, and crystallographic symmetry produces a likely physiological tetramer that buries 5736 Å² (19%) of the $\alpha\beta$ heterodimer surface area (Fig. 4.9). The large α subunit (538 residues) is composed of the PLP-binding TIM barrel domain and several additional α helices and β strands at the N and C termini (Fig. 4.8). These helices and strands form an intertwined "accessory clamp" structure that wraps around the sides of the TIM barrel, and extends up toward the Ado ligand of the Cbl cofactor. This accessory clamp provides most of the interactions between the protein and the Ado ligand of the Cbl (discussed below), suggesting that its role is mainly in stabilizing AdoCbl in the pre-catalytic resting state. The small β subunit (262 residues) comprises two domains: the N-terminal dimerization domain, which has the same fold as copper binding domain of the Alzheimer's disease amyloid precursor protein³² (PDB code 1OWT), and the AdoCbl-binding Rossmann-like domain, which also provides the imine bond to PLP. The Rossmann-like domain interacts with the C-terminal end of the TIM barrel, placing PLP into the top of the barrel, while projecting AdoCbl to the edge of the barrel, far from the PLP binding site. The dimerization domain of β forms a continuous β -sheet with the dimerization domain of the second $\alpha\beta$ unit and buries an extensive surface of hydrophobic residues. The dimerization domain also makes many hydrogen-bonding and hydrophobic contacts with the TIM barrel domain of the α subunit. No contacts are observed between the dimerization domain and the Rossmann domain, though these domains are linked by a disordered loop (85 β -101 β)

that we could not model. The average B-factor of the dimerization domain is approximately twice those of either the Rossmann-like domain or the TIM barrel and accessory clamp, suggesting a degree of mobility for the dimerization domain (Table 4.1). The $\alpha_2\beta_2$ tetramer is arranged such that there is no direct interaction between the active sites of either $\alpha\beta$ pair.

The presence of a TIM barrel and a Rossmann-like domain in 5,6-LAM is consistent with the domain usage in other Cbl-dependent base-off enzymes, such as GM, MCM, and methionine synthase (MS), but the orientation of the Rossmann domain relative to the TIM barrel is markedly different, and is likely to be mechanistically relevant (discussed below). It is also interesting that both subunits play a role in binding both cofactors; AdoCbl is bound at the C-terminal end of the Rossmann domain of β and by the accessory clamp at the edge of the α subunit, whereas PLP is bound at the C-terminal end of the TIM domain of α and by a lysine residue at the edge of the β subunit.

4.3.2. PLP-protein interactions

PLP-dependent enzymes of known structure can be sorted into families based on their respective folds. Enzymes of fold type I, II, III, IV, and V are represented by aspartate aminotransferase, tryptophan synthase, alanine racemase, D-amino acid aminotransferase, and glycogen phosphorylase, respectively³³ (Fig. 4.10). 5,6-LAM cannot be placed into any of these five PLP enzyme families, although it does share features with fold types II, III, and IV. As with fold type III, PLP is bound at the top of the TIM barrel pore, but the imine linkage is formed to the Rossmann domain rather than

to a lysine of the TIM barrel, and a least-squares superposition of 5,6-LAM and alanine racemase reveals that PLP does not occupy analogous positions at the C-terminal ends of the TIM barrels (Fig. 4.11). In addition, the second domain of fold type III is composed mainly of β strands rather than having a Rossmann-like fold. The similarity to fold type II proteins is more limited and focuses on the use of a serine residue (S238 α in 5,6-LAM), rather than the more typical aspartic acid, to hydrogen bond with the pyridine nitrogen. The presence of a Ser residue in this position suggests that the pyridine nitrogen is not protonated in 5,6-LAM. In agreement with fold types III and IV, the *si* face of PLP is solvent exposed³³.

The experimental electron density map indicates that K144 β forms a linkage to PLP (Fig. 4.5). Biochemical, mutagenesis and mass-spectrometry studies on 5,6-LAM from *P. gingivalis*³⁴, combined with sequence alignment against the *C. sticklandii* enzyme (~67% identity), support the assignment of K144 β as the Lys residue that forms an imine bond with PLP. K144 β resides at the N-terminus of a short glycine-rich loop (144 β -KGYAGHYG-151 β) that is highly conserved across all 5,6-LAM sequences. This short loop interrupts the second helix of the Rossmann domain (Figs. 4.8, 4.12b). The helix is reformed for one last turn before the peptide resumes the remainder of the Rossmann fold. As was previously recognized³⁴, this represents a novel PLP-binding motif. The terminal amino group of K144 β does not appear to be coplanar with the pyridine ring of PLP, leading us to believe that the internal aldimine was photoreduced in the X-ray beam, as has been observed in other structures (e.g. PDB codes 1GOP³⁵, 1B54³⁶, 1T3I³⁷). Significantly, all contacts to the PLP cofactor, except for the imine linkage, are made

from residues of the TIM barrel (Fig. 4.12a and Table 4.2), and are similar to PLP-protein interactions observed in other PLP-dependent enzymes. These interactions include π -stacking, electrostatic interactions with the phosphate, and hydrogen bonding. Y263 α forms π -electron stacking interactions with the pyridine ring and also hydrogen bonds to the phosphate moiety. The phenolic oxygen of PLP, proposed to be important for intermediate stabilization in PLP- and AdoCbl-dependent 1,2-aminomutases¹⁴, is observed to hydrogen bond to the side-chain of N299 α . The phosphate group interacts with two Arg sidechains (R184 α , R268 α), the sidechain of S189 α , and a number of main-chain amides (G187 α , Q188 α , S189 α). Like in all PLP enzymes of known structure, the phosphate moiety of PLP is bound near the N-terminus of an α helix (in this case, a short helical turn, composed of 188 α -QSL-190 α).

4.3.3. Cbl-protein interactions

AdoCbl binds to 5,6-LAM with $K_M = 6.6 \mu\text{M}$ and stabilizes the enzyme against thermal lability²³. AdoCbl was added to 5,6-LAM immediately prior to crystallization, and we observe electron density that is consistent with the cofactor (Fig. 4.13a,b). 5,6-LAM contains a "base-off" AdoCbl binding sequence (131 β -DxHxxG...Sxl...GG-222 β) and binds AdoCbl in the base-off conformation, with H133 β replacing the intrinsic dimethylbenzimidazole (DMB) substituent of the cofactor as the lower axial ligand to the cobalt²³ (the Co-N distance is 2.3 Å). Binding of AdoCbl by the Rossmann domain of 5,6-LAM is similar to Cbl binding in MS³⁸, MCM³, and GM² (see chapter 1), and is characterized by a hydrogen-bonding network designed to bind the Cbl cofactor (Fig 4.13a, b, and Table 4.3). The binding determinants for Cbl include several residues that

hydrogen bond to the propionamide side chains of the corrin ring (T130 β , A132 β , T134 β , V135 β , T191 β , Q192 β), and, as in the case of MS, MCM, and GM, a serine residue (S187 β) which hydrogen-bonds to the DMB N atom. One potential hydrogen bond between the ribose moiety of the DMB tail and the protein is observed: the main-chain carbonyl O of R243 β is 2.8 Å away from the 2'-OH. The DMB moiety is bound in a largely hydrophobic cavity, and is in van der Waal contact with I137 β , I140 β , V248 β , L185 β , and F239 β , as well as G221 β and G222 β , two residues of the base-off Cbl binding sequence motif. The phosphate moiety of the DMB tail, which is not observed to contact the protein directly, is bound near the surface of the Rossmann-like domain. Based on the structures of GM and MCM, we assume that the phosphate interacts with solvent, but due to the moderate resolution of our structure, we did not model water molecules.

All solutions and crystals containing AdoCbl were handled under red light until after cryo-cooling. Despite our stringent efforts to prevent the cleavage of the photolabile C-Co bond, the simulated annealing composite omit map suggest that this bond is mostly cleaved (Fig. 4.13b), and we have modeled the Ado moiety as AdoH. We believe that the cleavage of AdoCbl is nonenzymatic and is due to photoreduction of the C-Co bond in the X-ray beam. This phenomenon has previously been reported³⁹. In the structure of 5,6-LAM, AdoH adopts a *syn* conformation about the glycosidic bond, in contrast to GM⁴⁰ and MCM⁴¹, where the adenine ring of Ado is *anti* to the ribose ring. Interestingly, AdoH is forced to adopt the *syn* conformation because of a steric clash between the adenine ring and Y193 α that would arise if AdoH were in the *anti* conformation. AdoH

interacts mostly with residues of the accessory clamp: the 2' and 3' -OH groups of the ribose moiety of AdoH hydrogen bond to the main-chain carbonyls of E55 α and D54 α , respectively, and the exocyclic amino group of the adenine ring hydrogen bonds to D64 α . Y193 α and V56 α are positioned for hydrophobic interaction with the adenine moiety of AdoH. Interestingly, the AdoH binding loop, composed of residues 51 α -57 α , form a distorted β -hairpin structure that allows for two adjacent main-chain carbonyls to hydrogen bond with the 2'- and 3'-OH groups of AdoH (Fig. 4.13b, Table 4.3).

4.3.4. *The CxxCxxxC motif of 5,6-LAM*

Interestingly, 5,6-LAM contains a CxxCxxxC motif and is reported to adventitiously bind metals²³. Analysis of the 5,6-LAM structure suggests that the three-Cys sequence, which is reminiscent of the conserved CxxxCxxC motif of the AdoMet radical enzymes, plays no role in catalysis. The three Cys residues are not positioned for disulfide formation or metal binding (Fig. 4.14), and there is no additional electron density to suggest the presence of a metal in the area. Moreover, these Cys residues are not absolutely conserved across the sequenced 5,6-LAMs.

4.4 Discussion

4.4.1. A hypothetical conformational change to bring AdoCbl into the active site

As mentioned above, the relative orientation of the Rossmann-like domain to the TIM barrel in 5,6-LAM is markedly different from that observed in either GM or MCM. Whereas in 5,6-LAM the Rossmann domain is bound off-center on top of the TIM barrel (Fig. 4.15a), resulting in the $\sim 25\text{\AA}$ separation of the AdoCbl cofactor from the active-site PLP, in the enzyme-substrate complex of both MCM and GM, the Rossmann domain is docked directly over the center of the TIM barrel, thereby placing the Cbl cofactor in the active site and sequestering the active site from bulk solvent^{2,3}. MCM buries $\sim 15\%$ and $\sim 60\%$ of the TIM-barrel and Rossmann domain surface areas, respectively, at the TIM barrel-Rossmann interface. Likewise, GM buries $\sim 17.5\%$ of the TIM barrel surface area and $\sim 47\%$ of the Rossmann domain surface area. In contrast, 5,6-LAM buries only $\sim 6.6\%$ of the TIM barrel domain and 17% of the Rossmann domain at the TIM barrel-Rossmann interface. Therefore, we describe this structure of 5,6-LAM, in which the active site is solvent-accessible and the AdoCbl cofactor is not positioned for catalysis, as having the resting state "edge-on" conformation, in contrast to the hypothetical catalytic "top-on" conformation (Fig. 4.15b) that is analogous to the domain arrangement in the substrate-bound forms of MCM and GM (Fig. 4.15d).

A key feature that is unique to PLP binding in the resting-state structure of 5,6-LAM is the intersubunit nature of the imine linkage (Fig. 4.12). In this mode of PLP binding, the cofactor acts as an anchor, tethering the separate polypeptide chain of the Rossmann-like domain to the TIM barrel domain through PLP. We propose that the anchoring role of

PLP, which forces the unusual orientation of the Rossmann domain with respect to the TIM barrel, is important for positioning AdoCbl outside of the putative active site and for regulating the formation of the highly oxidizing Ado• in the absence of substrate. In the resting state, a large cleft separates the dimerization domain from the Rossmann-like domain (Fig. 4.16). This cleft, which leads to the top of the TIM barrel and the PLP cofactor, is presumably the path that the substrate must follow in order to arrive at the active site. Introduction of the substrate and transaldimination would then release K144β and effectively break the PLP-mediated anchoring interactions between the Rossmann-like and TIM barrel domains. With the Rossmann-like domain freed from its constrained position, a large-scale conformational change could occur. We suggest that such a conformational change must occur, and must result in the docking of the Rossmann-like domain directly atop the center of the TIM barrel domain, filling the cleft between the Rossmann domain and the dimerization domain (Fig. 4.15b). This catalytic "top-on" conformation would effectively sequester the active site and position Ado near the substrate-PLP complex, allowing for substrate radical generation and catalysis. Such a conformational change could provide the energy that is required for the large rate-acceleration of AdoCbl C-Co bond homolysis that characterizes this enzyme family. 5,6-LAM is not exceptionally fast ($k_{\text{cat}} = 750 \pm 44 \text{ min}^{-1}$ for D-lysine⁴²), and would not require a very fast conformational change for catalysis. The hypothetical conformational change that accompanies formation of the catalytic state of 5,6-LAM could not be rate-limiting, since a primary deuterium kinetic isotope effect is observed in the reaction of 5,6-LAM with deuterium labeled substrates.

There is precedent in the Cbl enzyme literature for a large-scale conformational change upon substrate binding^{41,43,44}. For methylcobalamin-dependent methionine synthase, the enzyme exists as an ensemble of conformational states that interconvert upon substrate or product binding⁴⁴. X-ray analysis reveals that the two active sites that alternatively methylate and demethylate the Cbl cofactor are ~50 Å apart⁴³, requiring large conformational rearrangements of the enzyme during each catalytic cycle. For AdoCbl-bound MCM, the presence of substrate has a dramatic effect on the structure of the TIM barrel⁴¹. In the X-ray structure of the substrate-free form of MCM, the TIM barrel is splayed open, leaving a large gap in the center of the barrel⁴¹ (Fig. 4.15c). Substrate binds in this gap, threading through the N-terminal end of the TIM barrel to the Cbl cofactor, which is located at the C-terminal end of the barrel³. Binding of substrate appears to trigger the barrel closure (Fig. 4.15d), which in turn, causes Y89 to swing toward the top of the AdoCbl corrin ring, presumably facilitating the homolytic cleavage of the Ado moiety to give Ado•^{41,45}. Thus, while MCM and 5,6-LAM have similar structures, the way in which conformational changes are linked to substrate binding is different, and takes advantage of the unique properties of the substrates. The ~23 Å-long methylmalonyl-CoA can bind along the entire length of the TIM barrel, causing the barrel to tighten, whereas lysine, a much smaller substrate, can release the enzyme's imine linkage from the PLP, freeing the Rossmann domain to rotate.

4.4.2. Questions arising from the structure of 5,6-LAM

Several open questions remain concerning the hypothetical conformational change that we propose is necessary for catalysis in 5,6-LAM. What role, if any, does the dimerization domain play in the conformational change? Could the accessory clamp swing up and down to facilitate the edge to top rotation of the Rossmann domain? What drives the reformation of the imine linkage with K144 β that would result in reversion to the edge-on conformation and product release? What is the structural rationale for the observed suicide inactivation of 5,6-LAM⁴⁶? Although many interesting details remain to be discovered, our structural analysis suggests a novel mechanism for substrate-mediated control of radical generation. The structure of 5,6-LAM shows that AdoCbl-dependent enzymes can control radical generation by using a covalent bond that must be broken when substrates binds, effectively locking AdoCbl into a non-catalytic position in the absence of substrate.

4.5. Tables

Table 4.1. 5,6-LAM data collection and refinements statistics

Data Set	Se Peak
Wavelength (Å)	0.97918
Resolution range (Å)	50.0-2.8
Unique Reflections ¹	45,836
Redundancy	6.8
Completeness (%)	99.8 (99.8)
I/σ(I)	18.6 (6.6)
R _{sym} ²	9.3 (28.4)
Non-hydrogen atoms in asymmetric unit	5864
Number of reflections (working set / test set)	24098 / 2378
R _{cryst} ³ (%) / R _{free} (%)	21.9 / 26.9
Overall B (Å ²)	
α (TIM barrel + accessory clamp)	
main chain	31.3
side chain	36.1
β (dimerization domain)	
main chain	62.9
side chain	67.7
β (Rossmann-like domain)	
main chain	31.6
side chain	38.1
Cofactors	
Cbl	34.8
AdoH	70.1
PLP	24.9
RMS deviations of	
protein bonds (Å)	0.009
protein angles (°)	1.4
Number of heavy atom sites in the asymmetric unit	
Se	29
Co	1

Values in parentheses are for the highest-resolution shell. ¹For the purpose of phasing, Friedel pairs were not merged, and this is accounted for in the number of unique reflections. $^2R_{\text{sym}} = [\sum_{hkl} \sum_i |I_i(hkl) - \langle I(hkl) \rangle|] / \sum_{hkl} \sum_i I_i(hkl)$ for hkl independent reflections and i observations of a given reflection. $\langle I(hkl) \rangle$ is the mean intensity of the miller index (hkl). $^3R_{\text{cryst}} = \sum_{hkl} ||F_o(hkl)| - |F_c(hkl)|| / \sum_{hkl} |F_o(hkl)|$. $R_{\text{free}} = R_{\text{cryst}}$ for a test set of reflections (9.9% of all reflections) not included in refinement. No σ cutoff was used in the refinement.

Table 4.2. Potential PLP-5,6-LAM hydrogen bonding and electrostatic interactions

Atom	Contacting residue	Contacting atom	distance (Å)
Pyridoxal			
N1	Ser 238 α	OG	2.7
O3	Asn 299 α	ND2	2.5
O3	Asn 299 α	OD1	3.2
Phosphate			
O1P	Arg 268 α	NE	2.6
O1P	Ser 189 α	OG	2.5
O1P	Tyr 263 α	OH	3.0
O2P	Gln 188 α	N	3.3
O2P	Ser 189 α	N	3.0
O2P	Arg 184 α	NH1	2.5
O2P	Ser 189 α	OG	3.1
O3P	Arg 268 α	NH1	2.7
O3P	Gly 187 α	N	2.5
O4P	Tyr 263 α	OH	2.9

Table 4.3. Potential AdoCbl-5,6-LAM hydrogen bonding interactions			
Atom	Contacting residue	Contacting atom	distance (Å)
AdoH			
O3'	Asp 54 α	O	3.1
O2'	Glu 55 α	O	2.9
N6	Asp 64 α	OD1	3.8
Corrin ring			
N33	Thr 191 β	OG	3.0
O34	Thr 191 β	N	2.9
O34	Gln 192 β	N	3.1
O44	Ala 132 β	N	2.7
N45	Thr 130 β	O	3.1
O51	Val 135 β	N	3.1
O51	Thr 134 β	N	2.6
N52	Thr 134 β	OG1	3.5
Ribose			
O8R	R243 β	O	2.8
DMB			
N3B	S187 β	OG	2.6

4.6. Figures

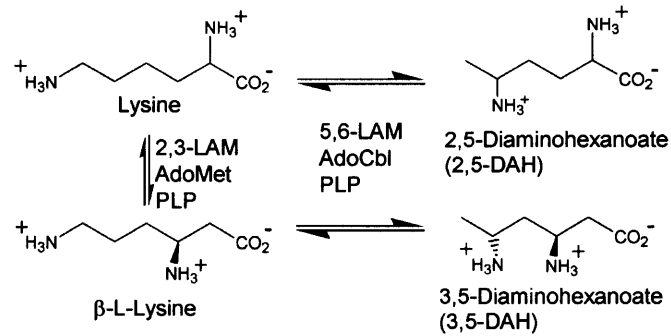


Figure 4.1. Aminomutases in the bacterial lysine fermentation pathway. 5,6-LAM and 2,3-LAM catalyze similar reactions and act on similar substrates. Both enzymes require PLP, but 5,6-LAM is AdoCbl dependent, whereas 2,3-LAM is an AdoMet-dependent iron-sulfur enzyme. The natural substrates of 5,6-LAM include DL-Lysine and β -L-Lysine. 2,3-LAM acts on L-Lysine and does not accept D-Lysine as a substrate.

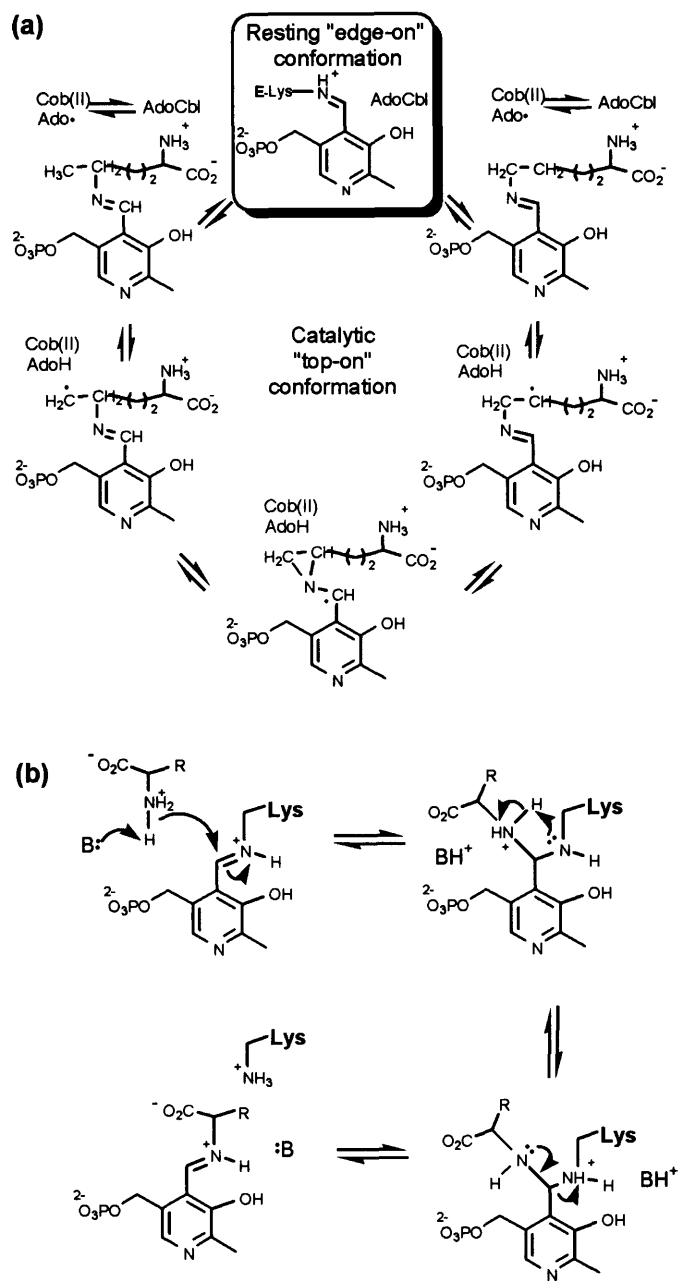


Figure 4.2. Proposed mechanism of 5,6-LAM. **(a)** Proposed mechanism of 5,6-LAM, modified from reference⁴². The boxed step represents the state of the enzyme observed in our crystal structure. The unboxed steps are proposed to occur while 5,6-LAM is in the hypothetical "top-on" conformation (see text). **(b)** Mechanism of a general-base catalyzed transaldimination with PLP⁴⁷⁻⁵³.

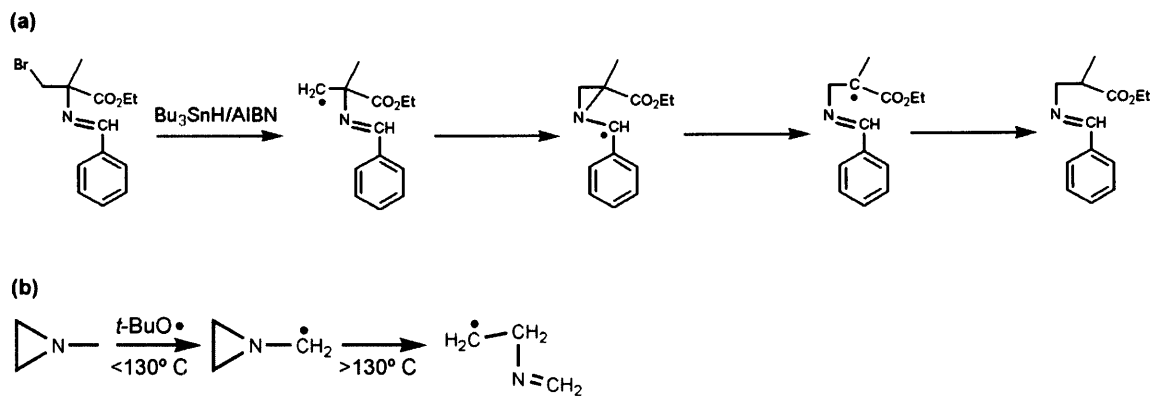


Figure 4.3. (a) 1,2-imino shift under radical-generating conditions, as observed by Han and Frey¹⁵ (b) Rearrangement of the aziridylcarbinyl radical, as observed by Danen and West¹⁶.



Figure 4.4. Various crystal forms of 5,6-LAM. All crystals were produced using the conventional hanging-drop vapor diffusion method (by mixing 1 μ L of protein solution with 1 μ L of precipitant solution), and drops were equilibrated over a 0.5 mL well of precipitant solution. **(a)** The form used to solve the structure (form 1). Only this crystal form diffracts to give data of reasonable quality. Protein solution supplemented with AdoCbl (12 mg/mL 5,6-LAM, 0.5 mM β -mercaptoethanol, 10 mM triethanolamine pH 7.2, 4.5 mM AdoCbl; the molar ratio of AdoCbl to protein is 30) was mixed in a 1:1 ratio with precipitant solution (0.1 M Tris hydrochloride pH 8.0, 0.2 M sodium acetate, 24% w/v PEG 2000 monomethyl ether). Crystals appeared within 24 hours. **(b)** Protein solution supplemented with AdoCbl (same as part **a**) was mixed in a 1:1 ratio with precipitant solution (0.1 M sodium Cacodylate pH 6.5, 0.2 M sodium acetate, 24% w/v PEG 2000 monomethyl ether). Crystals appeared within 24 hours. **(c)** Protein solution supplemented with AdoCbl (same as part **a**) was mixed in a 1:1 ratio with precipitant solution (0.1 M Tris hydrochloride pH 8.0, 0.2 M sodium acetate, 19% w/v PEG 2000 monomethyl ether, 5 mM NiCl_2). Crystals appeared within 48 hours. **(d)** A solution of protein, adeninylnpentylcobalamin, and substrate (12 mg/mL 5,6-LAM, 0.5 mM β -mercaptoethanol, 10 mM triethanolamine pH 7.2, 2 mM adeninylnpentylcobalamin, 5 mM D-lysine or L-lysine) was mixed in a 1:1 ratio with precipitant solution (0.1 M Bis-tris pH 7.0, 2 M ammonium sulfate). The molar ratio of adeninylnpentylcobalamin to protein is 13. Crystals appeared within 7 days. **(e)** A solution of protein, CNCbl, and substrate (12 mg/mL 5,6-LAM, 0.5 mM β -mercaptoethanol, 10 mM triethanolamine pH 7.2, 4.5 mM CNCbl, 5 mM D-lysine or L-lysine) was mixed in a 1:1 ratio with precipitant solution (0.1 M Bis-tris pH 6.5, 2 M ammonium sulfate). The molar ratio of CNCbl to protein is 30. These crystals are small and only faintly pink, and appeared within 10 days. In this picture, several are identified with arrows. Dark red crystals are probably CNCbl.

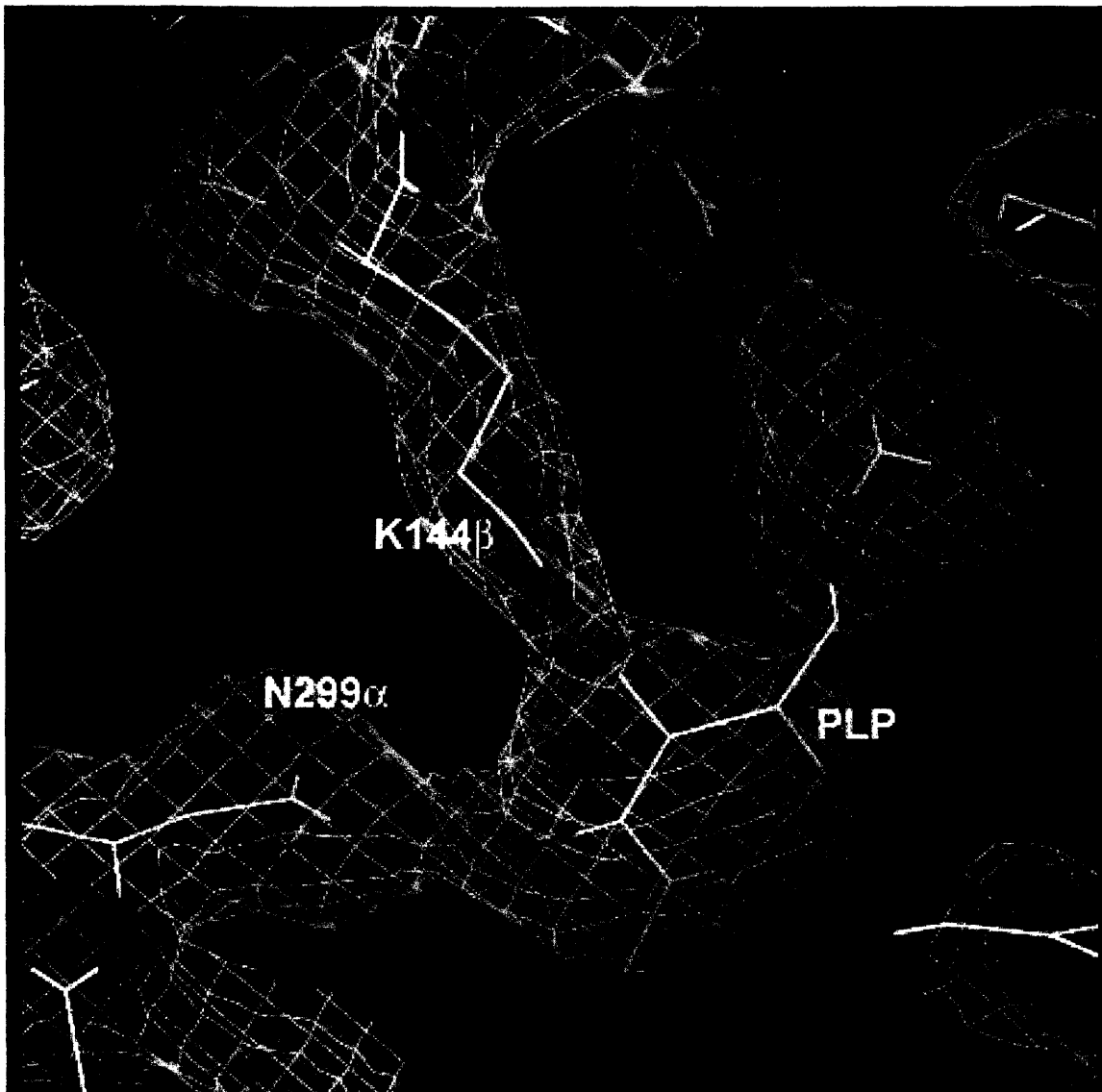


Figure 4.5. Solvent-flattened 3.0 Å resolution experimental electron density of 5,6-LAM. The map is contoured at 1.0 σ . Residues K144 β and N299 α , along with PLP, are shown.

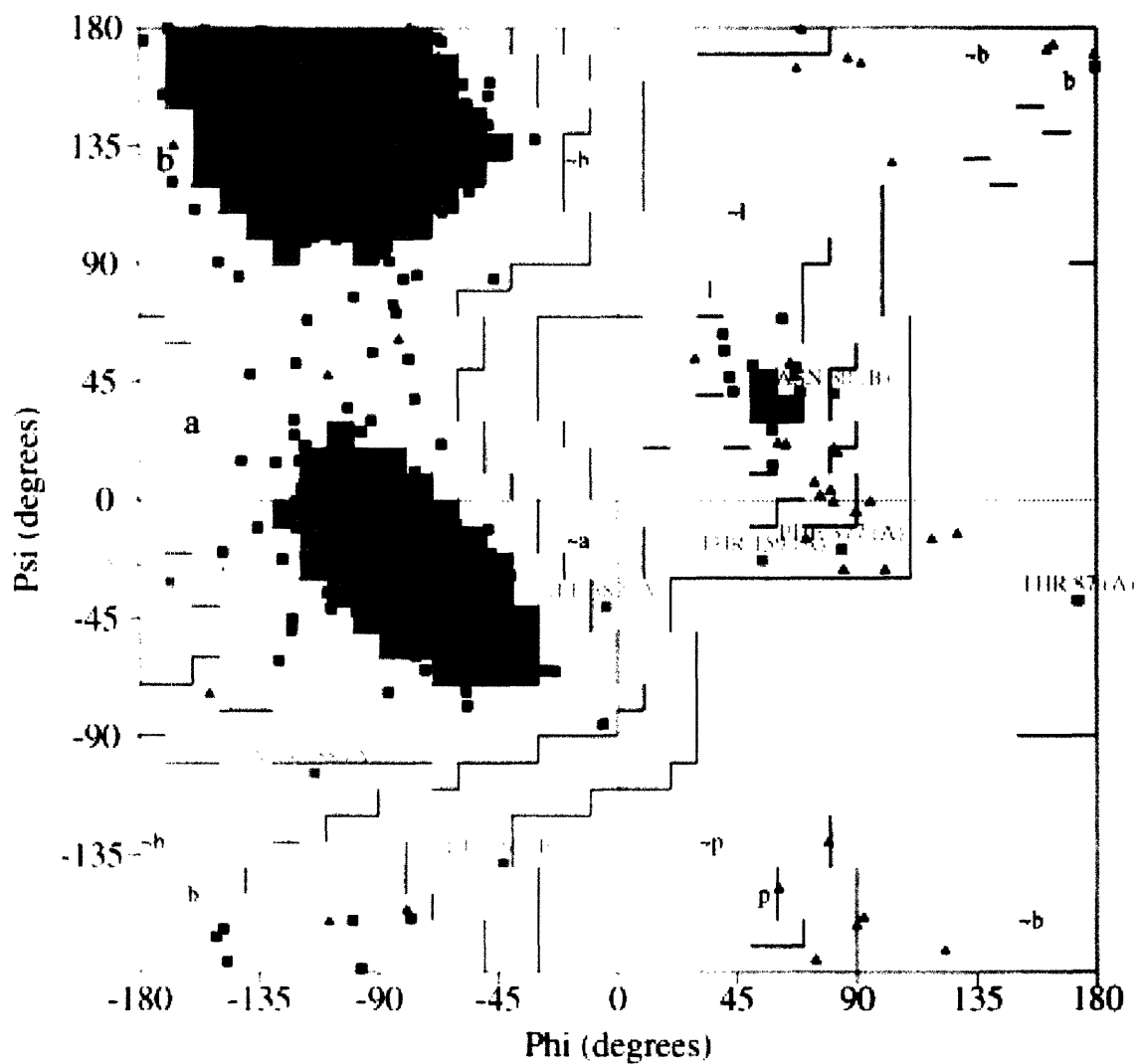


Figure 4.6. Ramachandran plot of 5,6-LAM. The plot is colored as follows: red, most favoured regions; yellow, additional allowed regions; light yellow, generously allowed regions; white, disallowed regions. Glycine residues are shown as triangles. Figure made using PROCHECK³⁰.

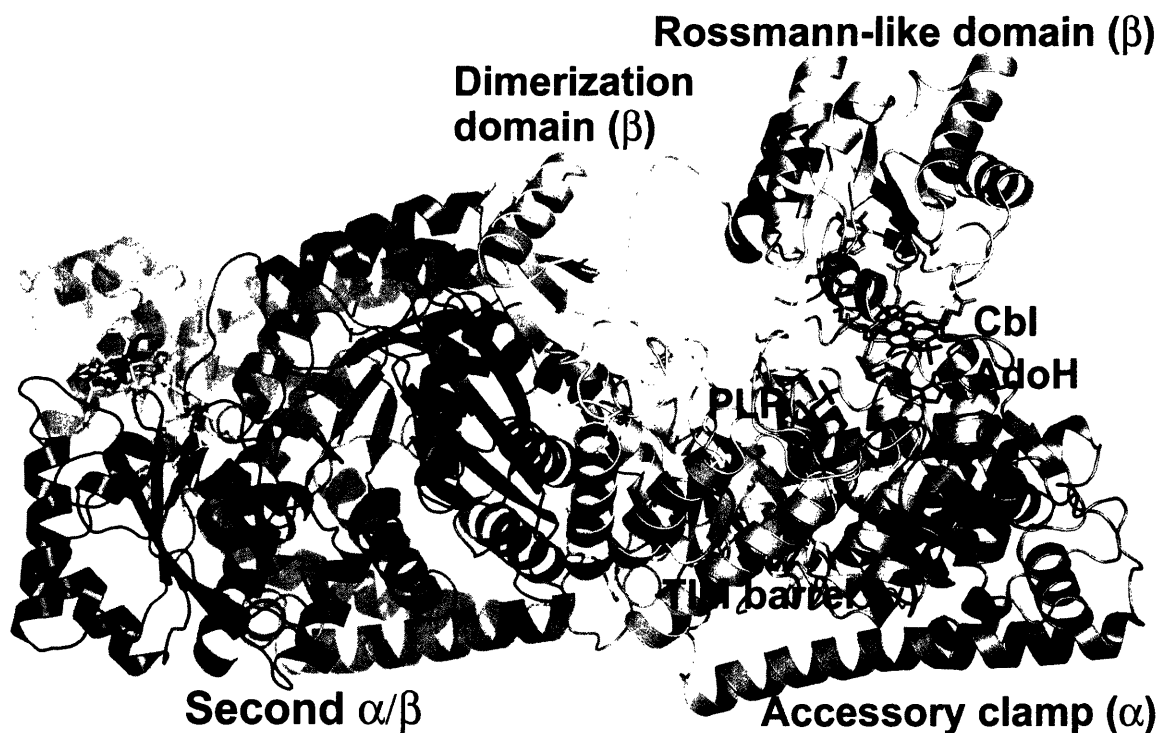


Figure 4.7. Overall structure of 5,6-LAM and location of cofactors. Ribbon diagram of the $\alpha_2\beta_2$ 5,6-LAM tetramer with the “accessory clamp” of α in brown, the TIM barrel of α in green, the Rossmann-like domain and the dimerization domain of β in blue. The dashed line represents the disordered loop connecting the two domains of β . The second $\alpha\beta$ unit is represented in darker colors of blue, green, and brown. AdoH is shown in red sticks; Cbl in pink sticks and sphere; PLP in black sticks. With the exception of Figs. 4.1, 4.2, and 4.3b, all figures were prepared using PyMOL⁵⁴.

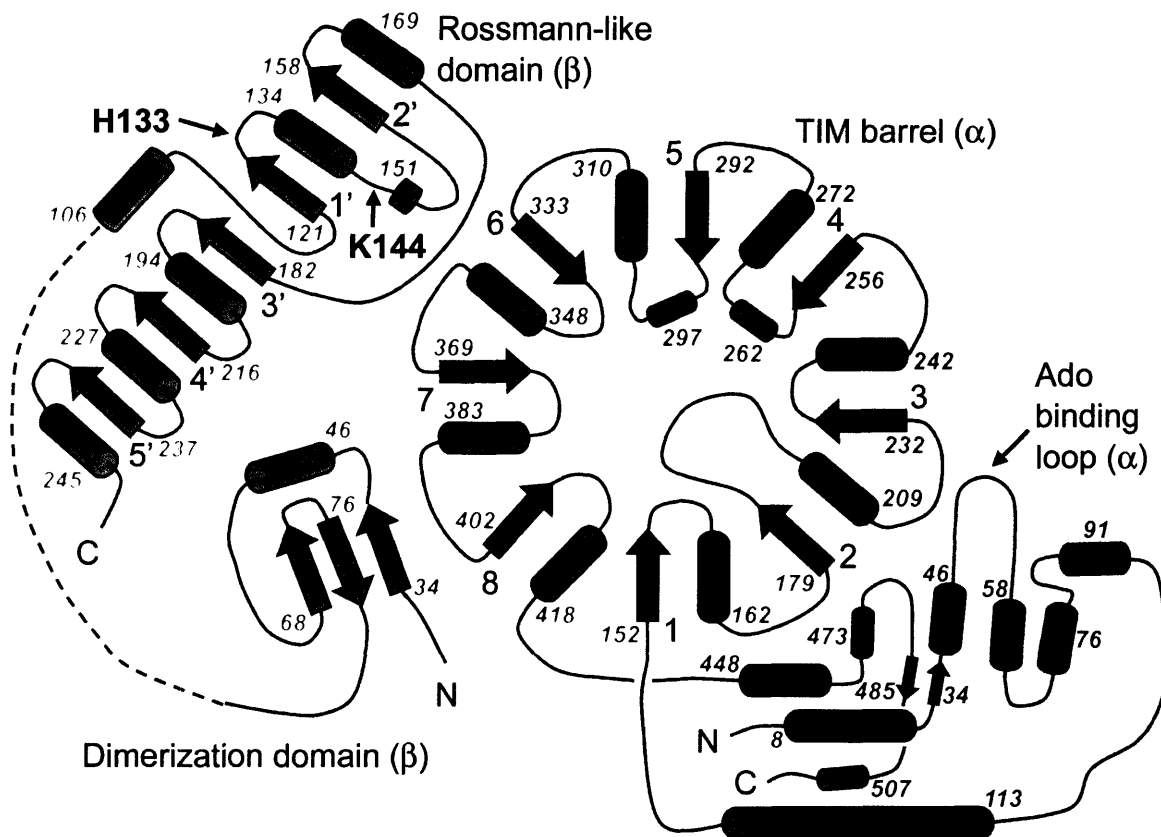


Figure 4.8. Topology diagram of the 5,6-LAM $\alpha\beta$ heterodimer. The β strands of the TIM barrel and Rossmann-like domains are numbered in large black numerals. Red numerals next to secondary structure elements indicate the N-terminal residue of that element. The locations of H133 β , which is the lower axial ligand to the cobalt of Cbl, and K144 β , which forms the imine bond to PLP, are emphasized with arrows. The Ado binding loop, which forms most of the interactions between the protein and AdoH, is also emphasized.

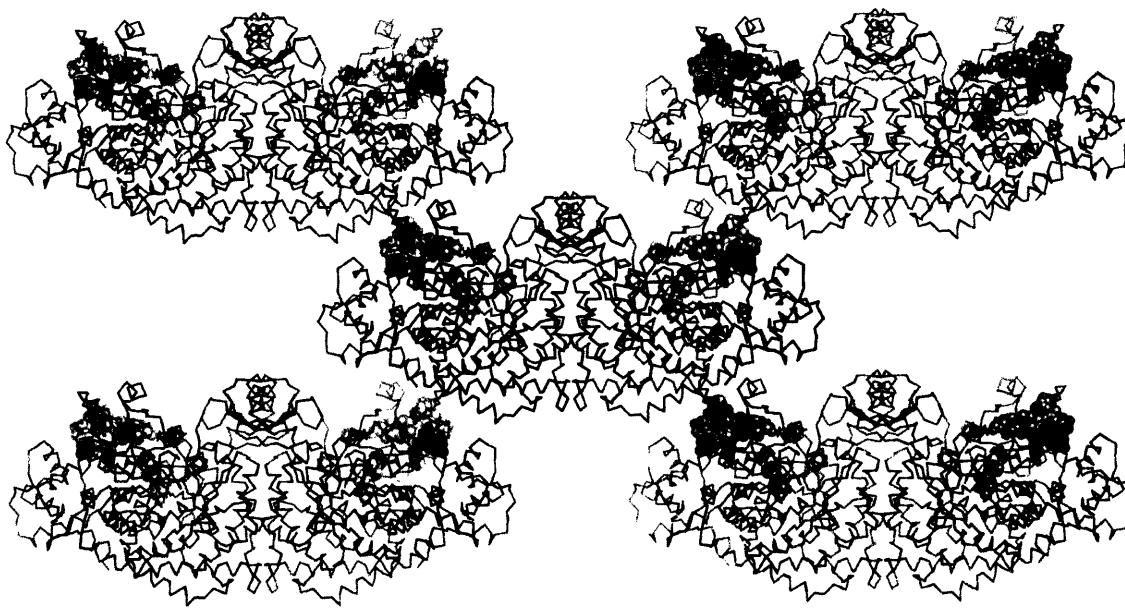


Figure 4.9. Lattice packing interactions of 5,6-LAM. The proposed physiologically relevant 5,6-LAM tetramers in the crystal are shown in different colors. Each $\alpha\beta$ unit interacts with three other $\alpha\beta$ units of neighboring tetramers. PLP, Cbl, and AdoH are shown in orange, pink, and red spheres, respectively.

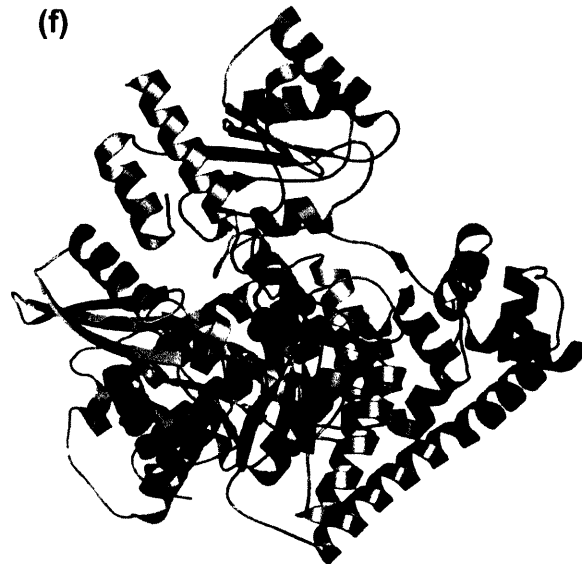
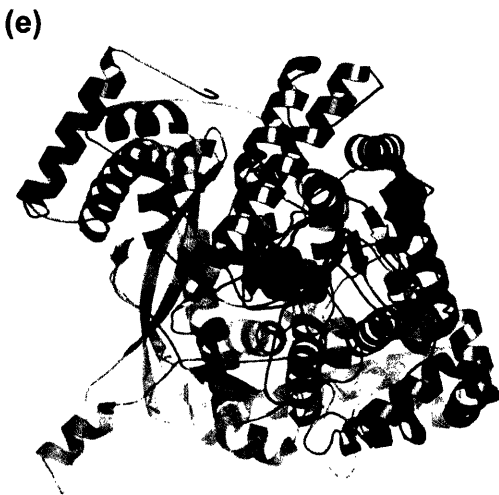
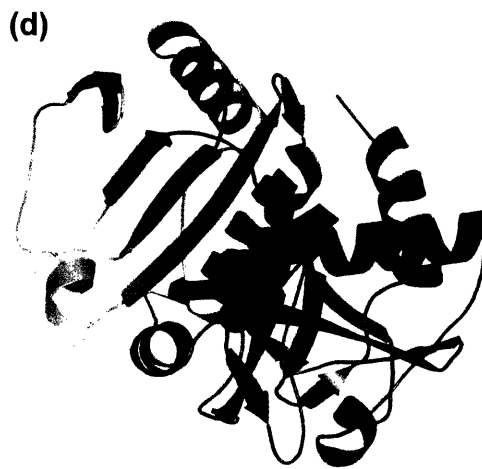
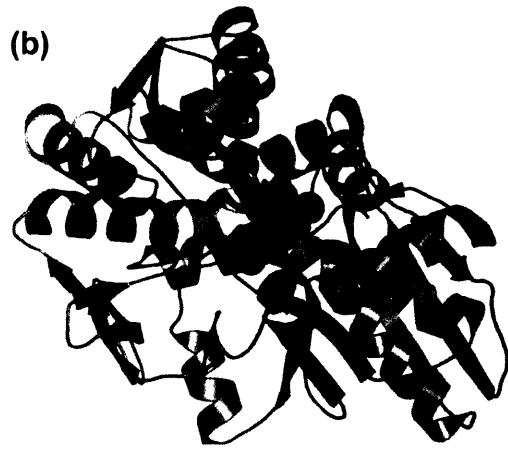
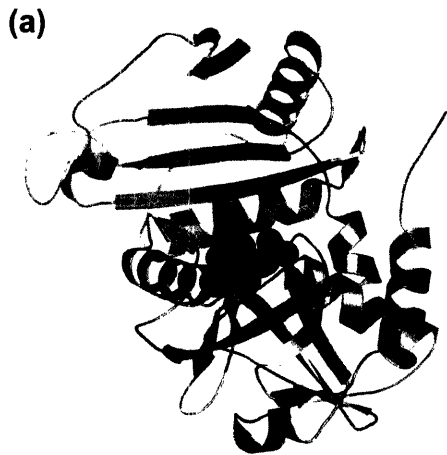


Figure 4.10. The five established PLP-binding enzyme families, plus 5,6-LAM. The structures shown are those of **(a)** aspartate aminotransferase (PDB code 1A0G); **(b)** tryptophan synthase (PDB code 1BKS); **(c)** alanine racemase (PDB code 1SFT); **(d)** D-amino acid aminotransferase (PDB code 1DAA); **(e)** glycogen phosphorylase (PDB code 1FU4); **(f)** 5,6-LAM. The PLP binding subunits are colored in blue. PLP (black spheres) and its associated Lys residue (black sticks) are shown. The PLP binding subunit of 5,6-LAM (β , the Rossmann-like domain) has a structure unlike that of any known PLP binding protein.



Figure 4.11. Superposition of the TIM barrels of alanine racemase and 5,6-LAM. alanine racemase (pink) and 5,6-LAM (light green) are shown in cartoon representations. The structures superimpose with an RMSD of 2.0 \AA^2 for 66 α carbons, as determined by LSQMAN⁵⁵. The view is from the top of the TIM barrel. The PLP cofactor of alanine racemase (red spheres) does not superimpose with the PLP of 5,6-LAM (dark green spheres).

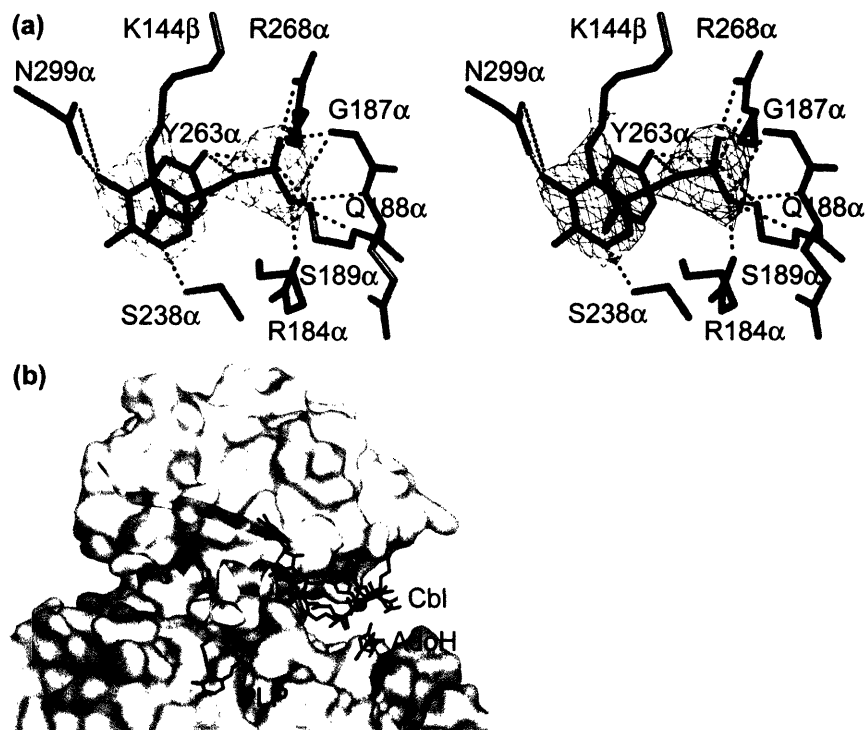


Figure 4.12. PLP in the putative active site of 5,6-LAM **(a)** Stereo view of the putative active site of 5,6-LAM. K144 β forms an imine bond to PLP; all other protein-PLP interactions are made by residues of the TIM barrel. A simulated annealing composite $2|F_o|-|F_c|$ omit electron density map (orange mesh), contoured at 1.5σ , is shown around the PLP. Unless otherwise noted, the coloring scheme for all stick or ball-and-stick representations is as follows: grey, C; red, O; blue, N; green, P; pink, Co. **(b)** Relative positions of PLP and AdoCbl. PLP is inserted into the C-terminal end of the TIM barrel by K144 β , which anchors the Rossmann-like domain in an off-center conformation on the top corner of the TIM barrel. H133 β , K144 β , PLP, Cbl, and AdoH are all depicted in black sticks. The secondary structural elements of the Rossmann-like domain that contain H133 β and K144 β are shown in a ribbon representation. Opaque domain surfaces are shown, colored as in Fig. 4.7.

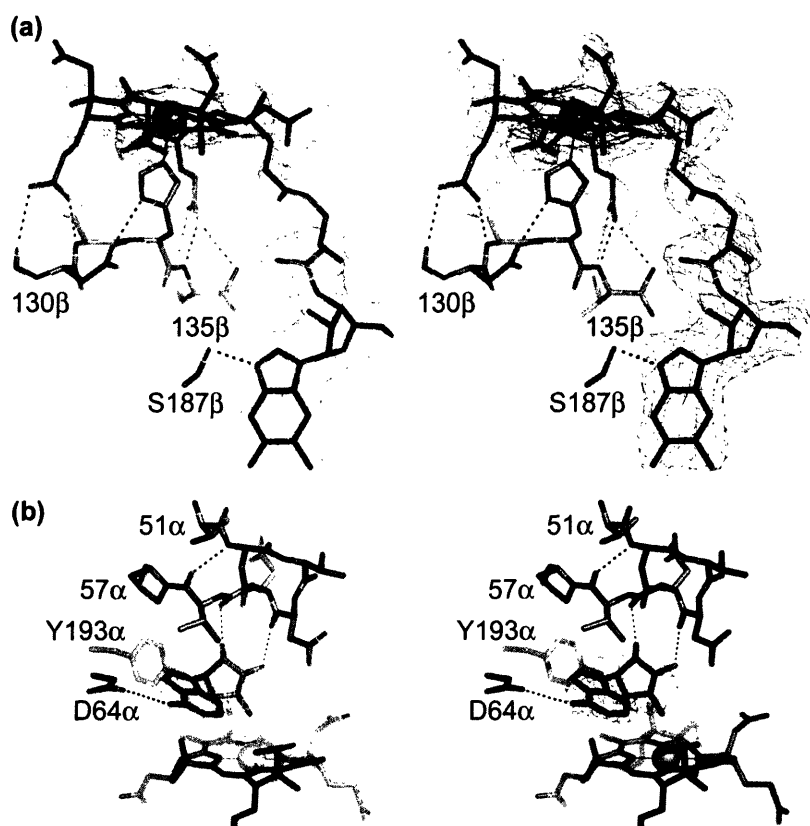


Figure 4.13. The AdoCbl binding site of 5,6-LAM. **(a)** Stereo view of Cbl within a 1.8 Å-radius simulated annealing composite $2|F_o|-|F_c|$ omit electron density map, contoured at 1.0σ . Hydrogen bonds between a propionamide side chain of the corrin ring and residues T191 β and Q192 β are omitted for clarity. **(b)** Stereo view of AdoH. AdoCbl appears to have cleaved in the X-ray beam, and we modeled the Ado moiety as AdoH. AdoH is shown in a 1.8 Å-radius simulated annealing $2|F_o|-|F_c|$ omit electron density map contoured at 1.0σ . Y193 α is part of the TIM barrel domain; otherwise, all protein-AdoH contacts are made by residues of the accessory clamp.



Figure 4.14. A stereo view of the local structure of the CxxCxxxC sequence. The three Cys residues are not positioned for disulfide formation or metal ligation.

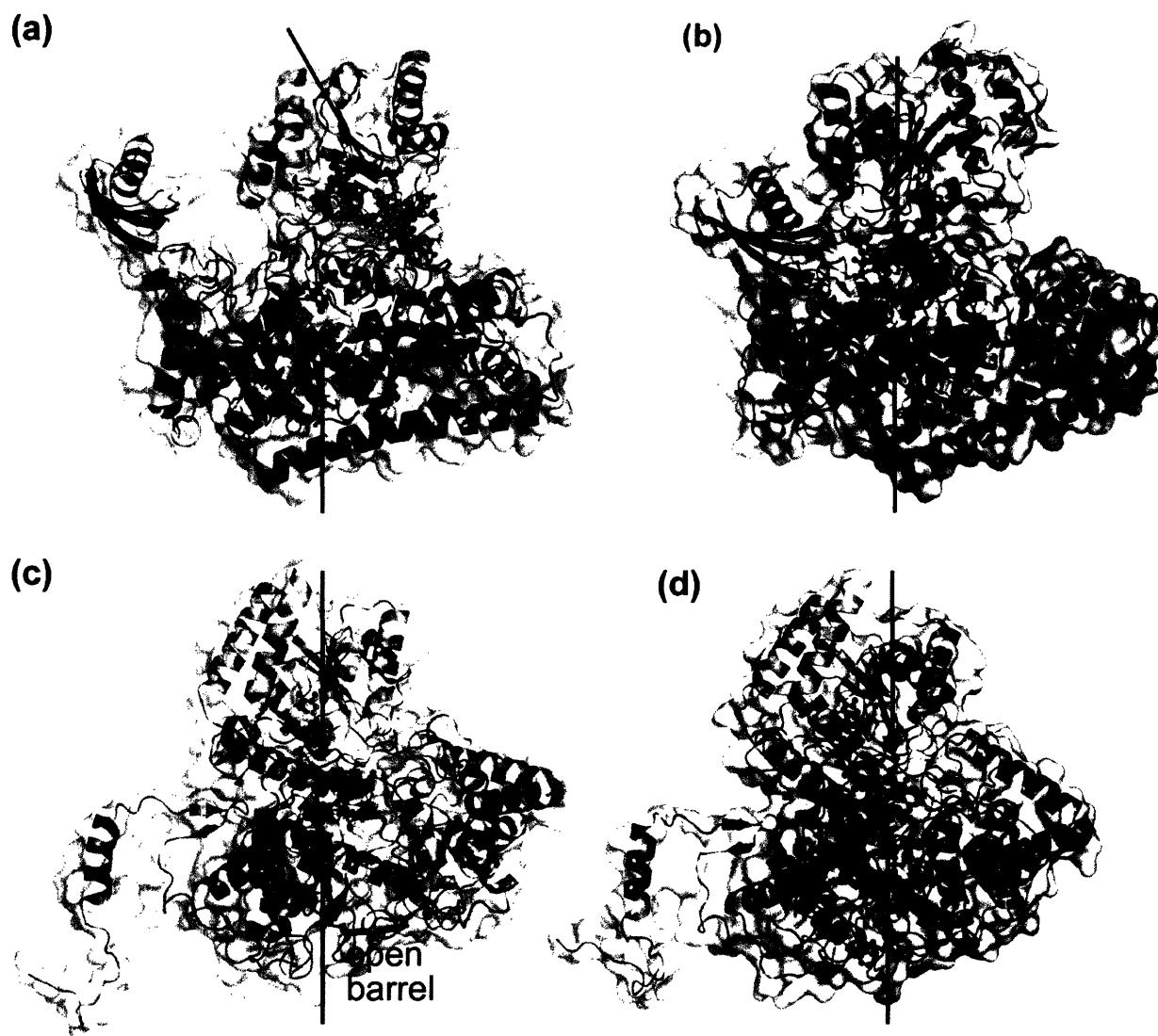


Figure 4.15. Hypothetical conformational change of 5,6-LAM and observed conformational change of MCM. (a) Structure of the substrate-free form of 5,6-LAM, as determined in this study. Protein domains and cofactors are colored as in Fig. 4.4a. Arrows represent the axes of the TIM barrel and Rossmann-like domains. (b) Hypothetical structure of the substrate-bound 5,6-LAM. The Rossmann-like domain is modeled to cap the C-terminal end of the TIM barrel in a manner resembling the structure of MCM. (c) Structure of the substrate-free form of MCM (PDB code 3REQ). The Rossmann-like domain sits directly atop the center of the TIM barrel, which is pried open in preparation for substrate binding. The Ado moiety of intact AdoCbl is shown in red, and the Cbl portion is shown in pink. (d) Structure of substrate-bound MCM (PDB code 1REQ). The substrate fragment, desulfo-CoA (dark blue), threads through the TIM barrel domain, effecting the closure of the TIM barrel to a much more compact structure. The Ado moiety of AdoCbl was not observed.

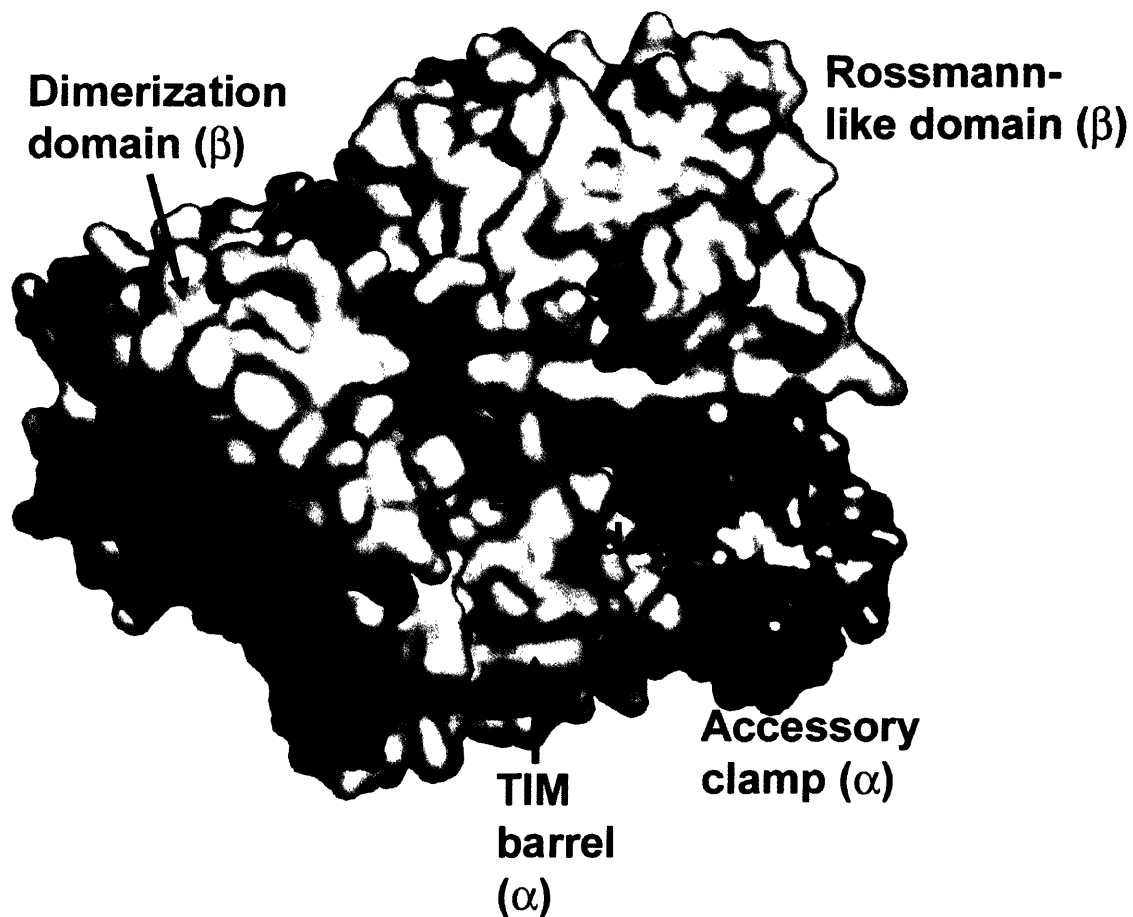


Figure 4.16. A cleft leading to the putative active site of 5,6-LAM. Protein and cofactor surfaces are shown, colored as in Fig. 4.4a, except that PLP is shown in orange. PLP is entrenched in the active site. The cleft leading to the active site is formed by the Rossmann-like domain and the dimerization domain.

4.7. References

1. Barker, H.A., Kahn, J.M. & Hedrick, L. Pathway of lysine degradation in *Fusobacterium nucleatum*. *J. Bact.* **152**, 201-207 (1982).
2. Reitzer, R. et al. Glutamate mutase from *Clostridium cochlearium*: the structure of a coenzyme B₁₂-dependent enzyme provides new mechanistic insights. *Structure Fold. Des.* **7**, 891-902 (1999).
3. Mancina, F. et al. How coenzyme B₁₂ radicals are generated: the crystal structure of methylmalonyl-coenzyme A mutase at 2 Å resolution. *Structure* **4**, 339-350 (1996).
4. Shibata, N. et al. A new mode of B₁₂ binding and the direct participation of a potassium ion in enzyme catalysis: X-ray structure of diol dehydratase. *Structure* **7**, 997-1008 (1999).
5. Berkovtich, F., Nicolet, Y., Wan, J.T., Jarrett, J.T. & Drennan, C.L. Crystal structure of biotin synthase, an *S*-adenosylmethionine-dependent radical enzyme. *Science* **303**, 76-79 (2004).
6. Berkovtich, F. et al. A locking mechanism preventing radical damage in the absence of substrate, as revealed by the X-ray structure of lysine 5,6-aminomutase. *Proc. Natl. Acad. Sci.*, manuscript in press (2004).
7. Dekker, E.E. & Barker, H.A. Identification and Cobamide Coenzyme-dependent Formation of 3,5-Diaminohexanoic Acid, and Intermediate in Lysine Fermentation. *J. Biol. Chem.* **243**, 3232-3237 (1968).
8. Morley, C.G.D. & Stadtman, T.C. Studies on the fermentation of D- α -Lysine. Purification and properties of an adenosine triphosphate regulated B₁₂-coenzyme-dependent D- α -Lysine mutase complex from *Clostridium sticklandii*. *Biochemistry* **9**, 1970 (1970).
9. Chirpich, T.P., Zappia, V., Costilow, R.N. & Barker, H.A. Lysine 2,3-aminomutase. Purification and properties of a pyridoxal phosphate and *S*-adenosylmethionine-activated enzyme. *J. Biol. Chem.* **245**, 1778-1789 (1970).
10. Petrovich, R.M., Ruzicka, F.J., Reed, G.H. & Frey, P.A. Metal cofactors of lysine-2,3-aminomutase. *J. Biol. Chem.* **266**, 7656-7660 (1991).
11. Moss, M. & Frey, P.A. The role of *S*-adenosylmethionine in the lysine 2,3-aminomutase reaction. *J. Biol. Chem.* **262**, 14859-14862 (1987).
12. Morley, C.G.D. & Stadtman, T.C. The role of pyridoxal phosphate in the B₁₂ coenzyme-dependent D- α -Lysine mutase reaction. *Biochemistry* **11**, 600-605 (1972).
13. Wetmore, S.D., Smith, D.M. & Random, L. How B6 Helps B12: The Roles of B6, B12, and the Enzymes in Aminomutase-Catalyzed Reactions. *J. Am. Chem. Soc.* **122**, 10208-10209 (2000).
14. Wetmore, S.D., Smith, D.M. & Random, L. Enzyme catalysis of 1,2-amino shifts: the cooperative action of B6, B12, and aminomutases. *J. Am. Chem. Soc.* **123**, 8678-8689 (2001).
15. Han, O. & Frey, P.A. Chemical model for the pyridoxal 5'-phosphate dependent lysine aminomutases. *J. Am. Chem. Soc.* **112**, 8982-8983 (1990).

16. Danen, W.C. & West, C.T. An electron spin resonance investigation of the 1-Aziridylcarbonyl and related free radicals. *J. Am. Chem. Soc.* **96**, 2447-2453 (1973).
17. Zhao, Y., Such, P. & Rétey, J. Radical intermediates in the coenzyme B₁₂ dependent methylmalonyl-CoA mutase reaction shown by ESR spectroscopy. *Angew. Chem. Int. Engl.* **31**, 215-216 (1992).
18. Marsh, E.N. & P., B.D. Coupling of cobalt-carbon bond homolysis and hydrogen atom abstraction in adenosylcobalamin-dependent glutamate mutase. *Biochemistry* **37**, 11864-11872 (1998).
19. Zelder, O., Beatrix, B., Leutbecher, U. & Buckel, W. Characterization of the coenzyme-B-12-dependent glutamate mutase from *Clostridium-cochlearium* produced in *Escherichia-coli*. *European Journal of Biochemistry* **226**, 577-585 (1994).
20. Finlay, T.H., Valinsky, J., Mildvan, A.S. & Abeles, R.H. Electron spin resonance studies with dioldehydrase. Evidence for radical intermediates in reactions catalyzed by coenzyme B 12. *J. Biol. Chem.* **248**, 1285-1290 (1973).
21. Tamao, Y. & Blakley, R.L. Direct spectroscopic observation of an intermediate formed from deoxyadenosylcobalamin in ribonucleotide reductase. *Biochemistry* **12**, 24-34 (1973).
22. Budisa, N. et al. High-level biosynthetic substitution of methionine in proteins by its analogs 2-aminohexanoic acid, selenomethionine, telluromethionine and ethionine in *Escherichia coli*. *Eur. J. Biochem.* **230**, 788-796 (1995).
23. Chang, C.H. & Frey, P.A. Cloning, sequencing, heterologous expression, purification, and characterization of adenosylcobalamin-dependent D-lysine 5, 6-aminomutase from *Clostridium sticklandii*. *J. Biol. Chem.* **275**, 106-114 (2000).
24. Otwinowski, Z. & Minor, W. Processing of X-ray diffraction data collected in oscillation mode. *Methods Enzymol.* **276**, 307-326 (1997).
25. Rice, L.M., Earnest, T.N. & Brunger, A.T. Single-wavelength anomalous diffraction phasing revisited. *Acta. Cryst. D* **56**, 1413-1420 (2000).
26. Dodson, E. Is it jolly SAD? *Acta. Cryst. D* **59**, 1958-1965 (2003).
27. Terwilliger, T.C. & Berendzen, J. Automated structure solution for MIR and MAD. *Acta. Cryst. D* **55**, 849-861 (1999).
28. McRee, D.E. XtalView/Xfit--A versatile program for manipulating atomic coordinates and electron density. *J. Struct. Biol.* **123**, 156-165 (1999).
29. Brunger, A.T. et al. Crystallography & NMR system: A new software suite for macromolecular structure determination. *Acta. Cryst. D* **55**, 905-921 (1998).
30. Laskowski, R.A., MacArthur, M.W., Moss, D.S. & Thornton, J.M. PROCHECK: a program to check the stereochemical quality of protein structures. *J. Appl. Cryst.* **26**, 283-291 (1993).
31. Baker, J.J., van der Drift, C. & Stadtman, T.C. Purification and properties of β -lysine mutase, a pyridoxal phosphate and B₁₂ coenzyme dependent enzyme. *Biochemistry* **12**, 1054-1063 (1973).
32. Barnham, K.J. et al. Structure of the Alzheimer's disease amyloid precursor protein copper binding domain. A regulator of neuronal copper homeostasis. *J. Biol. Chem.* **278**, 17401-17407 (2003).

33. Schneider, G., Kack, H. & Lindqvist, Y. The manifold of vitamin B6 dependent enzymes. *Structure Fold. Des.* **8**, R1-R6 (2000).
34. Tang, K.H., Harms, A. & Frey, P.A. Identification of a novel pyridoxal 5'-phosphate binding site in adenosylcobalamin-dependent lysine 5,6-aminomutase from *Porphyromonas gingivalis*. *Biochemistry* **41**, 8767-8776 (2002).
35. Hester, G. et al. Crystal structure of phosphoserine aminotransferase from *Escherichia coli* at 2.3 Å resolution: comparison of the unligated enzyme and a complex with alpha-methyl-l-glutamate. *J. Mol. Biol.* **286**, 829-850 (1999).
36. Weyand, M. & Schlichting, I. Crystal structure of wild-type tryptophan synthase complexed with the natural substrate indole-3-glycerol phosphate. *Biochemistry* **38**, 16469-16480 (1999).
37. Tirupati, B., Vey, J.L., Drennan, C.L. & Bollinger, J.M., Jr. Kinetic and structural characterization of Slr0077/SufS, the essential cysteine desulfurase from *Synechocystis* sp. PCC 6803. *Biochemistry* **In press**(2004).
38. Drennan, C.L., Huang, S., Drummond, J.T., Matthews, R.G. & Ludwig, M.L. How a protein binds B12: A 3.0 Å X-ray structure of B₁₂-binding domains of methionine synthase. *Science* **266**, 1669-1674 (1994).
39. Champloy, F., Gruber, K., Jogl, G. & Kratky, G. XAS spectroscopy reveals X-ray-induced photoreduction of free and protein-bound B-12 cofactors. *J. Synch. Rad.* **7**, 267-273 (2000).
40. Gruber, K., Reitzer, R. & Kratky, G. Radical Shuttling in a Protein: Ribose Pseudorotation Controls Alkyl-Radical Transfer in the Coenzyme B(12) Dependent Enzyme Glutamate Mutase. *Angew. Chem. Int. Ed.* **40**, 3377-3380 (2001).
41. Mancia, F. & Evans, P.R. Conformational changes on substrate binding to methylmalonyl CoA mutase and new insights into the free radical mechanism. *Structure* **6**, 711-720 (1998).
42. Tang, K.H., Casarez, A.D., Wu, W. & Frey, P.A. Kinetic and biochemical analysis of the mechanism of action of lysine 5,6-aminomutase. *Arch. Biochem. Biophys.* **418**, 49-54 (2003).
43. Evans, J.C. et al. Structures of the N-terminal modules imply large domain motions during catalysis by methionine synthase. *Proc. Natl. Acad. Sci.* **101**, 3729-3726 (2004).
44. Bandarian, V., Ludwig, M.L. & Matthews, R.G. Factors modulating conformational equilibria in large modular proteins: a case study with cobalamin-dependent methionine synthase. *Proc. Natl. Acad. Sci.* **100**, 8156-8163 (2003).
45. Vlasie, M.D. & Banerjee, R. Tyrosine 89 accelerates Co-carbon bond homolysis in methylmalonyl-CoA mutase. *J. Am. Chem. Soc.* **125**, 5431-5435 (2003).
46. Tang, K.H., Chang, C.H. & Frey, P.A. Electron transfer in the substrate-dependent suicide inactivation of Lysine 5,6-Aminomutase. *Biochemistry* **40**, 5190-5199 (2001).
47. Auld, D.S. & Bruice, T.C. Catalytic reactions involving azomethines. VII. Rates and equilibria of aldimine formation with 3-hydroxypyridine-4-aldehyde and alanine. *J. Am. Chem. Soc.* **89**, 2083-2089 (1967).

48. Auld, D.S. & Bruice, T.C. Catalytic reactions involving azomethines. VIII. Water and alanine catalysis of the transamination of 3-hydroxypyridine-4-aldehyde by alanine. *J. Am. Chem. Soc.* **89**, 2090-2097 (1967).
49. Auld, D.S. & Bruice, T.C. Catalytic reactions involving azomethines. IX. General base catalysis of the transamination of 3-hydroxypyridine-4-aldehyde by alanine. *J. Am. Chem. Soc.* **89**, 2098-2106 (1967).
50. Harris, S.A., Webb, T.J. & Folkers, K. Chemistry of vitamin B6. I. Tautomerism. *J. Am. Chem. Soc.* **62**, 3198-3203 (1940).
51. Metzler, D.E. Equilibria between pyridoxal and amino acids and their imines. *J. Am. Chem. Soc.* **79**, 485-490 (1957).
52. Metzler, D.E. & Snell, E.E. Spectra and ionization constants of the vitamin B6 group and related 3-hydroxypyridine derivatives. *J. Am. Chem. Soc.* **77**, 2431-2437 (1955).
53. Thanassi, J.W., Butler, A.R. & Bruice, T.C. Catalytic reactions involving azomethines. VI. The mechanism of the transamination of 3-hydroxypyridine-4-aldehyde by glutamic acid. *Biochemistry* **4**, 1463-1472 (1965).
54. DeLano, W.L. The PyMOL Molecular Graphics System. (<http://pymol.sourceforge.net>).
55. Kleywegt, G.J. Use of non-crystallographic symmetry in protein structure refinement. *Acta. Cryst.* **D52**, 842-857 (1996).

Chapter 5
Conclusions

Abbreviations:

2,3-LAM	Lysine 2,3-aminomutase
5,6-LAM	Lysine 5,6-aminomutase
Ado	5'-deoxyadenosyl group
Ado•	5'-deoxyadenosyl radical
AdoCbl	Adenosylcobalamin, Coenzyme B ₁₂
AdoH	5'-deoxyadenosine
AdoMet	<i>S</i> -adenosylmethionine
BioB	Biotin synthase
Cbl	Cobalamin
CNCbl	Cyanocobalamin, Vitamin B ₁₂
DDH	Diol dehydratase
DTB	Dethiobiotin
HemN	Coproporphyrinogen III oxidase
RNR	Ribonucleotide reductase
SAM	<i>S</i> -adenosylmethionine

The crystal structures of biotin synthase (BioB) and lysine 5,6-aminomutase (5,6-LAM) allow for a comparison of the adenosylcobalamin (AdoCbl) and the adenosylmethionine (AdoMet) -dependent radical enzymes. In particular, we learn that at least one AdoMet radical enzyme has a TIM barrel fold¹, like most of the Cbl-dependent enzymes²⁻⁶. In a break from the TIM barrel trend, the structure of HemN, the only other AdoMet radical enzyme structure that is published, has an α/β fold (referred to as a “3/4 barrel”) that is reminiscent of the TIM barrel⁷.

The elucidation of the structure of 2,3-LAM is currently under way (P. A. Frey, personal communication). It is not known if its structure resembles the 3/4 barrel of HemN, the TIM barrel of BioB and 5,6-LAM, or some other structure.

5.1 Structural comparison of BioB with HemN

Superposition of BioB with HemN reveals that the two enzymes share a core set of β -strands and α helices (Fig. 5.1a). The common set of strands and helices superimpose with a root mean square deviation of 1.9 Å² for 99 alpha carbons (Fig. 5.1b). Additionally, the 4Fe-4S cluster, its coordinating AdoMet, and several important residues are structurally equivalent (Fig. 5.1c). In BioB, these residues are: Y59 and I192, which interact with the adenine ring of AdoMet; D155, which hydrogen bonds to the 2' and 3' -OH groups of the ribose moiety; and R173, which forms a salt bridge with the carboxyl group of AdoMet. Interestingly, a second AdoMet molecule, proposed to give rise to the second Ado• in the hypothetical HemN mechanism⁷, was modeled into the structure of

HemN. The second AdoMet molecule is located near the DTB site of BioB, possibly suggesting that this AdoMet might be occupying the binding site of the heme substrate.

5.2 Structural comparison of BioB with diol dehydratase

One tentative indication of an evolutionary link between the AdoMet and the AdoCbl radical enzymes is evident upon structural comparison of BioB and diol dehydratase (DDH). Superposition of the alpha carbons of both crystal structures (DDH PDB code 1DIO⁵) reveals several remarkable similarities (Fig. 5.2). The Co atom of cyanocobalamin (CNCbl) occupies the same space as the 4Fe-4S cluster of BioB, a catalytic K⁺ ion in DDH coincides with the 2Fe-2S cluster of BioB, the substrates of both enzymes superimpose, and both substrates are covered by similar loops.

Clearly, BioB, as well as the AdoCbl-dependent enzymes (with the exception of the class II RNR), are able to properly arrange their catalytic elements using the TIM barrel fold. It is possible that the TIM barrel is especially adept at catalyzing Ado• chemistry because the radical intermediates can be effectively sequestered inside the barrel.

The structure of BioB is more like the structure of DDH than that of HemN. Both BioB and DDH have relatively small substrates, compared to the HemN substrate, a tetrapyrrole macrocycle. Accordingly, the 3/4 barrel fold of HemN envelopes more volume than does a TIM barrel, allowing for a larger active site. It is tempting to speculate that substrate size dictates the use of a 3/4 barrel fold over a TIM barrel; a 3/4 barrel would be required for large substrates which could not fit inside an eight-stranded

β -barrel structure. With the current limitations on the number of AdoMet radical enzyme structures, there is no convincing support for this theory. To this end, the structure of 2,3-LAM is of special interest, since its substrate is identical to one of the 5,6-LAM substrates. If substrate size does determine the fold of an Ado• enzyme, then we expect 2,3-LAM to have a TIM barrel fold, like 5,6-LAM.

5.3. A novel role for PLP in an Ado• enzyme

We propose that in 5,6-LAM, PLP has a novel role in keeping AdoCbl out of the active site in the absence of substrate. Transimination of the covalent PLP-K144 β imine linkage with the substrate releases the Rossmann domain from its constrained position, allowing it to rotate and place AdoCbl into the active site of the TIM barrel domain. To our knowledge, this is the first reported instance of PLP being used to lock an enzyme in a certain conformation.

5.4. Ado• enzymes: barrel structures with reaction-specific accommodations

Ado• enzymes commonly utilize barrel-like structures, which are adapted to the particular enzymatic reaction. BioB appears to be very similar in structure to AdoCbl enzymes, but the AdoCbl-binding domain is replaced by a loop at the top of the barrel that binds the essential 4Fe-4S cluster. The structure of 5,6-LAM is generally similar to those of other AdoCbl enzymes, in that it contains a TIM barrel and a Rossmann-like domain. However, these domains are modified to create a mechanism by which a small substrate, lysine, can trigger a large conformational change upon binding and transimination. A broken helix of the Rossmann-like domain creates a novel PLP

binding motif. This motif allows for PLP-mediated interactions to control the conformation of the enzyme, keeping AdoCbl out of the active site in the absence of substrate. Thus, we expect to see more variation on the general theme of $\alpha\beta$ barrel structures as more AdoMet and AdoCbl radical enzymes are structurally characterized.

5.5. Figures

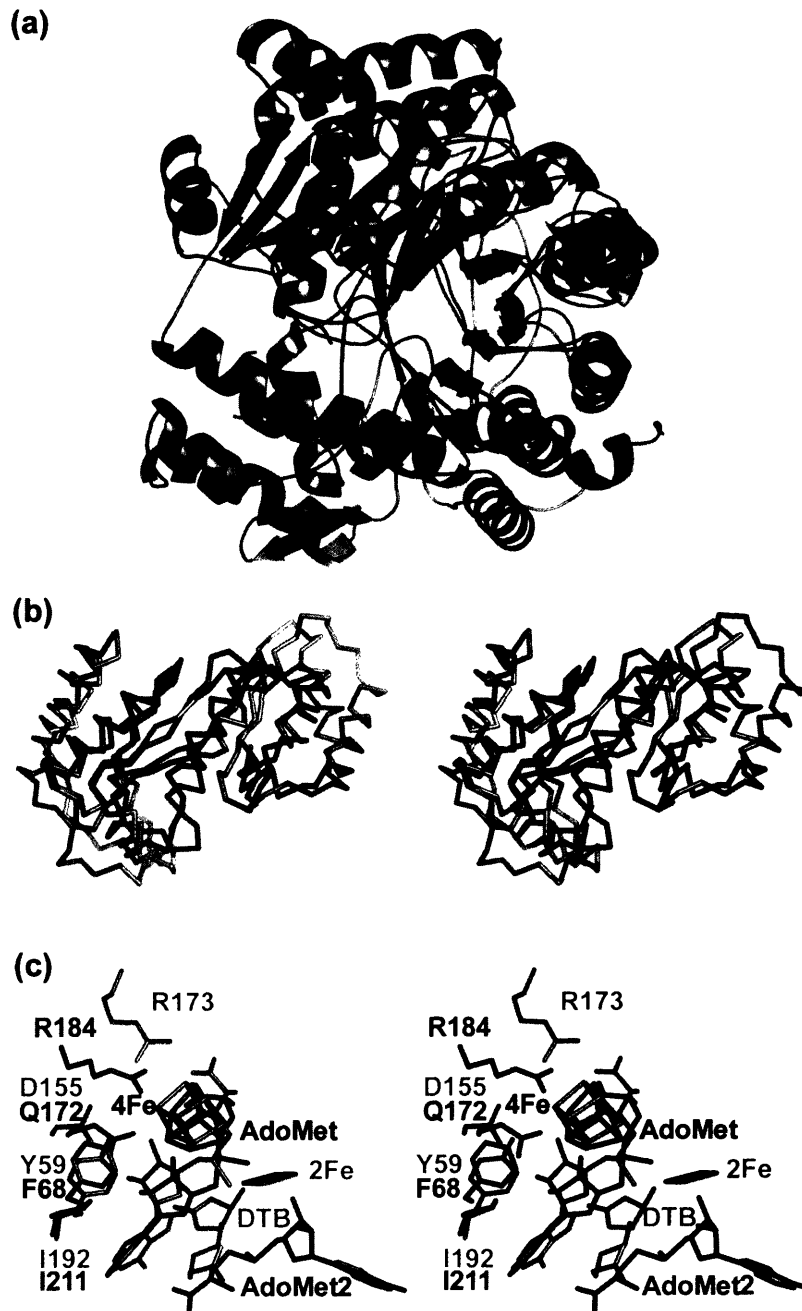


Figure 5.1. (a) Superposition of BioB (blue) and HemN (grey). The view is from the bottom of the BioB TIM barrel. Cofactors and substrates are omitted for clarity. (b) Stereo view alpha carbon trace of the structurally homologous regions of BioB and HemN. The color scheme for parts b and c are the same as for part a. (c) Analogous residues in the active sites of BioB and HemN (see text). Residues are labeled according to the coloring scheme of part a. The 4Fe-4S clusters and associated AdoMet of both proteins are labeled in black typeface. The second AdoMet of HemN is labeled "AdoMet2" in grey. The 2Fe-2S cluster of BioB is labeled "2Fe" in blue. Figures 5.1 and 5.2 were made using PyMOL⁸.

References

1. Berkovtich, F., Nicolet, Y., Wan, J.T., Jarrett, J.T. & Drennan, C.L. Crystal structure of biotin synthase, an *S*-adenosylmethionine-dependent radical enzyme. *Science* **303**, 76-79 (2004).
2. Berkovtich, F. et al. A locking mechanism preventing radical damage in the absence of substrate, as revealed by the X-ray structure of lysine 5,6-aminomutase. *Proc. Natl. Acad. Sci.*, manuscript in press (2004).
3. Drennan, C.L., Huang, S., Drummond, J.T., Matthews, R.G. & Ludwig, M.L. How a protein binds B₁₂: A 3.0 Å X-ray structure of B₁₂-binding domains of methionine synthase. *Science* **266**, 1669-1674 (1994).
4. Mancia, F. et al. How coenzyme B₁₂ radicals are generated: the crystal structure of methylmalonyl-coenzyme A mutase at 2 Å resolution. *Structure* **4**, 339-350 (1996).
5. Shibata, N. et al. A new mode of B₁₂ binding and the direct participation of a potassium ion in enzyme catalysis: X-ray structure of diol dehydratase. *Structure* **7**, 997-1008 (1999).
6. Reitzer, R. et al. Glutamate mutase from *Clostridium cochlearium*: the structure of a coenzyme B₁₂-dependent enzyme provides new mechanistic insights. *Structure Fold. Des.* **7**, 891-902 (1999).
7. Layer, G., Moser, J., Heinz, D.W., Jahn, D. & Schubert, W.D. Crystal structure of coproporphyrinogen III oxidase reveals cofactor geometry of Radical SAM enzymes. *EMBO J.* **22**, 6214-6224 (2003).
8. DeLano, W.L. The PyMOL Molecular Graphics System. (<http://pymol.sourceforge.net>).

Appendices

Appendix 1. Summary of 5,6-LAM crystallization experiments. Commercially available screens (Hampton Research Corp.) were used (denoted by “yes”) or not used (denoted by “no”) in crystallization experiments with 5,6-LAM, AdoCbl, cyanocobalamin (CNCbl), Adenylpentylcobalamin (APCbl), substrate (D or L-lysine), or inhibitors (L-ornithine [L-orn] or thialysine [Thialys]), in various combinations. For details of crystallization experiments, see chapter 4.

Protein sample	Crystal screen 2	Crystal screen lite	Index I	Index II	Memb-Fac	AS grid	PEG/Ion grid	PEG 6000 grid	Natrix
5,6-LAM	Yes	Yes	Yes	Yes	Yes	Yes	Yes	Yes	Yes
5,6-LAM +AdoCbl	Yes	Yes	Yes	Yes	Yes	Yes	Yes	Yes	Yes
5,6-LAM +AdoCbl +Thialys	No	Yes	Yes	Yes	Yes	Yes	Yes	Yes	No
5,6-LAM +AdoCbl +L-Orn	No	Yes	Yes	Yes	Yes	Yes	Yes	Yes	No
5,6-LAM +APCbl + D-Lys	No	Yes	Yes	Yes	Yes	Yes	Yes	Yes	No
5,6-LAM +CNCbl + D-Lys	No	Yes	Yes	Yes	Yes	Yes	Yes	Yes	No
5,6-LAM +CNCbl + L-Lys	No	No	Yes	Yes	No	Yes	Yes	Yes	No



Room 14-0551
77 Massachusetts Avenue
Cambridge, MA 02139
Ph: 617.253.5668 Fax: 617.253.1690
Email: docs@mit.edu
<http://libraries.mit.edu/docs>

DISCLAIMER OF QUALITY

Due to the condition of the original material, there are unavoidable flaws in this reproduction. We have made every effort possible to provide you with the best copy available. If you are dissatisfied with this product and find it unusable, please contact Document Services as soon as possible.

Thank you.

PAGES 165, 166, 167 APPEAR TWICE.